SITE CHARACTERIZATION AND 3-D GEOLOGIC MODELING OF THE RIVAL FIELD

Second Target Area Completed

Plains CO_2 Reduction (PCOR) Partnership Phase III
Task 1 – Deliverable D5

Prepared for:

Andrea T. McNemar

National Energy Technology Laboratory
U.S. Department of Energy
3610 Collins Ferry Road
PO Box 880
Morgantown, WV 26507-0880

DOE Cooperative Agreement No. DE-FC26-05NT42592

Prepared by:

Jason R. Braunberger
Jordan M. Bremer
Dayanand Saini
Hadi Jabbari
Wesley D. Peck
Charles D. Gorecki
Edward N. Steadman

Energy & Environmental Research Center
University of North Dakota
15 North 23rd Street, Stop 9018
Grand Forks, ND 58202-9018

March 2012
2012-EERC-04-16
Approved

EERC DISCLAIMER

LEGAL NOTICE This research report was prepared by the EERC, an agency of the University of North Dakota, as an account of work sponsored by the U.S. Department of Energy National Energy Technology Laboratory and TAQA North Ltd. Because of the research nature of the work performed, neither the EERC nor any of its employees makes any warranty, express or implied, or assumes any legal liability or responsibility for the accuracy, completeness, or usefulness of any information, apparatus, product, or process disclosed or represents that its use would not infringe privately owned rights. Reference herein to any specific commercial product, process, or service by trade name, trademark, manufacturer, or otherwise does not necessarily constitute or imply its endorsement or recommendation by the EERC.

DOE DISCLAIMER

This report was prepared as an account of work sponsored by an agency of the United States Government. Neither the United States Government, nor any agency thereof, nor any of their employees, makes any warranty, express or implied, or assumes any legal liability or responsibility for the accuracy, completeness, or usefulness of any information, apparatus, product, or process disclosed, or represents that its use would not infringe privately owned rights. Reference herein to any specific commercial product, process, or service by trade name, trademark, manufacturer, or otherwise does not necessarily constitute or imply its endorsement, recommendation, or favoring by the United States Government or any agency thereof. The views and opinions of authors expressed herein do not necessarily state or reflect those of the United States Government or any agency thereof.

NDIC DISCLAIMER

This report was prepared by the Energy & Environmental Research Center (EERC) pursuant to an agreement partially funded by the Industrial Commission of North Dakota, and neither the EERC nor any of its subcontractors nor the North Dakota Industrial Commission nor any person acting on behalf of either:

(A) Makes any warranty or representation, express or implied, with respect to the accuracy, completeness, or usefulness of the information contained in this report or that the use of any information, apparatus, method, or process disclosed in this report may not infringe privately owned rights; or

(B) Assumes any liabilities with respect to the use of, or for damages resulting from the use of, any information, apparatus, method, or process disclosed in this report.

Reference herein to any specific commercial product, process, or service by trade name, trademark, manufacturer, or otherwise does not necessarily constitute or imply its endorsement, recommendation, or favoring by the North Dakota Industrial Commission. The views and opinions of authors expressed herein do not necessarily state or reflect those of the North Dakota Industrial Commission

TABLE OF CONTENTS

Continued . . .

TABLE OF CONTENTS (continued)

LIST OF FIGURES

Continued . . .

LIST OF FIGURES (continued)

LIST OF TABLES

SITE CHARACTERIZATION AND 3-D GEOLOGIC MODELING OF THE RIVAL FIELD

EXECUTIVE SUMMARY

Site characterization and 3-D geologic modeling were completed for the Rival Field, Burke County, North Dakota, as part of the Plains CO_2 Reduction (PCOR) Partnership's advanced characterization efforts targeting oil fields with potential for future carbon dioxide (CO_2) enhanced oil recovery and long-term CO_2 storage. Predictive static 3-D geologic models were built with the goal of better understanding spatial distribution of reservoir properties across the 100-square-mile study area centered on the Rival Field.

The oil reservoir of interest represents an updip stratigraphic trap comprising carbonate rocks that were deposited 300–340 million years ago in a tidal flat depositional system positioned on a much larger carbonate shelf in the present-day northeast corner of the Williston Basin. The Rival Field and several nearby unitized fields all produce from the Midale and Rival Members of the Charles and Mission Canyon Formations at depths ranging from 6000 to 6900 ft. From 1957 to 2010, the Rival Field produced over 16.2 million barrels (Mbbl) of oil and 14.5 billion cubic feet of gas. Primary production peaked at 5000 bbl oil/day in October 1960, but current production is less than 200 bbl oil/day.

As part of the characterization efforts, core analysis was performed by the Applied Geology Laboratory at the Energy & Environmental Research Center to complement historically available data. Twenty-eight thin sections were prepared from Wells 16409 and 13700 and prepared for pertrographic analysis. In addition, five core plugs were cut from Well 16409 to estimate values for the following: bulk and grain density, porosity, permeability, and bulk mineralogy. These data, along with the historic data, were used to identify different macro- and microfacies and were then correlated to the geophysical logs.

Once the facies were determined, several well data normalization and petrophysical analysis techniques were performed on the geophysical logs available from the 312 wells. Five prominent tops were picked and correlated amongst 140 wells that passed the normalization and petrophysical analysis workflows, ultimately comprising the 3-D structural model. A petrophysical model was built with the following interpreted properties: effective porosity, net-to-gross (porosity), permeability, water saturation, temperature, and pressure. Random seeds were used to generate 31 realizations for each property where values were distributed across the model geostatistically using Gaussian random function simulation.

Volumetric EOR and CO_2 required were calculated based on original oil in place (OOIP), industry standard recovery and utilization factors, and a literature-derived formation factor. This resulted in 6.0–9.0 Mbbl of incremental oil from the Rival Field which required 1.5–2.9 Mt of CO_2 and would be ultimately stored.

A CO_2 Prophet model was calibrated using historic water injection data and simulated to make predictions for total CO_2 storage volume and IOR within the Rival Member. Sensitivity analysis was performed, resulting in a total of 36 cases of simulation of which 23 were successful. 60-acre, 80-acre, and 100-acre spacing units were used, with 12 cases for each. Two patterns were simulated for each spacing unit, or six cases for each of the seven-spot and line drive patterns. Upon injection of 1 hydrocarbon pore volume (HCPV), the patterns continually showed an additional 13–15 Mbbl of oil (15%–18% OOIP), while 2 HCPV resulted in an additional 22.8–24.4 Mbbl of oil (26.9%–28.6% OOIP). The injection of CO_2 for EOR ultimately would result in an incidental cumulative storage of an estimated 2.5 to 3.5 million tons of CO_2.

This method, along with the volumetric EOR and CO_2 method, gives good estimations of the potential for incremental oil recovery in the Rival Field, although they do not replace calculations made by detailed history-matching and subsequent predictive simulations.

SITE CHARACTERIZATION AND 3-D GEOLOGIC MODELING OF THE RIVAL FIELD

INTRODUCTION

Project Objectives

The efforts described in this report are part of a larger characterization component of Plains CO_2 Reduction (PCOR) Partnership activities funded by the U.S. Department of Energy (DOE) National Energy Technology Laboratory (NETL). Phase III characterization of the PCOR Partnership region comprises identifying, gathering, and evaluating information on locations within the region that have potential to serve as sites for large-scale injection, enhanced oil recovery (EOR), and storage of carbon dioxide (CO_2). Detailed subsurface mapping and modeling must be conducted prior to large-scale CO_2 injection for project design, including the use of tertiary oil production techniques if applicable. As part of the PCOR Partnership's Phase I and II regional characterization activities, evaluations of potential geological storage targets were completed on a reconnaissance level using readily available public sources of data. These investigations resulted in assessment of the theoretical storage capacity for oil fields and identification of saline aquifer potential throughout the PCOR Partnership region, which provides a basis for further evaluation.

Early in Phase III, the PCOR Partnership identified three target areas for further evaluation with regard to the utilization of CO_2 for EOR (Figure 1): 1) the Eland Field, which is part of the Dickinson Lodgepole Mound (DLM) complex located in western North Dakota; 2) the Rival Field in northwestern North Dakota, which is located near a gas-processing plant that currently disposes of acid gas into the subsurface; and 3) the Sleepy Hollow Field in southwestern Nebraska. Detailed characterizations of the Eland Field and DLM complex were completed in May 2009 (Knudsen and others, 2009).

Characterization activities have been completed in greater detail than previous studies of the field and have utilized all sources of data available through the PCOR Partnership. These data sources include, but were not limited to, geophysical logs, core analysis, bottomhole pressure tests, production decline curves, drillstem tests, and produced fluid analysis. Site characterization has culminated in the production of a predictive 3-D static geologic model with multiple realizations using industry-standard software that address critical parameters of the target formation:

Figure 1. Location of the three target areas within the PCOR Partnership region.

- Member thickness
- Basic reservoir properties
- Volumetric capacity of the reservoir
- Potential CO_2 EOR volume and recovery factor
- Prospective CO_2 storage within the reservoir

The Rival Field, represented by 12,800 unitized acres, located in Burke County, North Dakota (Figure 2), is currently operated by TAQA North Ltd. The oil reservoir comprises an updip stratigraphic trap created by facies change. Rocks that make up this reservoir were deposited in a tidal flat environment from within a larger carbonate shelf platform that was active in the late Paleozoic Era. Lithification, diagenesis, and oil migration followed deposition, ultimately forming this hydrocarbon reservoir. Primary production from the Rival and adjacent unitized oil fields (Portal, Black Slough, and Lignite) comes from the Charles and Mission Canyon Formations, part of the much larger Madison Group (Figure 3).

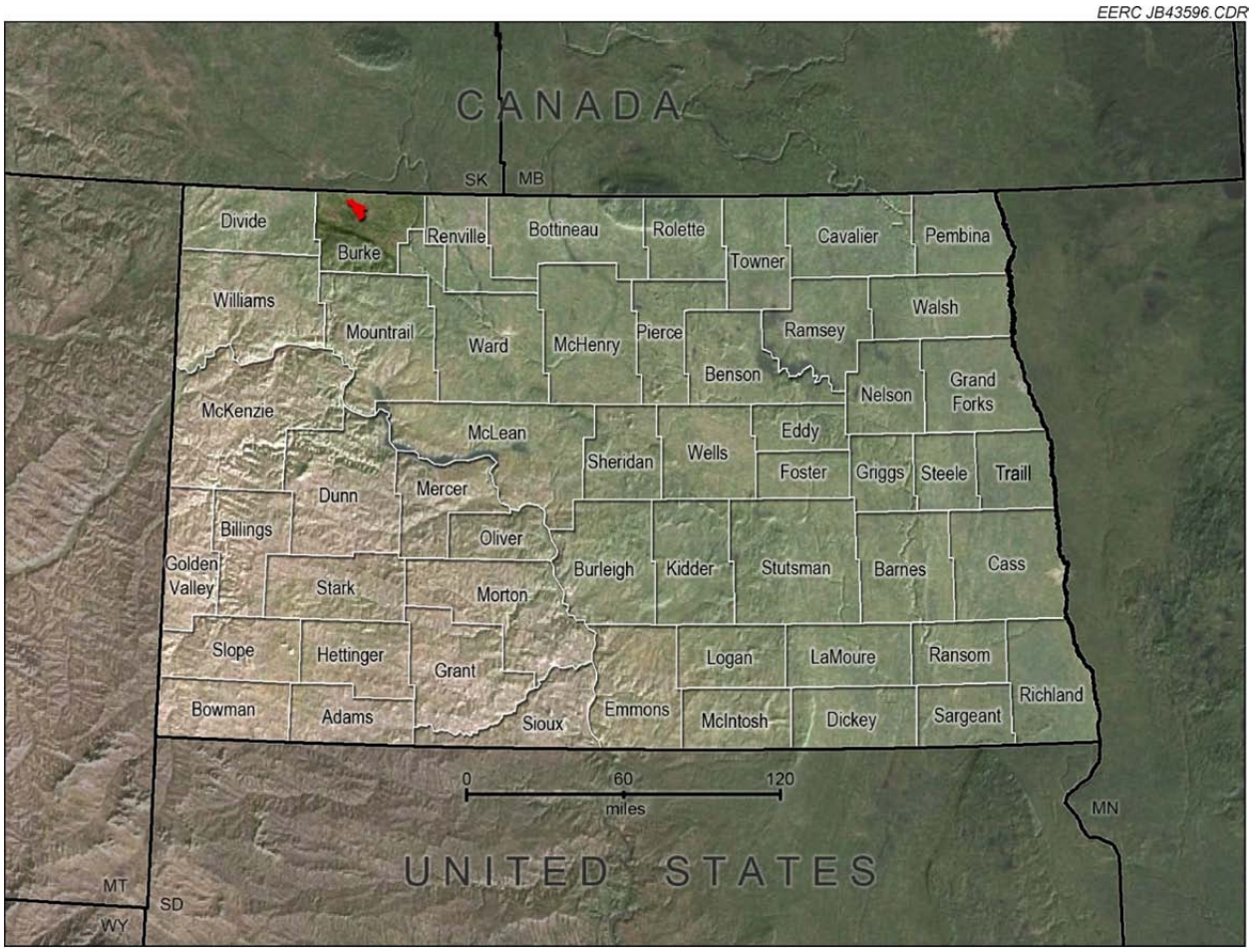

Figure 2. Location of the Rival Field in Burke County, North Dakota.

Geologic History

The Madison Group is traditionally known as a thick sequence of carbonate rock deposited between 300 and 340 million years ago (Ma) when the present-day Williston Basin sat just north of the equator in Earth's tropical region (Figure 4). Furthermore the present-day oil reservoir was part of an extensive tidal flat environment, forming a belt near the marine shore where the primary mode of sedimentation resulted in overlapping sequences in response to seawater rise (transgression), retreat (regression), and lateral shifts. This cyclicity is also known as sequence stratigraphy, where slight changes in sea level can affect the entire depositional system. The present-day analog tidal flat environment can be seen in two different settings: the Persian Gulf (Figure 5), with an extensive salt flat (sabkha), and the Little Bahama Bank, Caribbean Islands, without the sabkha (Figure 6).

This tidal flat depositional environment was built on a major carbonate shelf system containing several cycles of shallow sabkha sediments, barrier islands, intertidal buildups,

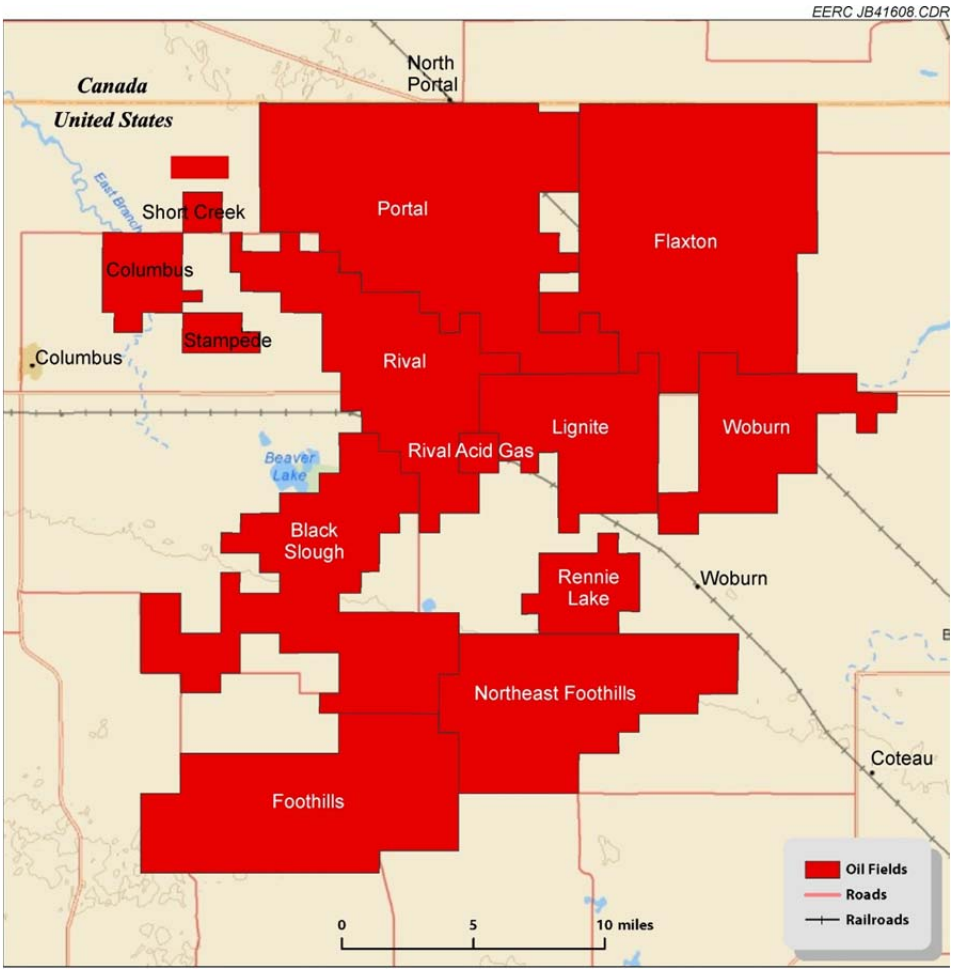

Figure 3. Map of the Rival Field and other nearby oil fields.

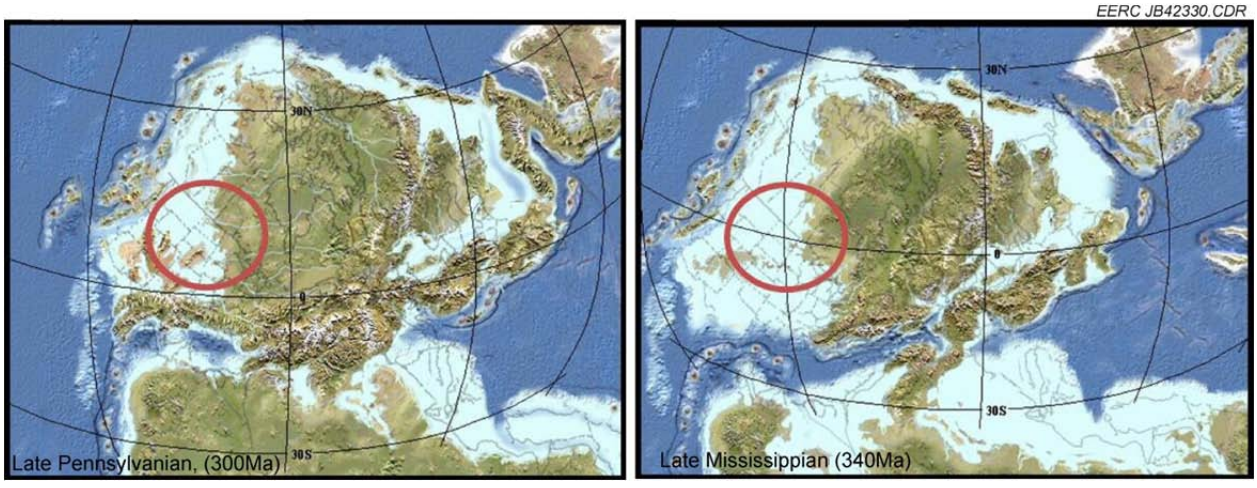

Figure 4. Paleogeographic representation of the depositional environment during the Pennsylvanian and Mississippian periods. The red circles highlight the areas of interest (Cook and Bally, 1975).

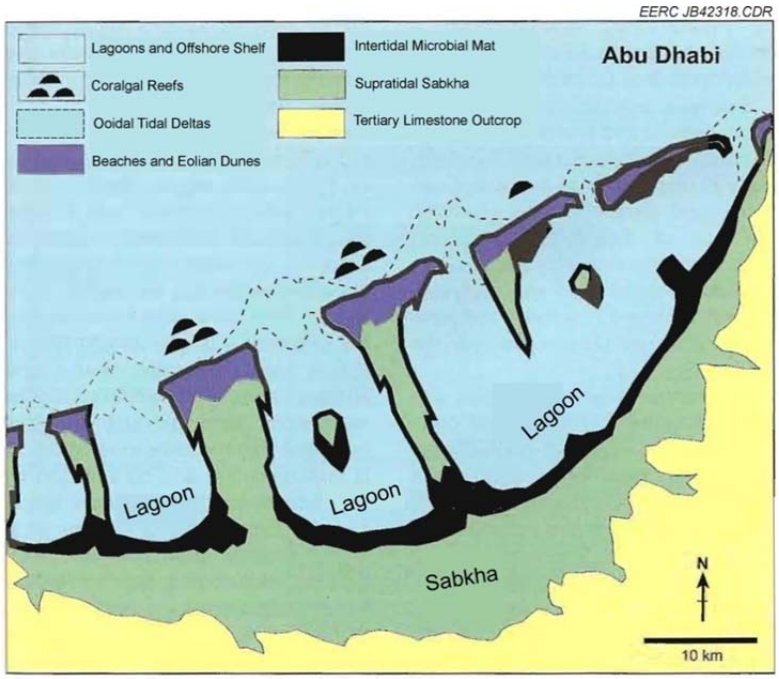

Figure 5. Simplified map of a modern tidal flat environment in the Persian Gulf near Abu Dhabi (James and Dalrymple, 2010).

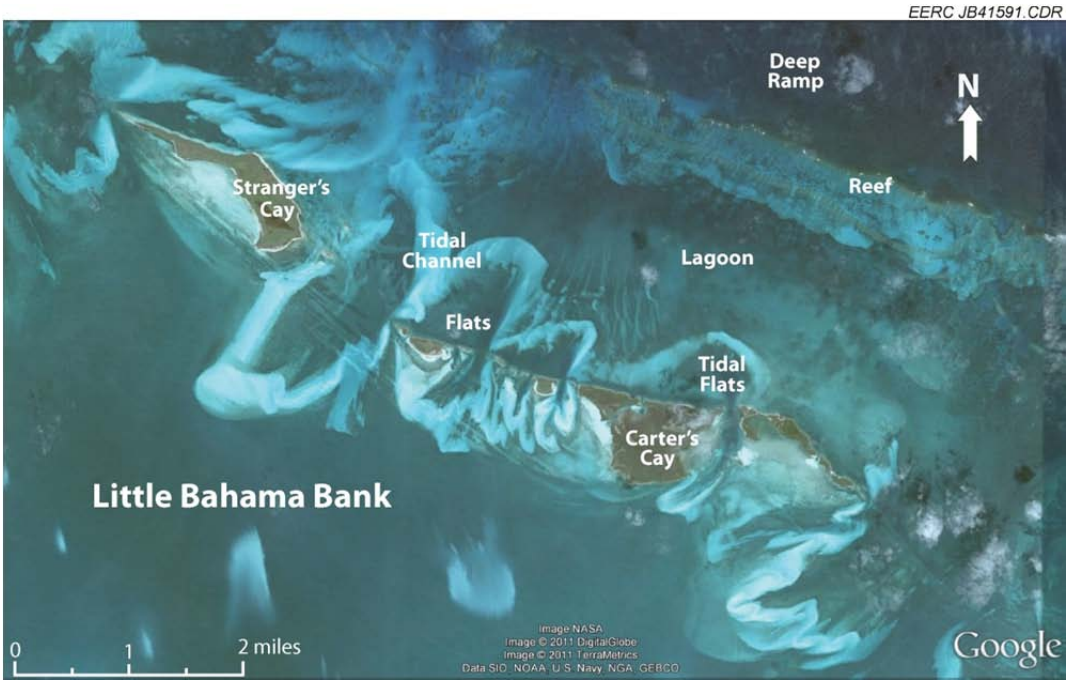

Figure 6. Little Bahama Bank, Caribbean Islands, a present-day analog of a tidal flat depositional environment system (image from Google Earth).

shoals, and deeper carbonate mud and marl (Lindsay, 1988) broken up into four conformable depositional categories: back ramp, shallow ramp, deep ramp, and basin (Figure 7). The backramp can comprise a sabkha further away from shore, with lagoons and tidal flats near shore. The sabkha commonly comprises evaporitic salt that has low permeability as a result of early cementation, development of algal mats, and formation of microcrystalline dolomite and evaporates, resulting in a capping or sealing layer when placed structurally updip of movable hydrocarbons. A similar configuration exists in the Rival Field and provides closure on the oil reservoir as it progresses updip to the northeast into the Lignite and Portal Fields. Additional closure on the reservoir comes from two primary diagenetic processes: sulfate-rich brines flowing through the sediments, heavily cementing the updip inner portion of the reservoir, and dolomitization of porous limestone moving updip into the nearby Lignite and Portal Fields.

The lagoons of the backramp depositional system represent a zone of calm water movement between the shore and the barrier islands. Skeletal lime muds that lithify into micritic muds are the dominant facies. Lagoon deposits can be affected by storm activity, homogenizing sediments and burying interclasts caused by destruction of nearby hardground. Restricted circulation can cause water to become suboxic or anoxic, at times leading to stagnation and evaporation that can raise salinity beyond the tolerance of many living organisms (James and Dalrymple, 2010), thus depositing organic material intermixed with carbonates.

Tidal flats commonly comprise supratidal, intertidal, subtidal, and channel deposits (Figure 8) that usually form reservoirs and seals with predictable cyclical distributions (Shinn, 1983). The supratidal zone is where sabkhas are created as a result of subaerial exposure and

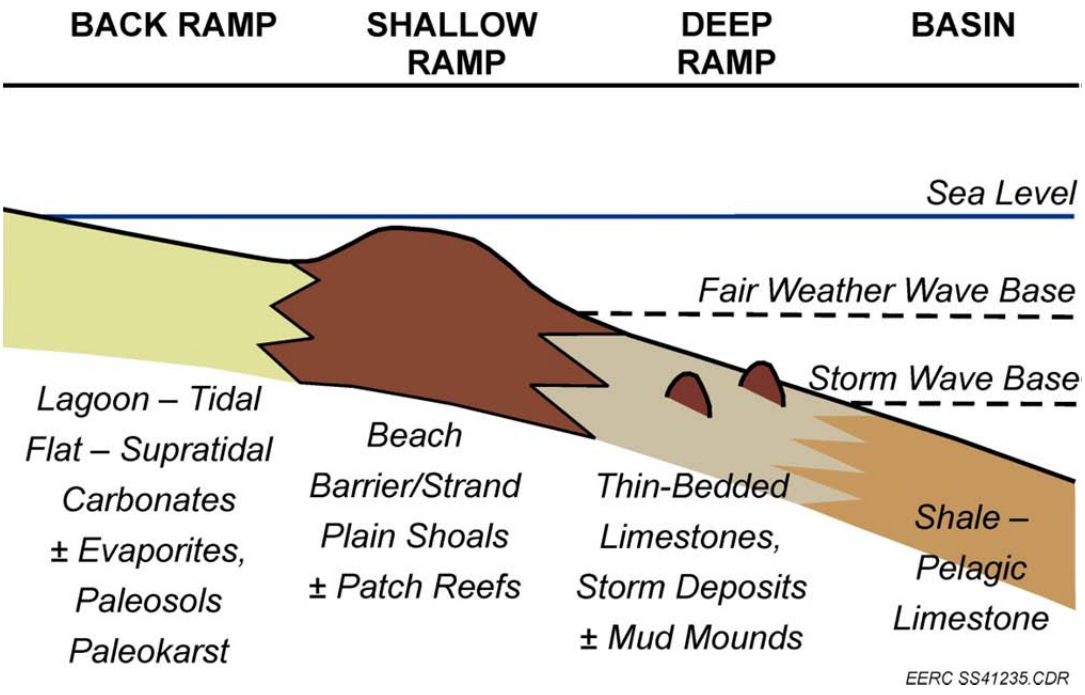

Figure 7. Depositional facies model of a warm-water, near-shore neritic carbonate system or, basically, a tidal flat environment without the sabkha (James and Dalrymple, 2010).

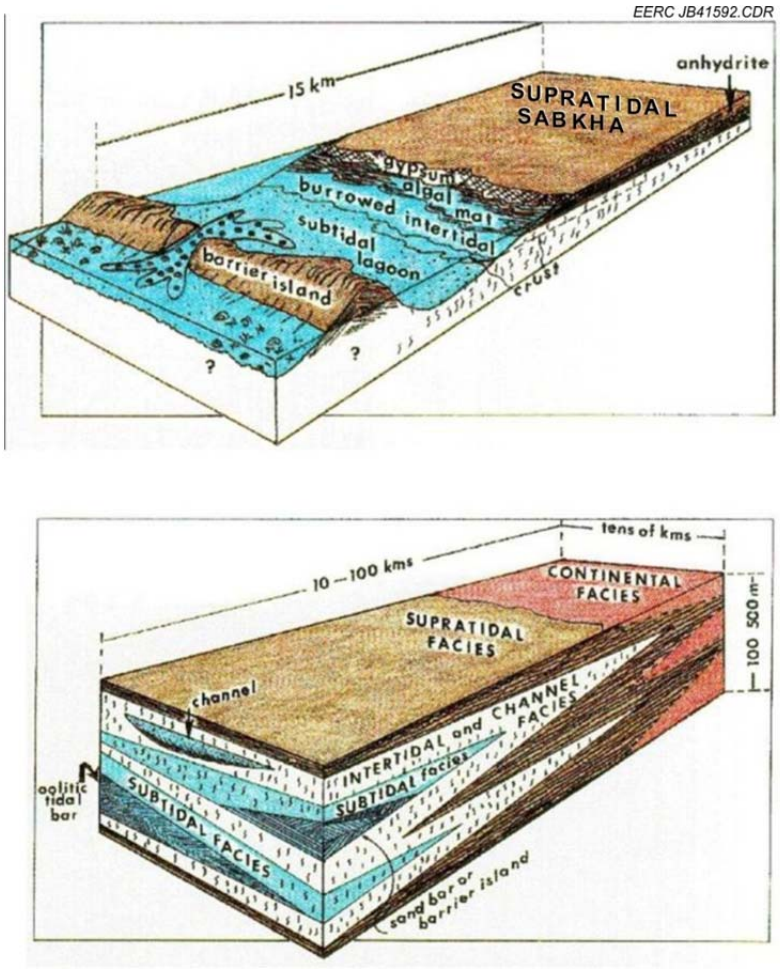

Figure 8. Tidal flat depositional environment with extensive supratidal sabkha (modified from Shinn, 1983).

evaporation of seawater into evaporites by capillary pressure forces. Fine-grained sand and mud can be brought onto the sabkha during storm events only, thus microbial algal mats are the only living organisms present during deposition. Microbial layers can become cemented with micrite, creating crusts or hardgrounds, which are susceptible to desiccation and eventually fragment into clasts. The intertidal zone lies between low- and high-tide levels and is frequently exposed and submerged by tidal swells. The facies are commonly bioturbated and burrowed including thin- to wavy-bedded mudstones and fine-grained grainstones. The subtidal zone is permanently submerged, containing lagoons, shoals, and reefs. The sediments are usually bioturbated and have a significant component of pelleted lime mud except for the nearby shoals and reefs which make up a small fraction of the subtidal zone. Common facies include laminated and thin-bedded mudstones, bioturbated and nonbioturbated mudstones, peloidal grainstones, and skeletal wackestones and packstones.

On the microdepositional level, individual thin laminae prograde or build up sediment as a result of levees and beach ridges being frequently flooded by storm tides carrying little sediment.

These laminations tend to be thinner toward the sea and gradually get thicker progressing toward the sabkha, where they can be destroyed by desiccation. Several living organisms create an ecosystem out of the tidal flat environment, burrowing into the layers of sediment and creating heterogeneity among the laminae. Tidal channels can completely rework intertidal buildups and carry clasts derived from the supratidal sabkha environment into the shallow-ramp and deep-ramp environments.

The shallow ramp primarily comprises high-energy wave-dominated barrier islands or shoals created by deposition of skeletal ooid and oncolith banks, providing excellent intragranular and vuggy porosity and creating the best situation for hydrocarbon accumulation. Coral reefs can also form in this environment but are commonly destroyed by storms. The deep ramp is the transition zone between the barrier islands and the basin. Storm deposits are common in this environment as it is left unprotected by the barrier islands. Thus the deep ramp can be extremely heterogeneous, containing all other types of depositional features seen among the tidal flat environment. The primary facies lacks structure and is commonly marl, a lime-rich mudstone containing copious amounts of clay-sized particles that remain suspended in the water longer and are deposited farther away from shore.

After millions of years, deposition and burial occurred from structural subsidence of the Williston Basin leading to lithification of the carbonate sediments into rock. During lithification, facies deposited in this tidal flat environment were susceptible to several rounds of diagenesis from moving groundwater. Diagenesis can be broken into three separate categories for this carbonate reservoir system: 1) secondary dolomitization caused by magnesium ions replacing calcium ions, 2) salt deposition caused by water flow carrying high concentrations of minerals, and 3) leaching of salt due to lower-than-in situ total dissolved solids (TDS) water flow dissolving minerals and carrying them out of the rock, leaving behind vugs or original intergranular porosity developed during deposition. Oil migration more than likely came from older strata, including the Upper Mississippian Madison Group, Lower Mississippian Basal Lodgepole, and Devonian–Mississippian Bakken Formation.

FIELD HISTORY

The area surrounding the Rival Field is home to several unitized oil fields, including the Portal, Black Slough, and Lignite Fields, all of which produce from the Madison Pool (Figure 3). The Rival Field has been in production since its discovery in the late 1950s and has produced over 16 million barrels (Mbbl) of oil through initial production and waterflood secondary recovery, along with 14.5 billion cubic feet (Bcf) of natural gas (Table 1). Production in the field is from the carbonate Mission Canyon and Charles Formations of the Madison Group, specifically the Midale and Rival Members which are vuggy, shoaly, and marly carbonate beds between two thick salt packages of approximately 30 feet each (Figure 9).

Primary production peaked at almost 5000 bbl oil/day (October 1960), and in the early 1960s, it was expected that production would drop off quickly without implementation of a waterflood for secondary recovery and pressure maintenance. Estimates from the early 1960s

Table 1. Well File History

Date	Activity
7/11/1957	First well in Lignite Field drilled (NDIC [North Dakota Industrial Commission] #1462). Well still in production, having produced 216,000 bbl oil and 728,000 Mcf gas.
9/2/1957	First well in Rival Field drilled (NDIC #1540). Well still in production, having produced 249,000 bbl oil and no gas.
10/3/1957	First well in Portal Field drilled (NDIC #1530); determined dry hole despite oil and gas shows in DST [drillstem test]. Productive well in Portal Field drilled later that month.
3/24/1958	Second discovery well drilled in Rival Field (NDIC #1752), leading to preliminary unitization of Rival North (NDIC #1540) and Rival South (this well). Well still in production, having produced 68,000 bbl oil and 236,000 Mcf gas.
6/15/1958	First well in Black Slough Field drilled (NDIC #1840); determined dry hole despite 180 ft of free oil in DST. Production did not begin until 1961.
7/1958	Rival Field placed on 160-acre spacing. Prior to that, 80-acre spacing used. Former Rival North and Rival South Pools consolidated. Forty completed wells present in the field, and three more being drilled.
4/1962	Poor producers in southwest Rival Field converted to water injection wells. Recognized earlier on that reservoir bubble-point pressure had been lost.
12/1962–2/1984	Injector well in the current Rival acid gas field intermittently used to inject water into Dakota Formation.
7/1963	Field operator Pan American Petroleum Corporation unsuccessfully attempted to merge a large portion of the Black Slough Field with the Rival Field; as many as 69 companies had interest in the field at this time.
1963–1994	Field continued to develop, boundaries extended/redefined, water injection wells permitted. No major activities reported.
1994	Field operator Camwest implemented the beginning of a horizontal reentry drilling program. Only a portion of the planned wells installed.
8/2002	Acid gas injection began in Rival acid gas field adjacent to Rival and Lignite Fields. Approximately 85 bbl/day of acid gas (50% hydrogen sulfide [H_2S], 42% CO_2) is disposed of daily into the Mission Canyon Formation.
2007	Field operator became Primewest, which contracted Hycal to run relative permeability tests on the Midale and Rival Members. More horizontal wells drilled as part of Jim Ehrets' evaluation for Camwest.
2008	TAQA North assumed majority ownership of Rival Field.

had a skeptical outlook on the field, expecting an economical waterflood to extend the life of the field by less than a decade. These early recovery estimates predicted the field would produce less than 10 Mbbl of oil, with production flatlining at 500 bbl/day. Fifty years later (September 2010), cumulative field production is over 16.2 Mbbl; however, the field now produces less than 200 bbl/day. The extended productive field life comes from higher-than-estimated waterflood success as well as better-than-expected reservoir decline (Figures 10 and 11).

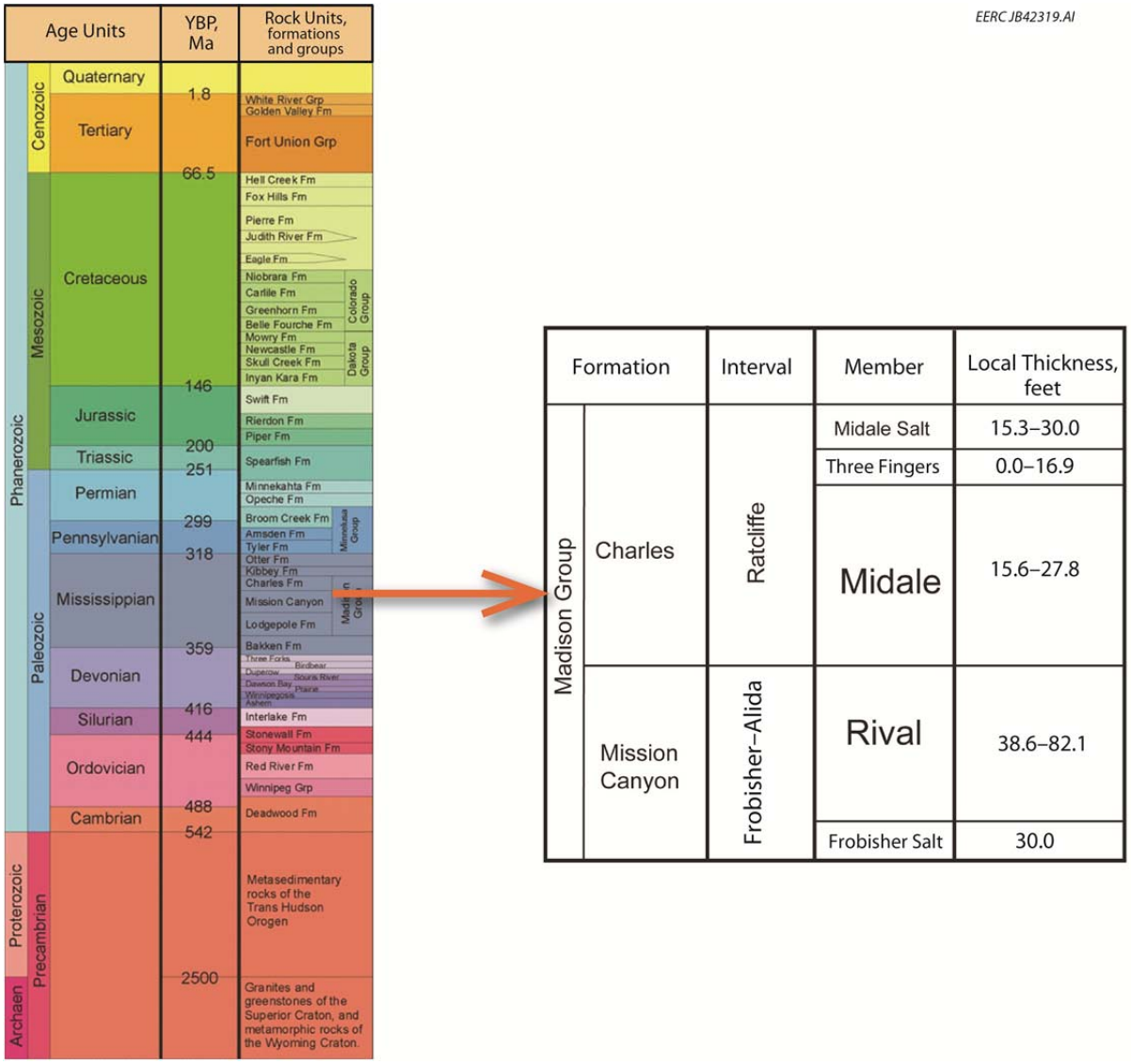

Figure 9. Williston Basin stratigraphy as presented by NDIC (left) and local stratigraphy of the Rival Field derived from literature and associated thicknesses derived from the 3-D geologic model (right).

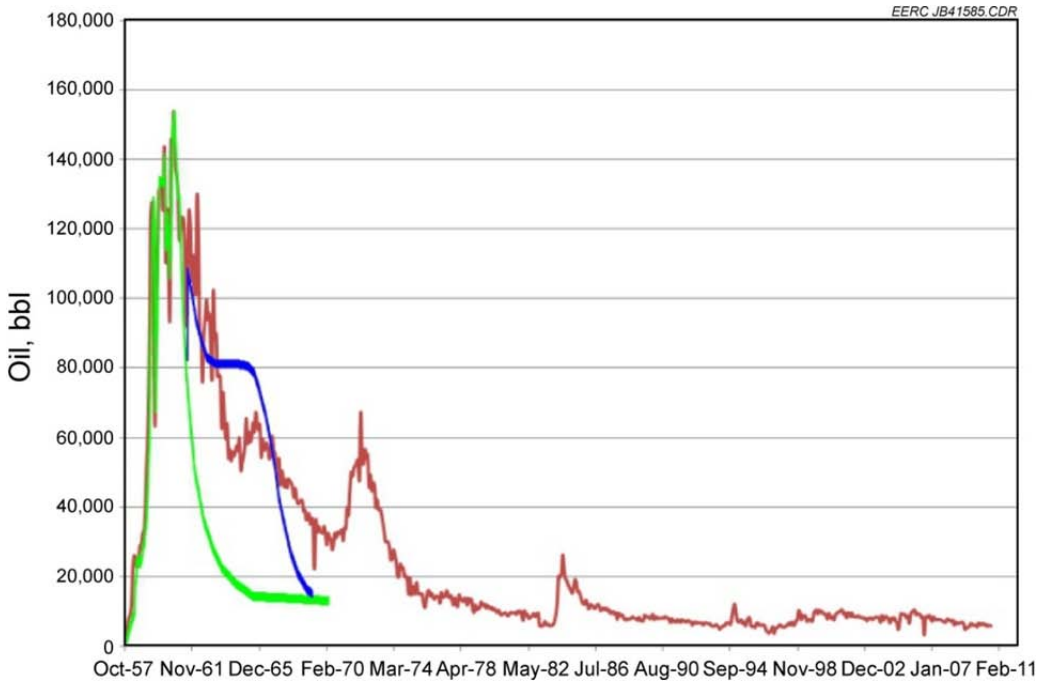

Figure 10. Decline curve to September 2010 (red) with 1957 estimation of initial production (green) and waterflood (blue).

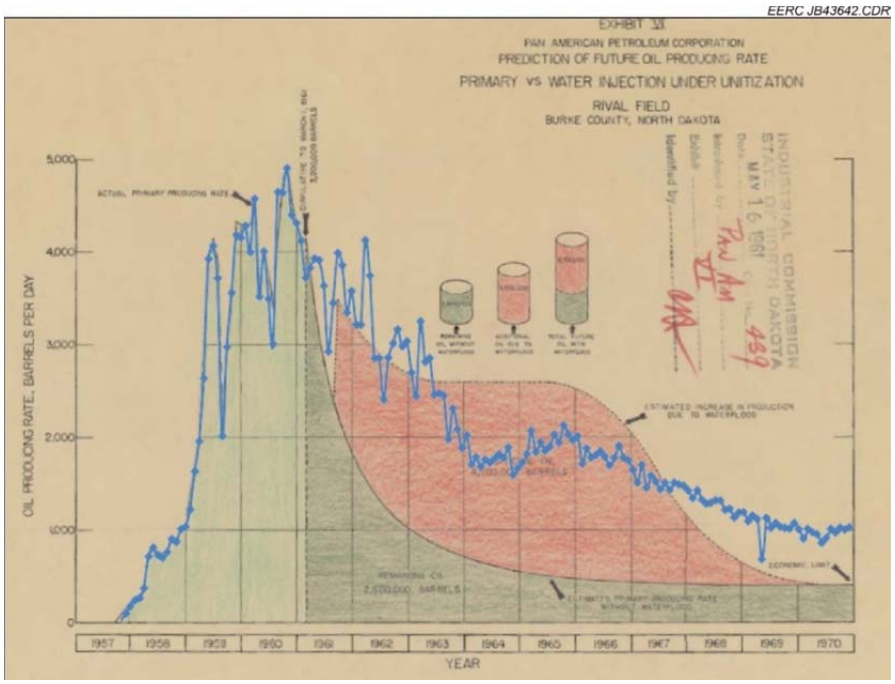

Figure 11. October 1957 – January 1971 production profile estimation under initial production (green) and with waterflood (red) (NDIC #0438) (blue line is actual field production profile through this time period).

PREVIOUS WORK

Rival and Surrounding Fields

Robert Lindsay compiled a report in 1988 targeting 25 oil fields that were productive in the Mission Canyon Formation at the time. Among them was the Rival Field, for which reservoir properties were reported (Table 2). Lindsay explains diagenesis within the Rival subinterval as being destructive to porosity in most cases but notes two cases in which secondary porosity was actually enhanced: partial leaching of primary anhydrite and solution enlargement of pores. These two processes not only lead to greater porosity but also would enhance pore connectivity (Figure 12).

Weyburn–Midale Fields

The Weyburn Field (60 miles to the northwest) is contained beneath a similar anhydrite seal and is productive from the Midale beds, both the vuggy shoal and marly facies from a similar carbonate shelf depositional system in the Williston Basin. These facies are similar to that of the Midale and Rival Members in the Rival Field and thus represent a great opportunity for EOR success.

The Weyburn Field is host to a CO_2 EOR operation in place since September 2000 that is expected to extend the life of the field by 25–30 years, increasing the recovery factor from 35% to 50%. The project was extended in 2005 to also encompass the adjacent Midale Field (Jensen and others, 2008). Thus far, 18 million tons of CO_2 has been stored in the fields out of the expected 40 million tons, and as of 2010, incremental oil recovery (IOR) estimates for the Weyburn and Midale Fields have totaled more than 215 Mbbl (Carbon Capture Journal, 2010).

Table 2. Rival Field Reservoir Properties (from Lindsay, 1988)

Representative Fields:	Rival, North and South Black Slough, and Foothills Fields
Reservoir Depth	6000 to 6900 ft (1800 to 2100 m)
Reservoir Thickness	Variable
Porosity	6% to 12%, average = 8%
Permeability	1 to 10 mD, average = 3.4 mD
Aerial Extent, acres	12,000 (Rival), 6400 (North Black Slough), 6713 (South Black Slough), and 5280 (Foothills)
Saturation, Sw	30% to 40%
Gravity, API (American Petroleum Institute)	37.6 to 39.1°, average 38.3°
Oil in Place, Mbbl	41.7 (Rival), 24.9 (North Black Slough), 15.3 (South Black Slough), and 19.9 (Foothills)
Ultimate Recovery	Not available
Cumulative Production, Mbbl	12.9 (Rival), 3.6 (North Black Slough), 2.6 (South Black Slough), 2.2 (Foothills) (mid-1982)

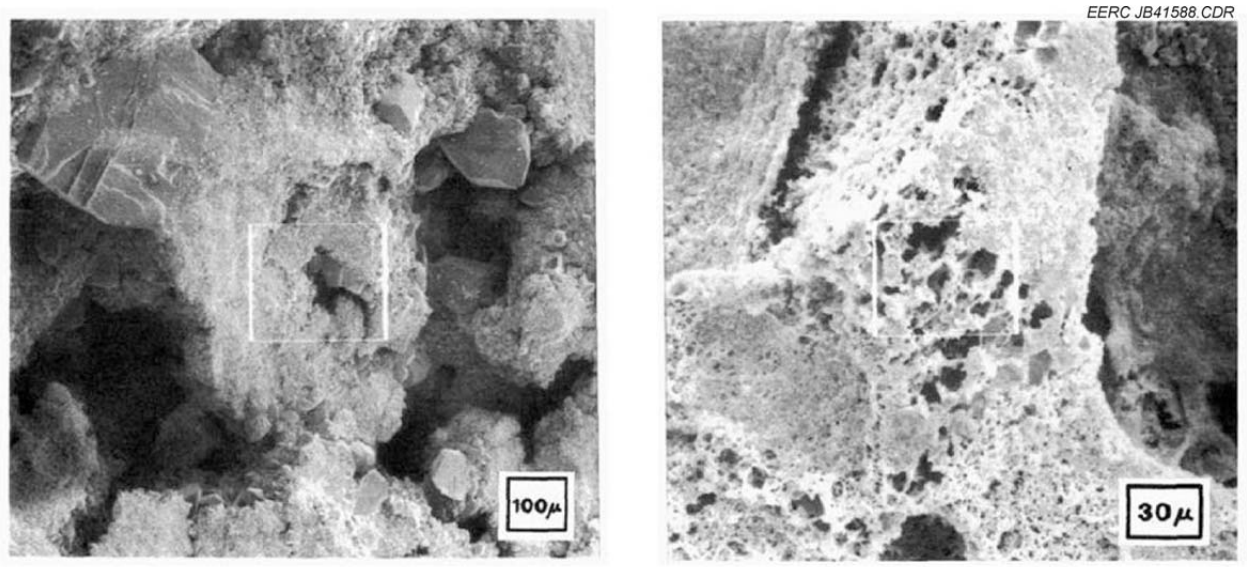

Figure 12. Scanning electron micrographs of the porous, productive Rival Member at a depth of 6180 ft. View of secondary moldic pores after anhydrite has been leached from them (left). A large unleached piece of anhydrite is still present in the upper left. Some calcite crystals have partially infilled some porosity. Calcite crystals growing into the pore system, resembling "swiss cheese," drastically reducing permeability and creating heterogeneity within the pore system (right). This phenomenon is one reason why waterflood operations in the Rival Field are not successful (Lindsay, 1988).

METHODS AND ANALYSIS

Current Core Analysis

Additional core analysis was performed to complement the historic core analysis performed by various personnel over the past 50 years. Previous to this study, petrographic analysis had not been accomplished on any available core. Several mud and facies logs exist for wells, but no descriptions of actual core were found. Thus seven of the 19 cores available at the Wilson M. Laird Core and Sample Library at the University of North Dakota were logged for geologic features (Table 3). Five wells were logged based on photos that were downloaded, cropped, and referenced using a track of feet and inches. Two wells, 16409 and 13700, were logged at the Core and Sample Library, followed by thin-section sampling.

Thin-section analysis was completed on Wells 16409 and 13700. Twenty-eight samples were collected from the Core and Sample Library which were prepared and analyzed by the Applied Geology Laboratory (AGL) at the Energy & Environmental Research Center (EERC) as part of this project (Appendix A). Petrographic analysis for each thin section included a description of the following: petrophysical class (Lucia, 2007), depositional environment (James and Dalrymple, 2010), and macro- and microfacies (Folk, 1959; Dunham, 1962). The descriptions were added to the project database, and attempts were made to extrapolate the thin-

Table 3. Geologic Features Noted During Core Photo Viewing

Facies	Sedimentary	Structural
Dolomite	Bird's-eye vugs	Fractures associated with chickenwire anhydrite
Limestone	Algal mats	Interclasts
Anhydrite	Ooids, peloids, and oncoids	Fining upward sequences
Shaley Marl	Burrows	Fining downward sequences
Packstone	Laminations	Shale lenses capping top of tidal flat cycle
Wackestone	Vuggy porosity	
Grainstone	Fenestral fabric	
Marl	Styolites	

section analysis to the remainder of the study area. The geophysical well data did not match well to either petrophysical class or macro- and microfacies. Thus rock fabric numbers were not computed from petrophysical class, and macro- and microfacies models were not built. However, the depositional environment descriptions did match the geophysical well data with regard to extrapolating two wells over a 100-square-mile area. This resulted in a depositional facies model (Appendix B).

Following initial thin-section analysis, five plug samples were acquired from Well 16409, with the goal of collecting pertinent sample properties (Table 4). Four horizontal plugs and one vertical plug (Figure 13) were cut from the two-thirds of the remaining original core. The vertical plug was cut from the shaley marl lithology along with a horizontal plug to help in analyzing the ratio of vertical to horizontal permeability in this potential flow barrier. Baseline mineralogy was obtained for the five core plugs using x-ray diffraction (XRD) analysis. The results are shown in Table 5. Correlation efforts were aimed at comparing property-to-property and property-to-facies relationships on highly characterized plugs. Procedures and results can be found in Appendix A.

Macrofacies

The Midale and Rival Members largely fall into two scenarios (Figures 14 and 15) identified from core descriptions and thin-section analysis: 1) micritic, fossiliferous, sometimes argillaceous mudstones that have experienced variable (sparry) dolomite recrystallization and 2) porous ooid/pellet grainstone banks partially cemented with sparry dolomite cement. These

Table 4. AGL Tests and Associated Parameters for All Five Core Plugs from Well 16409

Test	Gas Pycnometer	Permeameter	XRD	Petrographic Analysis
Parameters	Bulk density	Vertical permeability	Bulk mineralogy	Estimation of mineral/ carbonate grain assemblages
	Grain density	Horizontal permeability		Depositional facies
	Porosity	Maximum permeability		Petrophysical class

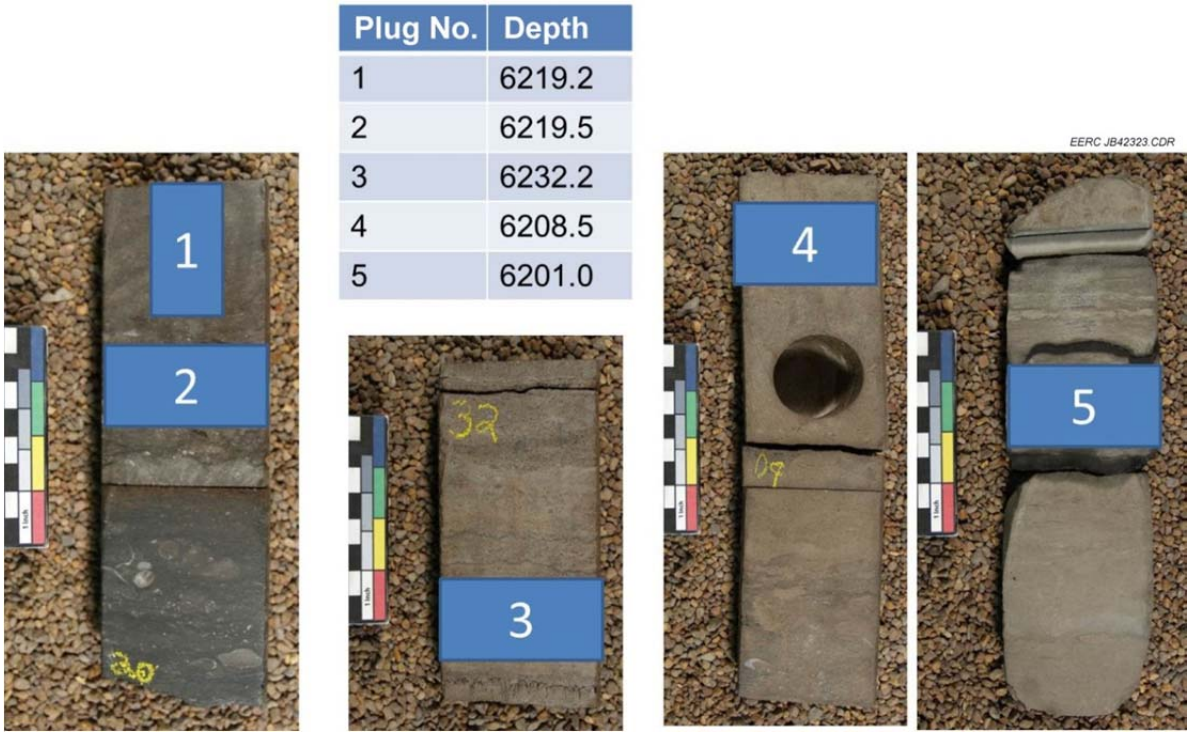

Figure 13. Schematic showing orientation of the five core plugs taken in the remaining two-thirds of the core from Well 16409.

fabrics are consistent with a standard warm-water neritic carbonate ramp experiencing fluctuating water depth.

Although two separate macrofacies are present in the Midale Member, their respective lithological properties are homogeneous when crossplotting core porosity vs. core permeability in type Well 16409 (Figure 16), suggesting that a degree of similarity exists within the porous networks between the facies. Heterogeneity found within the Midale Member is primarily associated with rock fabric and diagenesis, specifically dolomitization and secondary salt deposition and leaching. Secondary salt deposition occurs from high-TDS water flowing through the formation, filling voids and fractures with minerals that aid in salt accumulation. If water with TDS lower than in situ fluids flows through the formation, leaching may occur, in which the water dissolves the salt out of the voids and fractures and into the water. There have been many iterations of mineral deposition and leaching affecting definition of flow zones and overall reservoir performance.

The Rival Member comprises limestone containing vuggy and intragranular porosity, also affected by diagenesis. Heterogeneity is common throughout the pore network as calcite crystals grow into pore throats, causing an overall reduction in porosity and permeability. However, the mineral growth may be leached at later stages, creating localized patches of high permeability and effective porosity.

Table 5. XRD Results from Five Samples Derived from Core Plugs of Well 16409

AGL No.	Depth, ft	GoF[1]	Rwp[2]	Qtz[3]	Plag[4]	KFd[5]	Pyr[6]	Dol[7]	Cal[8]	Anh[9]	Gyp[10]	Kaol[11]	Ill[12]	Hem[13]	Mag[14]	Amr[15]
S-00696	6219.2	1.30	20.26	4.39	–	–	0.310	5.24	67.07	–	1.68	–	–	–	–	2.13
S-00697	6219.5	1.24	19.07	3.88	–	–	0.290	12.10	56.86	0.90	2.43	0.25	1.49	0.20	0.20	21.3
S-00698	6232.5	1.24	20.26	1.55	–	–	–	–	83.89	–	2.54	–	–	–	–	12.0
S-00699	6208.5	1.29	20.19	2.489	–	–	0.816	36.88	46.36	1.13	2.45	–	1.36	–	–	7.52
S-00700	6201.0	1.49	23.05	9.128	1.43	5.03	1.626	59.49	21.749	–	–	–	–	–	–	1.55

[1] Goodness of fit.
[2] Residual with peaks.
[3] Quartz.
[4] Plagioclase.
[5] Potassium feldspar.
[6] Pyrite.
[7] Dolomite.
[8] Calcite.
[9] Anhydrite.
[10] Gypsum.
[11] Kaolinite.
[12] lllite.
[13] Hematite.
[14] Magnetite.
[15] Amorphous.

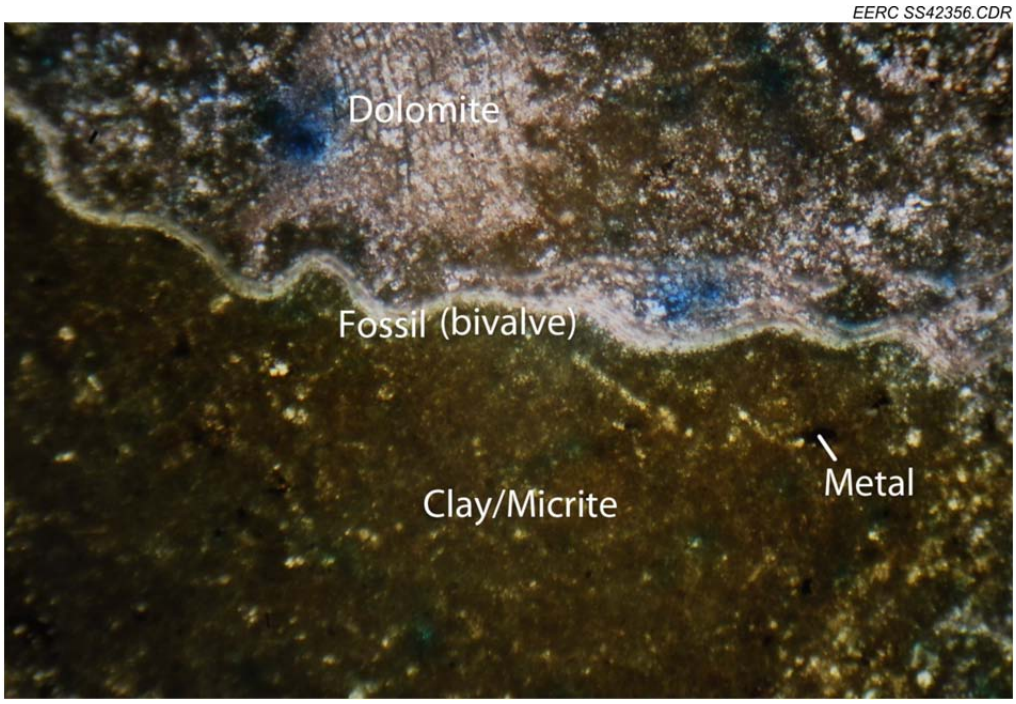

Figure 14. Type thin section representing tight mudstone (nonreservoir rock) – Well 16409, 6216 ft, 40× magnification, plane-polarized light.

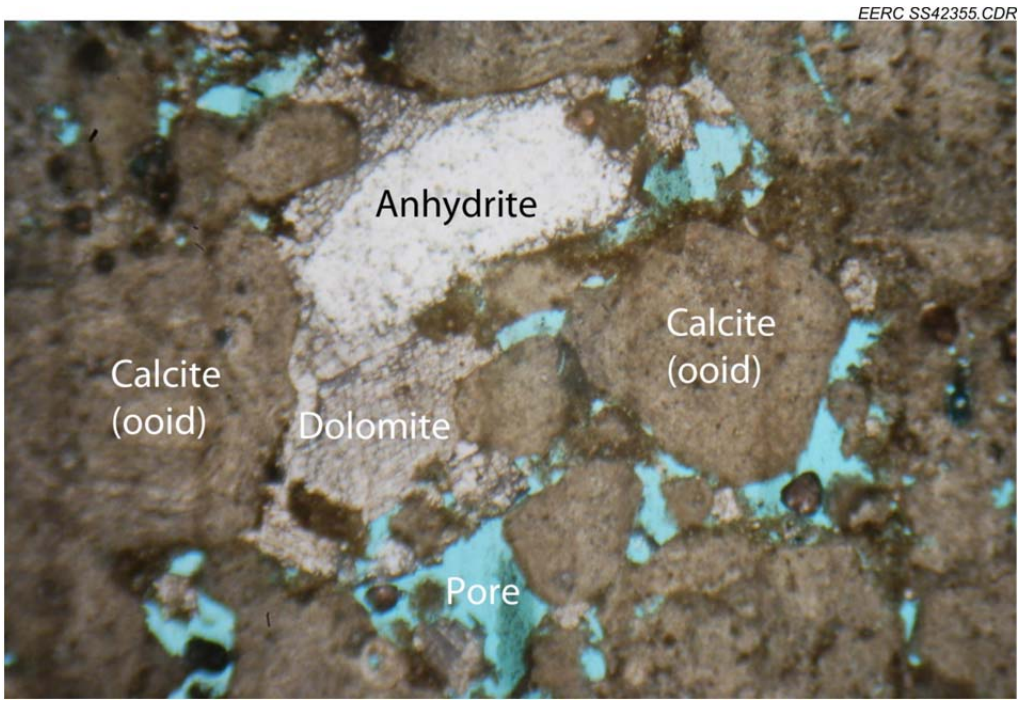

Figure 15. Type thin section representing porous grainstone (reservoir rock) – Well 13700, 6129 ft, 40× magnification, plane-polarized light.

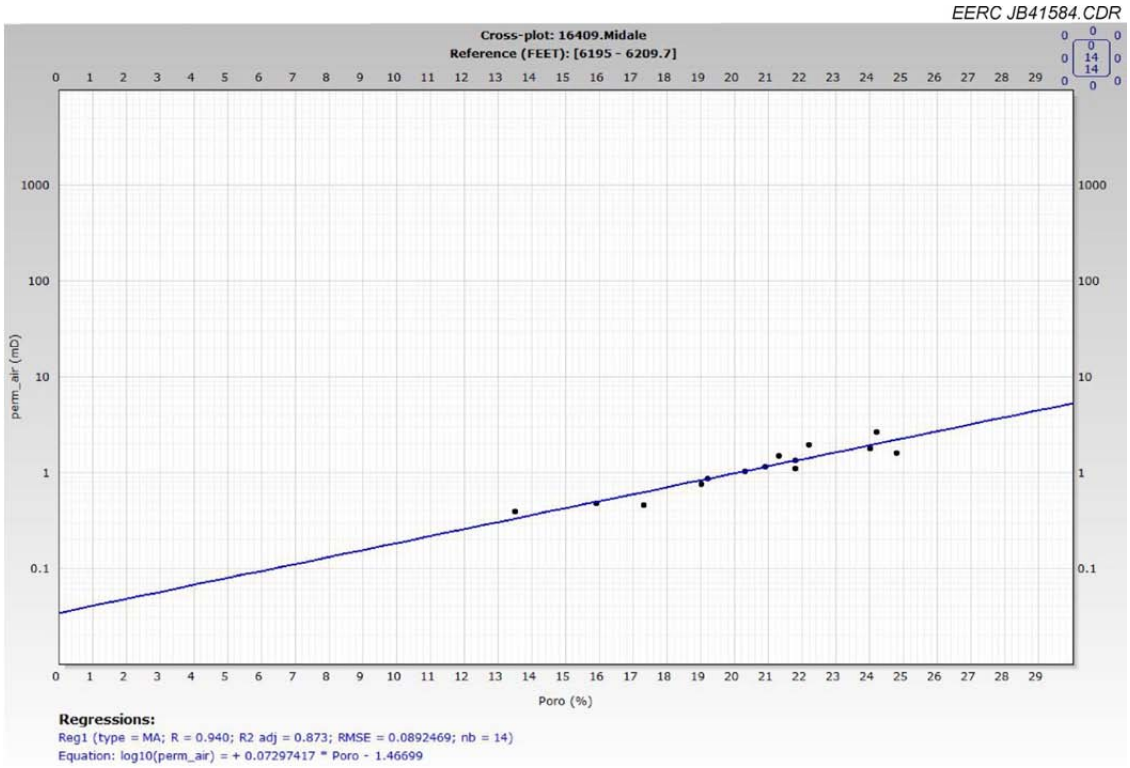

Figure 16. Techlog crossplot of core porosity vs. core permeability for type Well 16409 (R-squared value of 0.873).

Microfacies

The Rival Field is first differentiated into grainstone and peloidal packstone banks, which preserve a majority of the porosity and argillaceous carbonate mudstones, with virtually no porosity. Diagenesis of the reservoir is marked by fine- to coarse-grained secondary dolomite recrystallization (Appendix A). Additional microfacies were identified through thin-section analysis of Rival Field core, which are defined by a combination of carbonate classification according to Dunham (1962), lithologic fabric, interpreted depositional environment, and microstructure (Figure 17). Overall, analysis concluded that:

- Observed rocks represent a variety of depositional environments but may be grouped into carbonate grainstone banks (reservoir rock) and argillaceous carbonate mudstones (nonreservoir rock).

- Observed facies, fossil assemblages, and microstructures are consistent with a warm-water neritic carbonate ramp environment.

- A fair degree of secondary dolomite recrystallization has occurred throughout the interval.

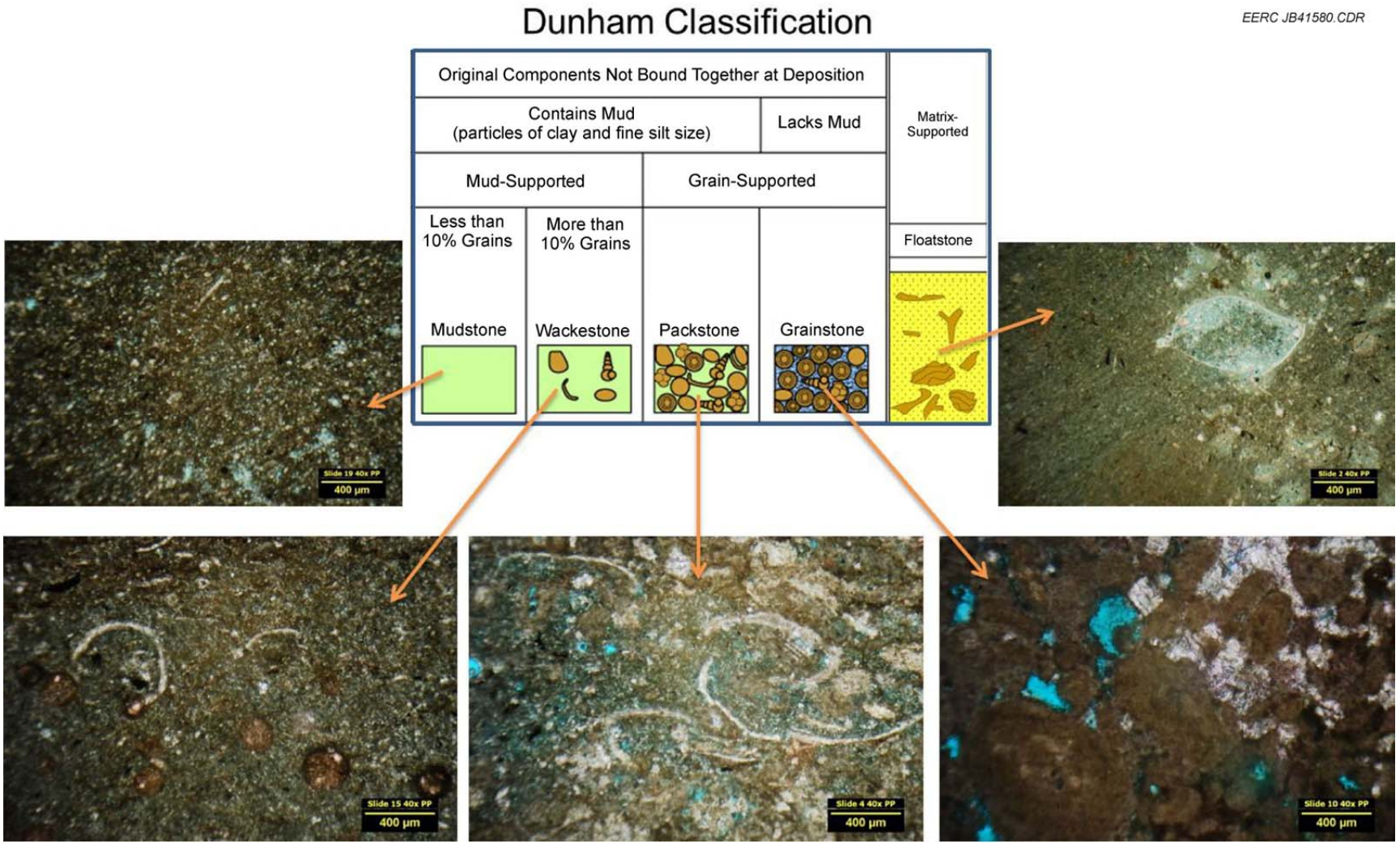

Figure 17. Dunham classification as applied to thin sections from the Rival Field. All sections shown are 40× magnification and viewed in plane-polarized light.

- Porosity in the Rival Field is present within carbonate grainstone banks that are loosely cemented by sparry dolomite.

Data Management

Two databases were utilized during the characterization process. A PETRA® database held the wells and all associated information, but it lacks the precision of spatial analysis found in ESRI's ArcGIS, so a geodatabase was also created to mirror PETRA. Having two similar databases allowed for easier quality control as new data were added to the project and permitted easier import and export operations from Petrel (Schlumberger's 3-D modeling software) and Techlog© (Schlumberger's petrophysical interpretation software).

A 100-square-mile study area was selected based on previously built models, publicly available well data (NDIC Department of Mineral Resources Oil and Gas Division), and previous geologic interpretation (Figure 18 and Table 6). Additional data were gleaned from previously published literature. The database of wells includes spud dates from 1957 to 2007. This range results in a variety of logging techniques and tools to be used. The data had to be separated based on logging tools utilized in order to correct for borehole error and uncertainty within the normalization process. 300 wells are within the current study area, with an additional 12 outside, which were included as an attempt to minimize uncertainty among the edges. 105 wells are in the Rival Field comprising roughly 160-acre spacing. Some infill horizontal producers and additional water injectors have been spudded at closer spacing arrangements. The closest water injector and producer pair are 540 feet apart.

Data for 80 wells included core analysis (Figure 19) with at least the following values: porosity, maximum permeability, water saturation, and oil saturation (Figure 20). Additional values for a few core analysis results included horizontal and vertical permeability, grain density, and bulk density. All calculated petrophysical data were correlated in some way to core analysis data by either petrophysical processing, crossplotting, or modeling workflows.

Well Data Normalization

Several normalization techniques were taken into consideration to account for the spread of spud dates among wells, attempting to eliminate systematic errors and inaccuracies from wireline log curves. Core-to-wireline log calibration took place on the order of shifting the core analysis up to 5 feet in measured depth to match the corresponding wireline log values. No interpolation or splining of data was done at this time. Core data analysis was both in whole core data and core plug format.

The gamma ray wireline log was normalized by a basic scale change. This process was completed in two ways. First, the highest gamma reading in the interval of interest is 66 gAPI (API gamma ray units). Thus a new scale of 0–66 gAPI was applied to all wells. Most vintage wells from the 1950s and 1960s have poor gamma ray logs with readings of 0–10 gAPI. These wells were subject to standardization or statistical normalization, where the low gAPI readings were transformed to the larger scale of 0–66 gAPI using a quantile method and a similar set of

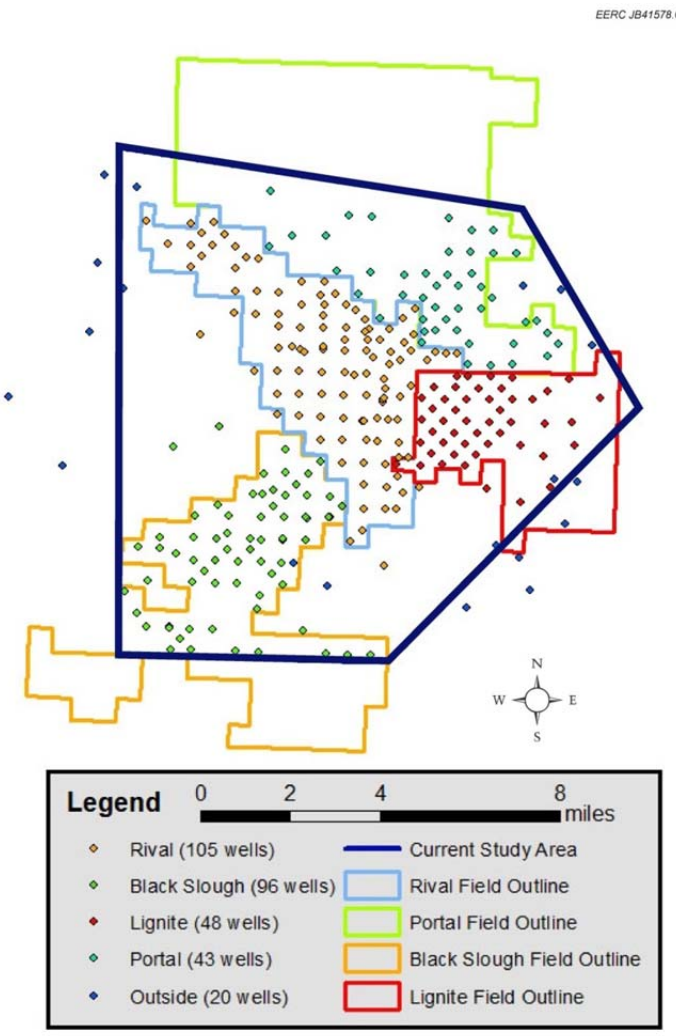

Figure 18. Map showing 312 total well locations. Current study area is dark blue, encompassing 100 square miles.

Table 6. Wireline Geophysical Logs Available for the 312 Wells

Geophysical Log	Abbreviation	Total Count from 312 Wells
Gamma Ray	GR	297
Compressional Travel Time	DT	225
Neutron Porosity	NPHI	101
Density Porosity	DPHI	19
Sonic Porosity	SPHI	150
Neutron Gamma Porosity	NEUT	45
Resistivity	RT	192
Bulk Density	RHOB	19
Photoelectric Factor	PEF	10

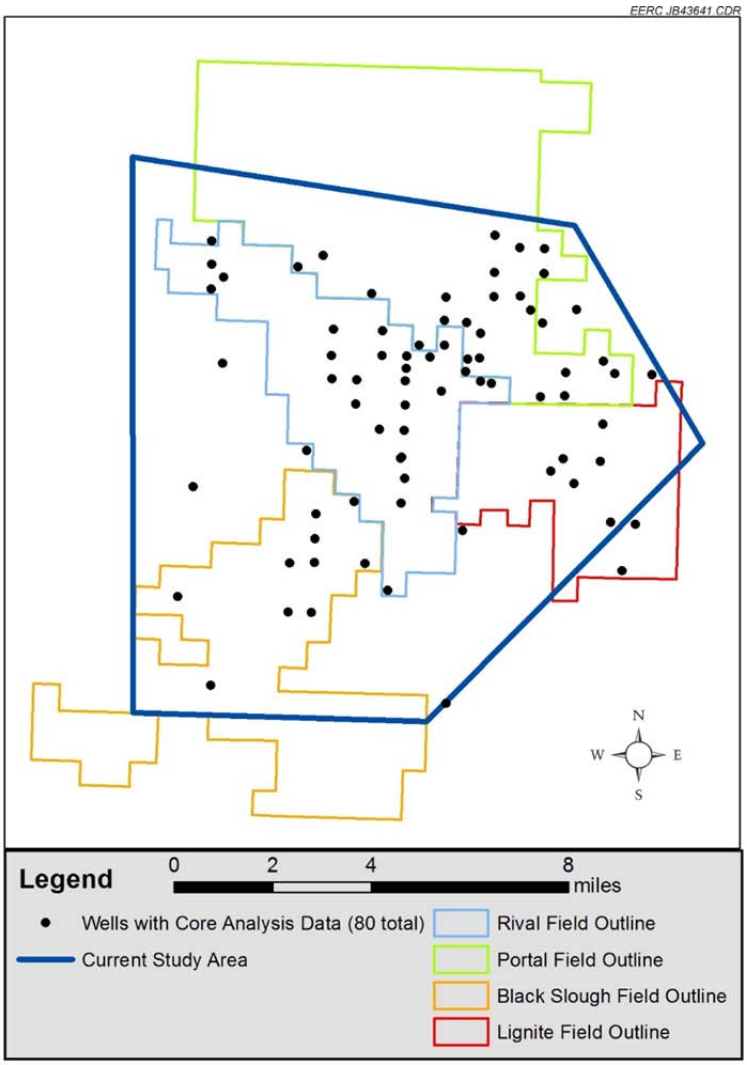

Figure 19. Map showing 80 well locations with core analysis data.

standard deviations found in the newer wells. This normalization technique assumes that the rocks are similar across the entire field. Without using this method, the gamma ray curves for the older wells would be considered useless.

A type well method was used to pick zones from wireline logs based on high-, mid-, and low-porosity values. Interpretation was added by gamma ray, density, and other pertinent logs. The original type well is 16409 (Figure 21). Well 16409 was selected as it had the best overall wireline log and core analysis suite. Well 16409 was spudded in 2006 as a primary water injector. Whole core was obtained for the interval of interest during drilling, and this core was targeted as part of this project to obtain new thin-section and core plug analysis. After 12 zones were selected in the type well, zone correlation continued across the entire well suite, with mixed degrees of success. Well log signatures were not as robust as the type well, leaving a sense of

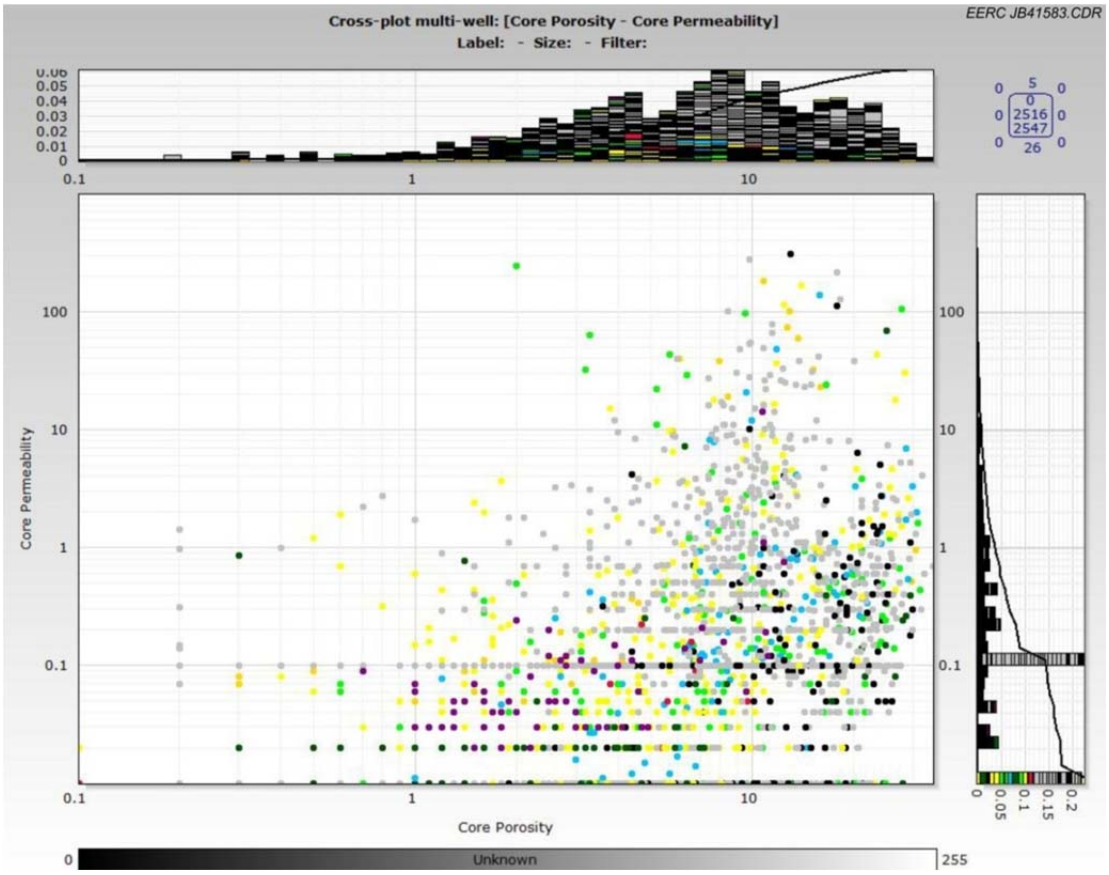

Figure 20. Techlog crossplot of core porosity vs. core permeability of the 80 wells, with 2547 total individual samples of core analysis data for the interval of interest.

uncertainty, especially when moving outside of the Rival Field. Since wells are placed at 160-acre spacing, there tends to be minimal change in geology between wells. The type well method works well in settings where there is little distance or geologic change between the wells in the data set (Shier, 2004).

Trend analysis regional normalization was used to confirm picked stratigraphic zones. This method is also called trial normalization, acting as a check and balance for the type well method used earlier. The workflow for trend analysis involves creating a single-layered 3-D model of the zone of interest, upscaled with the wireline log of choice, followed by kriging to determine outliers or unreasonable trends. Since kriging is an averaging algorithm, data that represent a large standard deviation are often seen as bull's eyes in the surface, upon selecting the appropriate contour scale factor. The outlier data are then corrected or thrown out depending on the reliability of the original data and ability to be normalized. If logs were suspect of poor logging standards, logging tool miscalibration, or operator negligence, they were most often dropped from the modeling database.

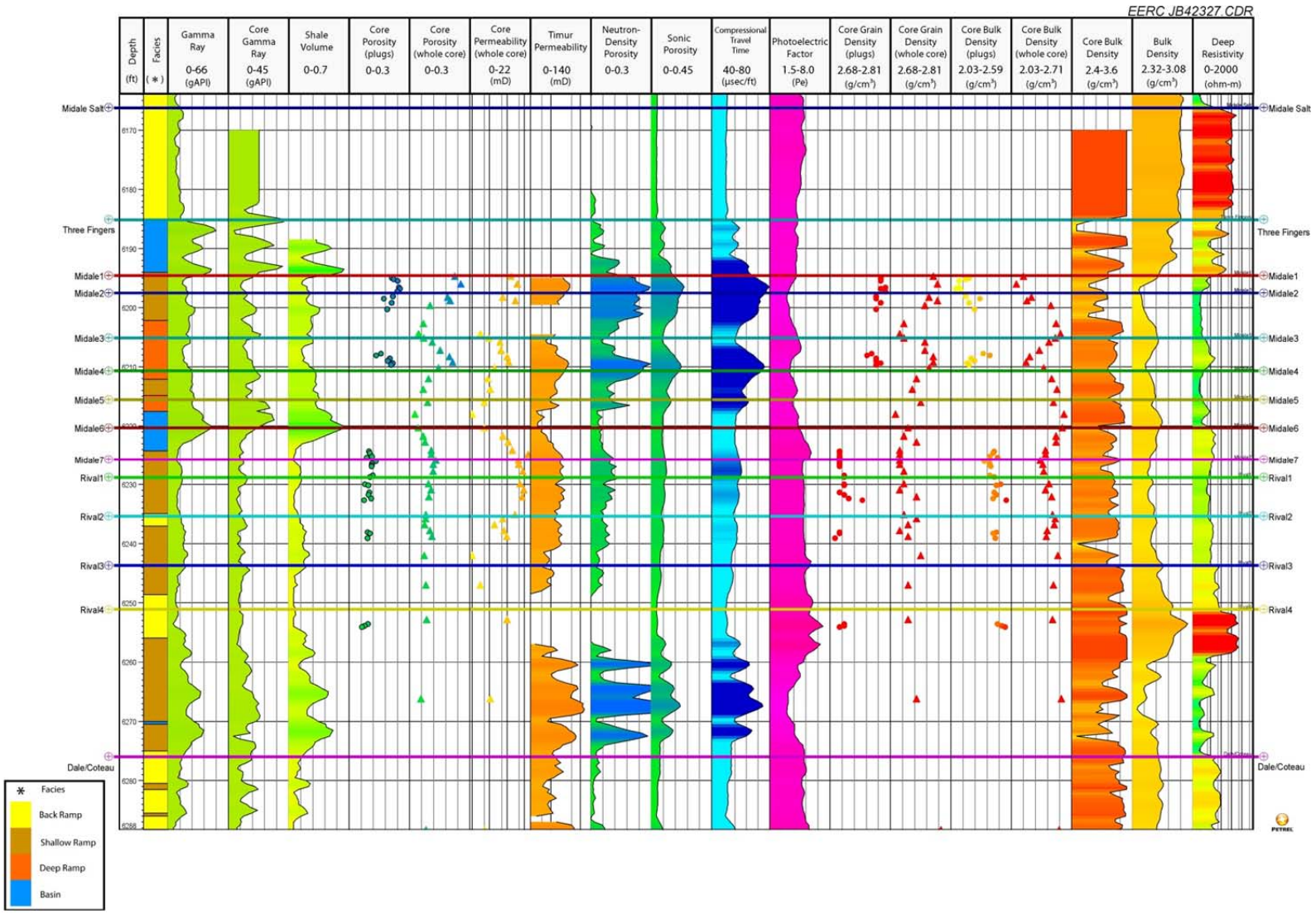

Figure 21. Type Well 16409, with 13 layers picked correlating to 12 zones.

With over 300 wells in the study area, it was appropriate to be robust in determining the best logs available for the model. After well log normalization, petrophysical analysis was performed on all available well logs. Many wells lacked reliable curves, values, or data. Wells that did not have gamma ray were excluded unless there were other sufficient curves, acoustic, neutron, or density, to allow for correlation. Three wells were dropped as they only had core analysis data and no complementing well logs, leaving 77 wells with core analysis to be used in the 3-D model. 140 wells with quality log suites passed the normalization and petrophysical analysis workflows (Figure 22).

Petrophysical Interpretation

The goal for petrophysical interpretation was to calculate basic reservoir properties based on well log curves, core analysis, and other variables using industry standard equations. A combination of Microsoft Excel, Python™, Techlog, and Petrel were all used in the workflow. Core analysis data were correlated to calculated values using crossplots, boxplots, and histograms. A glossary of equations and variables used during petrophysical interpretation are included in Appendix B. Calculated curves include total porosity, shale volume, effective porosity, permeability, water saturation, and net-to-gross (porosity).

Stratigraphic Framework

The Midale and Rival Members are formal subdivisions of formations within the massive Madison Group (Figure 23). Locally, the Midale Member represents the bottom of the Charles Formation (Lower Ratcliffe Interval), and the Rival Member represents the upper Mission Canyon Formation (Upper Frobisher–Alida Interval). The Rival Member denotes a transgressive event ending the upward shoaling of the Mission Canyon deposition and transferring into the regressive events leading to the deposition of the Midale and further deposition of the widespread Charles Formation salts.

Over 900 stratigraphic tops were picked for 275 wells representing 13 horizons during the normalization workflow. Of the 13 picked units, there are five prominent tops: “Midale Salt,” “Three Fingers,” “Midale,” “Rival,” and “Frobisher Salt.” These tops became the basis of five zones that were input into the structural model. The Midale salt is an extensive sabkha sequence locally represented by 30 feet of continuous evaporites. The Three Fingers unit is represented by three spikes on the gamma ray log, also described in previous literature as “a dense laminated and anhydritic dolomicrite zone” and considered 100% saturated with water (Laird, 1960). Both the Midale salt and Three Fingers represent the updip reservoir sealing formations. The Midale Member is highly argillaceous, as noted by the gamma ray wireline log. The higher-porosity zones within the Midale appear to be in the less argillaceous zones. There are two prominent high-porosity flow zones in the Midale represented primarily by grainstone ooid banks, each separated on the top and bottom by low- to midporosity and much lower permeability because of clay and micritic mud content. The Rival Member has an extremely low gamma ray signature, as its lithology is primarily limestone. Rival Member porosity and permeability are represented mainly by vugs that exist in the continuous shallow and back ramp depositional facies. These vugs have undergone several iterations of diagenesis, both infilling and leaching. This limestone

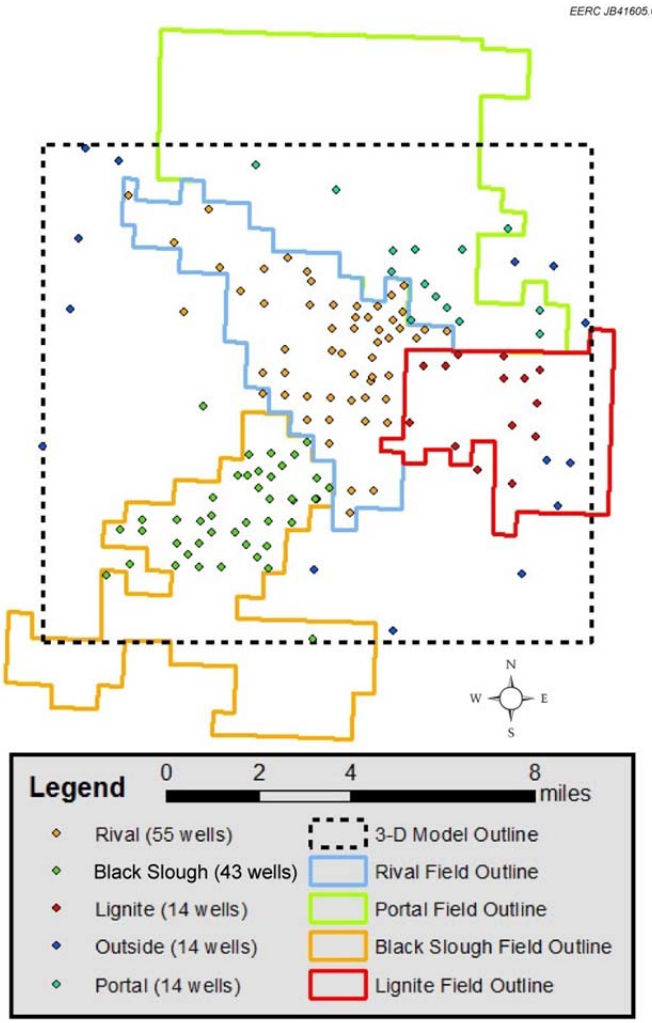

Figure 22. Map of the 140 wells that passed the normalization and petrophysical phases and were used to populate the 3-D geologic model.

interval thickens while migrating toward the southwest, unlike the Midale which gets thinner (Figure 24).

The five prominent zones were correlated across all of the 140 wells containing quality log suites. The minimum curvature algorithm was used to interpolate each surface. These surfaces were checked with isochore points to address any negative or zero values. Upon correction, the surfaces were input into a 3-D model, ultimately representing the structural model, since there are no faults included in this iteration. Layers were introduced into the model to better represent potential flow zones as seen in the 13 correlated zones of the normalization workflow.

EERC JB41589.CDR

Formation		Interval	Member	Zone	Zone Thickness, feet
Madison Group	Charles	Ratcliffe	Midale Salt	Top Seal – Midale Salt Zone	15.3–30.0
			Three Fingers	Top Seal – Three Fingers Zone	0.0–16.9
			Midale	Midale Zone (4 layers)	15.6–27.8
	Mission Canyon	Frobisher–Alida	Rival	Rival Zone (8 layers)	38.6–82.1
			Frobisher Salt	Bottom Seal – Frobisher Salt Zone	30.0

Figure 23. Local stratigraphy of the Midale and Rival Members.

3-D GEOLOGIC MODEL

Structure

Five zones were correlated across 140 wells in the Rival and surrounding fields: “Midale Salt,” “Three Fingers,” “Midale,” “Rival,” and “Frobisher Salt.” The base of the Frobisher salt was not picked; it was, instead, assigned an arbitrary thickness of 30 ft for modeling purposes.

Layers were created to add definition to the five zones: four layers in the Midale with a minimum thickness of 5 ft and eight layers in the Rival with a minimum of 5 ft. The 5-ft minimum is assumed as there are no major flow zone changes that occur in a 5-ft interval for either member.

Optimal grid cell size for the geologic model was determined to be 100 ft × 100 ft. The closest two injector wells are 147 ft apart, while the closest producers are 168 ft in the model. The closest injector and producer are 540 ft apart, meaning there are a minimum of four cells between an injector–producer pair.

Structural noses representing shallow-dipping anticlines seen in the Rival Field have some implication on production (Figure 25). The wells located on top of the structural noses produce significantly better than off of the nose. This increase in production can result from several factors, including the following: fractures can significantly increase permeability; a thicker oil column may be present on the structure; and biological preferences may have taken place during

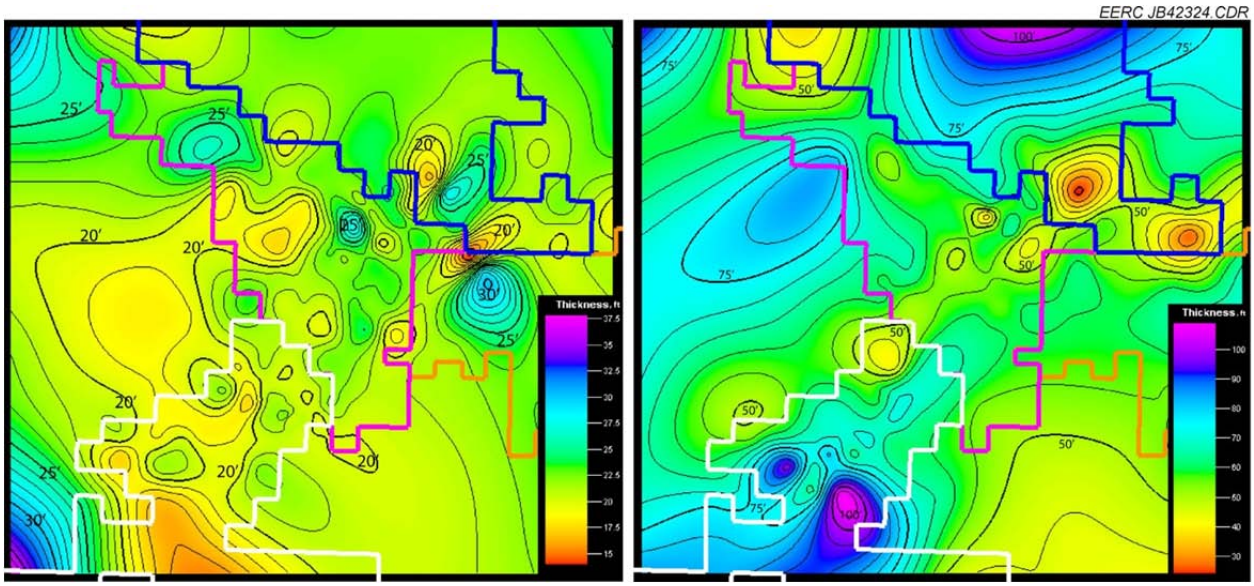

Figure 24. Isopach maps of the Midale (left) and Rival (right) Members. The Midale contour interval is 1 ft, and the Rival contour interval is 5 ft, with every fifth contour bolded and labeled.

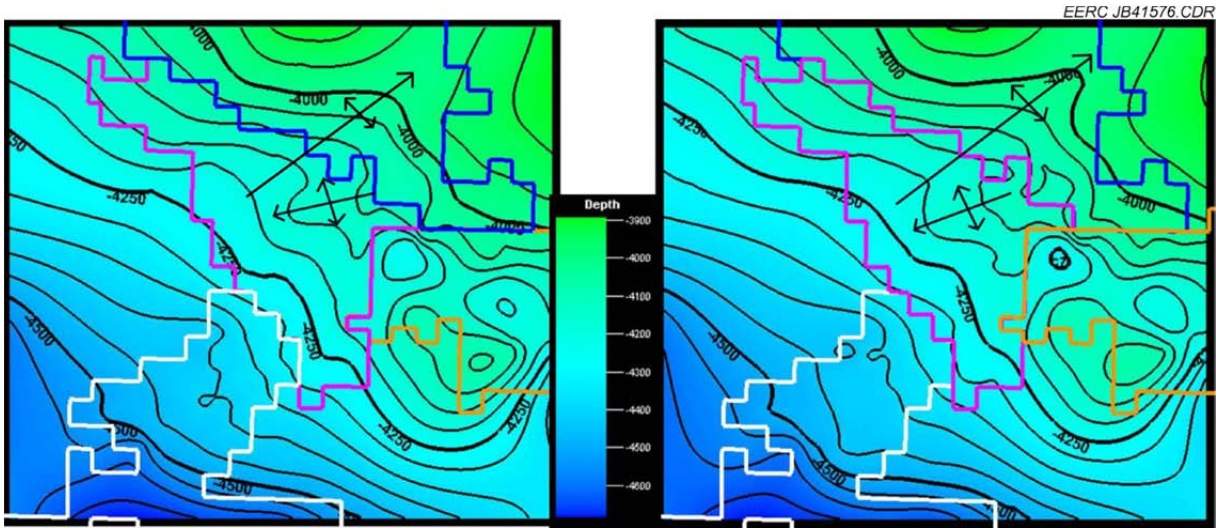

Figure 25. Structure contour maps of the Midale (left) and Rival (right) tops. Structural noses in the northeast portion of the Rival Field are noted by lines with arrows, representing the plunging direction.

deposition, lithification, and oil migration processes. There are also pressure differences implemented from either the structural noses or faulting in the reservoir.

The basement blocks structurally controlling the Rival Field were probably active during deposition, leading to associated fracture-influenced reservoir anisotropy. When the LANDSAT surface-derived lineaments (Anderson and others, 1960) are plotted on top of the Rival and

Midale structure, several lineaments run through the northeast corner of the field (Figure 26). Although salt doming is a possibility from large salt formations below, this fault–fracture pattern is probably related to wrench faulting (Brown and Brown, 1987).

Depositional Facies Model

Depositional environment classification was part of the thin-section analysis completed in the AGL. The data were brought into well section correlation workflow and extrapolated across the entire model based on petrophysical properties.

The depositional model was built with truncated Gaussian simulation (TGS) with trends and provided clues for facies classification within the reservoir (Appendix B). Petrophysical properties did not follow depositional facies, as several rounds of diagenesis have created and destroyed flow zones with similar reservoir properties. Thus a petrophysical model populated geostatistically was created for both the Midale and Rival Members, broken into equal-increment layers until flow zone simulation can be completed.

Petrophysical Model

Reservoir properties include effective porosity, net-to-gross (porosity), permeability, water saturation, temperature, and pressure that were upscaled into the structural framework model based on previously completed petrophysics. Data analysis was performed on the Three Fingers, Midale, and Rival zones for any given property, including transforms and variograms (Appendix B). The most common transform is normal score, which is required as part of geostatistical modeling with Gaussian function random simulation (GFRS). 1-D, 2-D, and 3-D trend transformations were tried but did not add any inherent value to the data analysis. Major and minor variograms were picked with confidence, while the vertical direction has some uncertainty

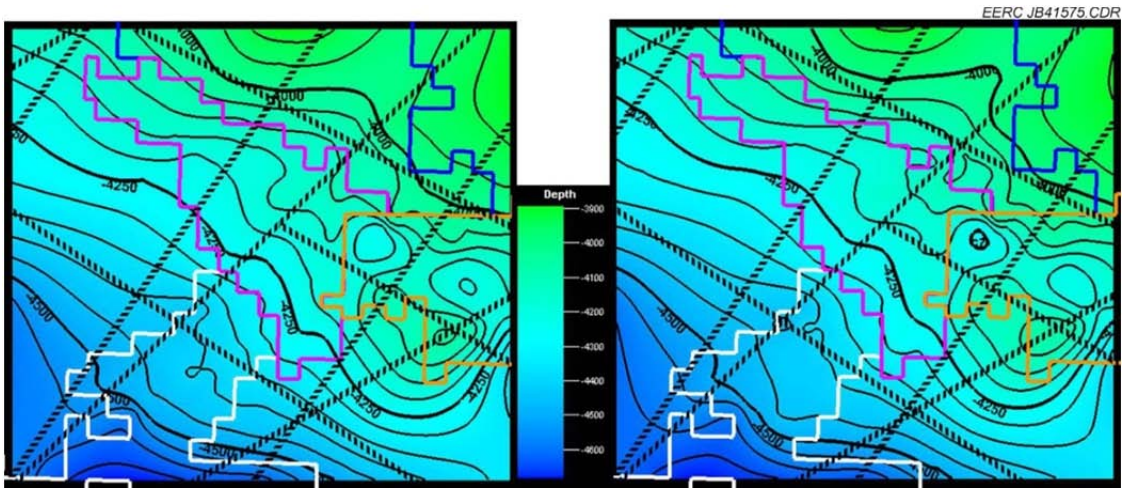

Figure 26. Lineaments overlain on structure contours of the Midale (left) and Rival (right) Members.

as there were not enough data points. The Midale salt and Frobisher salt zones are considered sealing members, thus a variogram was not needed; instead, they were assigned values during the petrophysical modeling process.

Both members show variations in porosity and permeability that reflect a combination of depositional, diagenetic, and structural nose control, reflecting reservoir development. Porosity and permeability have a poor relationship in the reservoir rocks. Thus a single porosity-to-permeability transform was deemed inadequate since diagenesis has controlled these properties locally throughout the reservoir. Instead, a cloud transform concept was followed. Permeability was modeled using bivariate distribution utilizing a crossplot of core porosity vs. core permeability (Appendix B).

The Archie equation was used to determine water saturation from all vintages of geophysical logs. The Archie equation results tended to be above average as compared with published literature (Laird, 1960). More reliable water saturation values were gleaned from core analysis data than the Archie equation. Thus the actual water saturation property was upscaled with core analysis data and cokriged with Archie equation results (Appendix B).

Random seed numbers were used to populate 31 realizations of each property. Care was taken to ensure that related properties utilized the same seed number for each individual realization. The realizations have not been ranked by any criteria.

Volumetric CO_2 EOR Potential and Estimated Storage Capacity

Industry standard formulas were used to calculate both EOR (Equation 1) and CO_2 required (Equation 2) based on OOIP.

$$V_{EOR} = OOIP * RF \quad \text{[Eq. 1]}$$

$$V_{CO2r} = [OOIP * RF* (V_{CO2}/V_{Oil})]/B_o \quad \text{[Eq. 2]}$$

The OOIP in the Rival Field is estimated to be approximately 59.7 million bbl. As a result, EOR potential based on the above equation resulted in 6.0–9.0 Mbbl of incremental oil from the Rival Field. Volume of CO_2 required (V_{CO2r}) was calculated for a range of recovery factors (RF) from 10% to 15%. V_{CO2r} is the necessary volume of CO_2 to achieve EOR potential and is equivalent to estimated storage capacity in the reservoir ranging from 1.5 to 2.9 Mt. V_{CO2}/V_{Oil} is the ratio of CO_2 injected to oil produced ranging from 5000 to 8000 scf/bbl. B_o is the formation factor to convert reservoir barrels of oil into stock tank barrels of oil (Table 7).

CO_2 PROPHET MODEL AND SIMULATION

A CO_2 Prophet model was used to estimate reservoir CO_2 storage capacity and incremental oil recovery from a simulated EOR CO_2 flood. CO_2 Prophet is a water- and CO_2-flooding prediction software which falls between crude empirical correlations and sophisticated numerical

Table 7. Volumetric Potential for EOR and Storage Capacity (M = 1,000,000)

OOIP, Mbbl	RF	EOR, Mbbl	Utilization, scf/bbl	B_o	CO_2, Mscf	CO_2, Mt
59.7	0.1	6.0	8000	1.2	39,800.0	2.3
59.7	0.1	6.0	6500	1.2	32,337.5	1.9
59.7	0.1	6.0	5000	1.2	24,875.0	1.4
59.7	0.125	7.5	8000	1.2	49,750.0	2.9
59.7	0.125	7.5	6500	1.2	40,421.9	2.3
59.7	0.125	7.5	5000	1.2	31,093.8	1.8
59.7	0.15	9.0	8000	1.2	59,700.0	3.5
59.7	0.15	9.0	6500	1.2	48,506.3	2.8
59.7	0.15	9.0	5000	1.2	37,312.5	2.2

simulators. It was designed to identify the influence of key variables such as reservoir heterogeneity and areal sweep efficiency on CO_2 project performance and economics prior to performing detailed numerical simulations. Different types of flooding patterns and many types of recovery processes can be simulated. The limitations include the balancing of injection and production rates and no gravity effect. The reservoir model can include up to 10 layers with no crossflow between the layers. The model uses the Dykstra–Parsons coefficient to calculate the permeability variations between the layers. The calculations of layer permeabilities are done internally in the program. This software is publicly available (U.S. Department of Energy National Energy Technology Laboratory, 2012; Petroleum Technology Transfer Council, 2012).

Prior to making CO_2 recovery and storage predictions, the model was calibrated by matching the observed field performance during historic secondary waterflooding activities. The main variables that were varied in a reasonable range during the calibration history match were Dykstra–Parsons coefficient, end point relative permeability values for oil and water, and current oil saturation to accommodate oil saturation change due to primary depletion. Several flooding patterns were considered during the initial model calibration. Two-spot, four-spot, five-spot, seven-spot, nine-spot, and line drive patterns were used based on 80-acre spacing. The seven-spot and line drive history matches were the most successful (Appendix C).

The calibrated models for the two successful patterns were then used to simulate CO_2 injection for overall storage capacity and IOR. Sensitivity analysis was performed, resulting in a total of 36 cases of simulation of which 23 cases were simulated successfully (Table 8). 60-acre, 80-acre, and 100-acre spacing units were used, with 12 cases for each. Two patterns were simulated for each spacing unit, or six cases for each the seven-spot and line drive patterns. Upon injection of 1 hydrocarbon pore volume (HCPV) the patterns continually showed an additional 13–15 Mbbl of oil (15%–18% OOIP), while 2 HCPV resulted in an additional 22.8–24.4 Mbbl of oil (26.9%–28.6% OOIP). CO_2 storage culminated in an estimated 2.5 megatons for the injection of 1 HCPV and up to 3.5 megatons for the injection of 2 HCPV (Appendix C).

Table 8. Results from CO_2 Simulation of 23 Cases Successfully Attempted (M = 1,000,000)

Spacing = 60 Acres

Pattern	Case	Cum. CO_2 Injection, HCPV	CO_2 Injection, Mscf/Day/Pattern	CO_2 Injection/ Year, Mt	Water Injection Time, Year	CO_2 Injection Time, Year	CO_2 Capt. Vol, Mscf	CO_2 Capt. Mass, Mt	CO_2 EOR Oil, Mstb	CO_2 Incremental EOR, % OOIP	CO_2 UT Factor, Mscf/Mstb	CO_2 Prod/Injection Ratio, scf/scf
Line	1	1	0.275	1	52.00	9.12	43,878	2.558	15.787	18.5	2780	0.73
Drive	2	1	0.551	2	52.00	4.54	43,844	2.556	15.650	18.5	2800	0.73
	3	2	0.275	1	52.00	18.75	61,662	3.595	24.422	28.6	2520	0.81
	4	2	0.551	2	52.00	9.29	61,611	3.592	24.235	28.5	2540	0.81
Seven-	1	1	0.275	1	52.00	9.28	38,298	2.233	13.193	15.5	2900	0.76
Spot	2	1	0.410	1.49	52.00	6.17	38,315	2.234	13.039	15.5	2940	0.76
	3	2	0.275	1	52.00	18.75	58,453	3.408	22.972	26.9	2540	0.82

Spacing = 80 Acres

Pattern	Case	Cum. CO_2 Injection, HCPV	CO_2 Injection, Mscf/Day/Pattern	CO_2 Injection/ Year, Mt	Water Injection Time, Year	CO_2 Injection Time, Year	CO_2 Capt. Vol, Mscf	CO_2 Capt. Mass, Mt	CO_2 EOR Oil, Mstb	CO_2 Incremental EOR, % OOIP	CO_2 UT Factor, Mscf/Mstb	CO_2 Prod/Injection Ratio, scf/scf
Line	1	1	0.367	1	52.50	9.23	43,853	2.557	15.757	18.5	2780	0.73
Drive	2	1	0.734	2	52.50	4.49	43,840	2.556	15.181	18.5	2890	0.73
	3	1	0.900	2.45	52.50	3.62	43,878	2.558	14.618	18.5	3000	0.73
	4	2	0.367	1	52.50	18.56	61,658	3.595	24.384	28.5	2530	0.81
	5	2	0.734	2	52.50	9.23	61,632	3.593	23.795	28.5	2590	0.81
	6	2	0.850	2.32	52.50	7.94	61,658	3.595	23.424	28.6	2630	0.81
Seven-	1	1	0.367	1	52.50	9.23	38,310	2.233	13.146	15.5	2910	0.76
Spot	2	1	0.550	1.50	52.50	6.08	38,310	2.233	12.749	15.5	3010	0.76
	3	2	0.367	1	52.50	18.71	58,470	3.409	22.925	26.9	2550	0.82
	4	2	0.450	1.23	52.50	15.22	58,445	3.407	22.797	26.9	2560	0.82

Spacing = 100 Acres

Pattern	Case	Cum. CO_2 Injection, HCPV	CO_2 Injection, Mscf/Day/Pattern	CO_2 Injection/ Year, Mt	Water Injection Time, Year	CO_2 Injection Time, Year	CO_2 Capt. Vol, Mscf	CO_2 Capt. Mass, Mt	CO_2 EOR Oil, Mstb	CO_2 Incremental EOR, % OOIP	CO_2 UT Factor, Mscf/Mstb	CO_2 Prod/Injection Ratio, scf/scf
Line	1	1	0.367	1	52.00	9.28	43,868	2.558	15.770	18.5	2780	0.73
Drive	2	1	0.734	2	52.00	4.54	43,878	2.558	15.657	18.5	2800	0.73
	3	2	0.367	1	52.00	18.76	61,655	3.594	24.402	28.6	2530	0.81
	4	2	0.734	2	52.00	9.28	61,645	3.594	24.279	28.6	2540	0.81
Seven-	1	1	0.367	1	52.00	9.28	38,308	2.233	13.210	15.5	2900	0.76
Spot	2	2	0.367	1	52.00	18.76	58,470	3.409	22.989	27.0	2540	0.82

CONCLUSIONS

Flow Zones

Four potential flow zones are represented in the interval of interest for type Well 16409 (Figure 27), two flow zones in each of the Midale and Rival Members. The Midale Member has a trend of high porosity and low permeability to midpermeability in its potential flow zones. Mud-dominated fabrics often have less porosity than grain-dominated fabrics. The low-porosity zones confining the flow zones are mostly mud-dominated fabrics as described in core photos and current petrographic analysis. While the actual flow zones exist in the grain-dominated fabrics. The Rival Member has a trend of high permeability and low porosity to midporosity in its potential flow zones. The Rival Member, being mostly limestone altered by diagenetic processes, relies heavily on vuggy porosity and permeability for flow properties.

Contacts

Multiple localized oil–water contacts may exist in both the Midale and Rival Members. Since much of the reservoir trap is represented by salt cementation zones created by diagenesis, there is a lack of well-defined oil–water contacts in the system. Traditional oil–water contacts do not exist in the Midale and Rival Members. The contacts are much more complex than the scope of this study. Impermeable and semipermeable extensive salt lenses and diagenetic salt zones present an unconventional reservoir system.

The Rival Member shows a considerable range of water saturation for any given structural horizon, reflecting significant variation of the oil–water contact across the field. The distribution of oil and water saturation in the Midale Member is a function of variation in size of the extremely fine pores and associated capillary forces. These fine pores and associated permeabilities probably influence the reservoir's productivity. There is a series of probable semipermeable barriers within the reservoir model, also affecting oil–water contacts. Reservoir simulation and history matching will help define and update oil–water contacts throughout both members.

IOR and CO_2 Storage Capacity

The Rival Field is an excellent candidate for tertiary CO_2 EOR. The Rival Field depositional environment and facies are similar to those found in the nearby Weyburn and Midale Fields in Saskatchewan where tertiary CO_2 EOR has been successful and ongoing since 2000, recovering an additional 215 Mbbl of oil. Volumetric calculations on the Rival Field suggest an EOR potential of 6.0–9.0 Mbbl based on industry standard recovery factors of 10%–15%. The CO_2 required for this recovery and, ultimately, stored is 1.5–2.9 million tons. These calculations were based on the net utilization factors ranging from 5000 to 8000 scf/bbl.

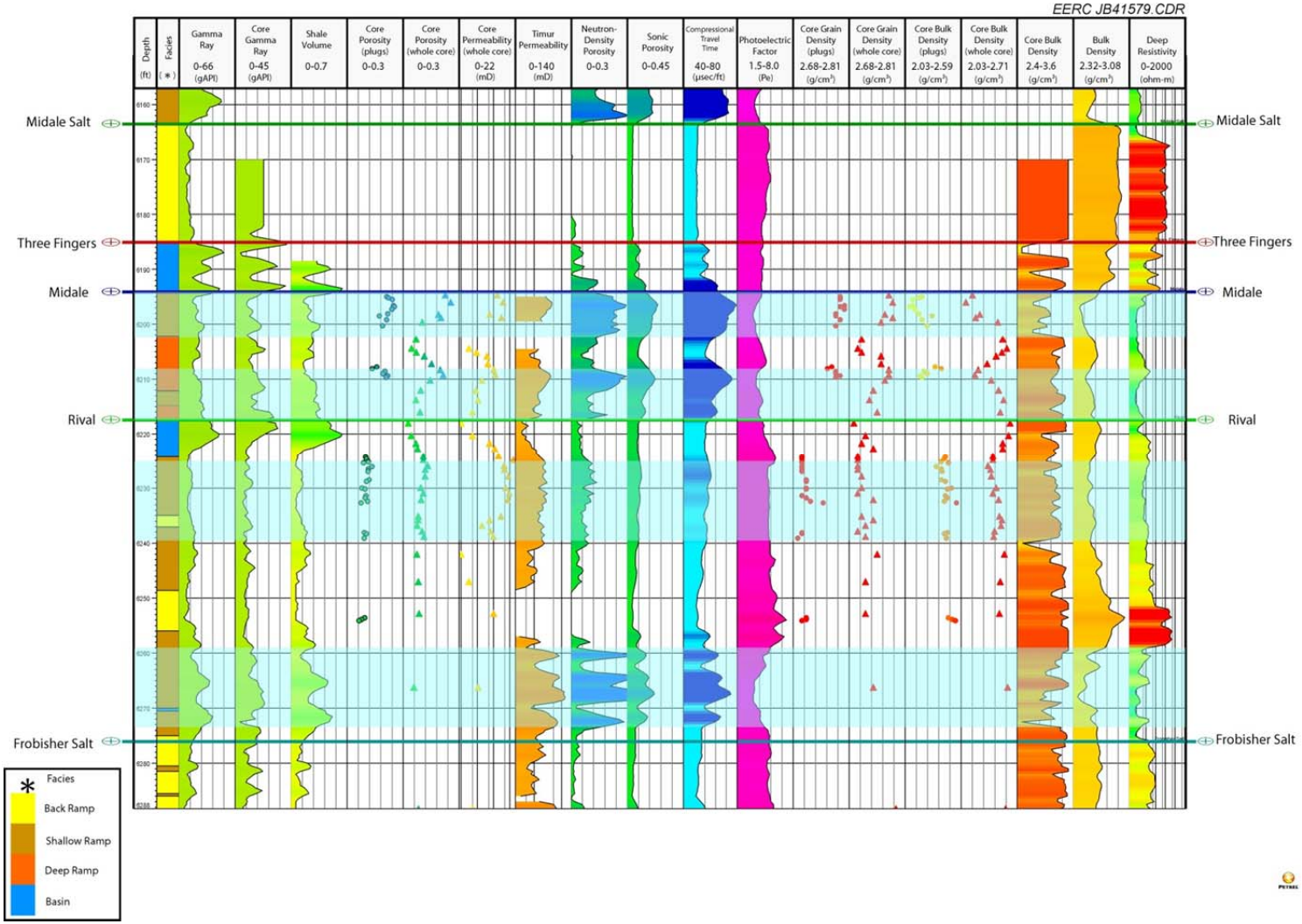

Figure 27. Zone correlation on type Well 16409. Two high-porosity zones in the Midale and one each of mid- and high-porosity zones in the Rival should be noted.

The CO_2 Prophet, a water and CO_2 flood prediction software, was used for more realistic estimates of incremental recovery factors, storage capacity, and net utilization factors. The simulation results suggested an incremental recovery of 15.8%–18.5% (12.74–15.5 Mbbl of oil) at 1 HCPV CO_2 injection in a miscible flood scheme for both the seven-spot and line drive patterns; this resulted in a utilization factor of 2780–3010 scf/bbl. Injection of 2 HCPV estimated 26.9%–28.6% recovery (22.8–23.8 Mbbl of oil) for miscible CO_2 flood for both the seven-spot and line drive patterns, resulting in a utilization factor of 2520–2630 scf/bbl. Volume of CO_2 required and estimated storage capacity were calculated to be 2.5 million tons for the injection of 1 HCPV and up to 3.5 million tons for the injection of 2 HCPV.

These CO_2 EOR and storage capacity estimations by volumetrics and CO_2 Prophet modeling show great potential for the Rival Field as an EOR target. Although these two methods do not replace the calculations based on history matching and predictive simulation, they do provide an initial screening of potential EOR in the reservoir. Updating the OWCs based on detailed log analysis would assist in adjusting OOIP, thus providing more accurate estimations. History matching and detailed predictive simulation could result in greater confidence in the numbers presented.

REFERENCES

Anderson, S.B., Hansen, D.E. and Eastwood, W.P., 1960, Oil fields in the Burke County area, North Dakota—geological, magnetic, and engineering studies: North Dakota Geological Survey Report of Investigation no. 36, p. 71.

Brown, D.L., and Brown, D.L., 1987, Wrench-style deformation and paleostructural influence on sedimentation in and around a cratonic basin: Rocky Mountain Association of Geologists, 1987 Symposium, p. 57–70.

Carbon Capture Journal, 2010, U.S. and Canada renew funding for Weyburn–Midale project: Carbon Capture Journal, no. 17, September–October 2010.

Cook, T.D., and Bally, A.W., 1975, Stratigraphic atlas of North and Central America: Princeton University Press, 271 p.

Dunham, R.J., 1962, Classification of carbonate rocks according to depositional texture, *in* Ham, W.E. (ed.), Classification of carbonate rocks: American Association of Petroleum Geologists Memoir, p. 108–121.

County, North Dakota: Report for Camwest Inc., Louisville, Colorado, Upstate Gas Exploration and Production.

Folk, R.L., 1959, Practical petrographic classification of limestones: American Association of Petroleum Geologists Bulletin, v. 43, p. 1–38.

James, N.P., and Dalrymple, R.W., 2010, Facies Models 4: Geological Association of Canada, IV Series, Geotext 6, p. 586.

Jensen, G.K.S., Nickel, E.H., Whittaker, S., and Rostron, B.J., 2008, Geological model and hydrogeological framework of an active CO_2 sequestration project in the Weyburn–Midale Area, Saskatchewan—leading to a further understanding of possible CO_2 migration: Energy Procedia, Greenhouse Gas Technologies (GHGT) 9.

Knudsen, D.J., Bremer, J.M., Gorecki, C.D., Sorensen, J.A., Peck, W.D., Harju, J.A., and Steadman, E.N., 2010, Plains CO2 Reduction (PCOR) Partnership (Phase III) – site characterization of the Dickinson lodgepole mounds for potential CO2 enhanced oil recovery—Task 1 Deliverable D2: Final report (October 1, 2007 – September 30, 2009) for U.S. Department of Energy National Energy Technology Laboratory Cooperative Agreement No. DE-FC26-05NT42592, EERC Publication 2010-EERC-03-02, Grand Forks, North Dakota, Energy & Environmental Research Center, March.

Laird, W.M., 1960, Oil fields in the Burke County area, North Dakota—geological, magnetic, and engineering studies: North Dakota Geologic Survey, Report of Investigation No. 36.

Lindsay, R.F., 1988, Mission Canyon Formation reservoir characteristics in North Dakota, in Goolsby, S.M., and Longman, M.W., (eds.), Occurrence and petrophysical properties of carbonate reservoirs in the Rocky Mountain region: Rocky Mountain Association of Geologists, p. 317–346.

Lucia, F.J., 2007, Carbonate reservoir characterization, an integrated approach: Berlin, Heidelberg, New York, Springer, p. 336.

Petroleum Technolgoy Transfer Council, 2012, www.pttc.org/co2prophet.htm (accessed January 2012).

Shier, D.E., 2004, Well log normalization—methods and guidelines: Petrophysics, the SPWLA Journal of Formation Evaluation and Reservoir Description, Houston, Texas, v. 45, no. 3, p. 268–280.

Shinn, E.A., 1983, Tidal flat environment, carbonate depositional environments: American Association of Petroleum Geologists Special Volumes, v. M33.

U.S. Department of Energy National Energy Technology Laboratory, 2012, www.netl.doe.gov/technologies/oil-gas/Software/e&ptools.html#CO2P (accessed January 2012).

APPENDIX A

RIVAL FIELD PETROGRAPHIC AND PHYSICAL ANALYSIS, OCTOBER 2011

RIVAL FIELD PETROGRAPHIC AND PHYSICAL ANALYSIS, OCTOBER 2011

Technical Report

Prepared for:

Bill Barnhart

TAQA North Ltd.
2100, 308 4th Avenue Southwest
CALGARY, AB T2P 0H7
CANADA

Prepared by:

Jordan M. Bremer
Corey D. Lindeman
Jonathan L. LaBonte
Benjamin W. Huffman
Blaise A.F. Mibeck
Steven A. Smith

Energy & Environmental Research Center
University of North Dakota
15 North 23rd Street, Stop 9018
Grand Forks, ND, 58202-9018

November 2011

DOE DISCLAIMER

EERC DISCLAIMER

TABLE OF CONTENTS

LIST OF FIGURES

LIST OF TABLES

RIVAL FIELD PETROGRAPHIC AND PHYSICAL ANALYSIS, OCTOBER 2011

EXECUTIVE SUMMARY

Petrographic analysis of core from the Rival Field has been conducted by the Energy & Environmental Research Center (EERC) as part of the Plains CO_2 Reduction Partnership Phase III Regional Characterization of Williston Basin deep geological storage resources. The Rival Field, located in Burke County, North Dakota, is currently operated by TAQA North and represents a strong opportunity for CO_2 enhanced oil recovery (EOR).

The goal of this analysis is to develop a basic understanding of petrographic rock properties which may serve as defining properties between facies types within the Rival reservoir. These data will be used to aid, form, and support petrophysical correlations, which will, in turn, be used in producing geologic models of the area.

Thin sections were created and analyzed on reservoir and nonreservoir samples collected from historical Rival Field core. Twenty-eight (28) samples were obtained with permission from the Wilson Laird Core and Sample Library by EERC personnel. Created sections represent vertical differentiation in two wells, North Dakota Industrial Commission (NDIC) Wells 16409 and 13700. Two thin sections from each sample (totaling 56) were created to an approximate thickness of 30 μm. Blue-dyed epoxy was used to easily differentiate pore spaces. Following thin-section analysis, five (5) 30-mm plug samples were taken representing various environments for the collection of petrophysical properties (Table ES-1). In all, plug sample measurements included the following:

- Bulk density
- Grain density
- Porosity (to gas)
- Permeability (to water)
- Mineralogy (by x-ray diffraction)
- Petrography (thin-section analysis)

Petrographic analysis for each interval included description, estimation of prevalent mineral/carbonate grain assemblages, expected depositional environment, and petrographic class (Table ES-2). Carbonate fabric descriptions were developed in accordance with classification schemes formalized by Folk (1959, 1962) and Dunham (1962). Microstructures and fossil assemblages, if present, were also identified (if possible) and noted. Thin-section analysis also included photomicrographs demonstrating plane- and cross-polarized light at 40× and 100× magnification.

Analysis and interpretation shows that the Rival Field is differentiated into grainstone banks, which contain a majority of the field's porosity, and argillaceous carbonate mudstones with virtually no porosity. The rocks were deposited in a warm-water neritic ramp environment that experienced sea-level fluctuations throughout their deposition. Diagenesis of the reservoir is marked by fine- to coarse-grained secondary dolomite recrystallization.

Table ES-1. Results of Analysis for Rival Plug Samples

Plug No.	Direction	Depth, ft	Porosity, %	Grain Density, g/cm³	Permeability, mD	Calcite, wt%	Dolomite, wt%
1	Vertical	6219.2	1.05	2.450	0.000134	67.1	5.20
2	Horizontal	6219.5	1.28	2.661	0.000426	56.9	12.1
3	Horizontal	6232.2	11.51	2.657	0.034	83.9	ND[1]
4	Horizontal	6208.5	16.79	2.679	0.021	46.4	36.9
5	Horizontal	6201.0	17.44	2.702	0.00176	21.7	59.5

[1] Not detected.

References

Dunham, R.J., 1962, Classification of carbonate rocks according to depositional texture, *in* Ham, W.E. (ed.), Classification of carbonate rocks: American Association of Petroleum Geologists Memoir, p. 108–121.

Folk, R.L., 1959, Practical petrographic classification of limestones: American Association of Petroleum Geologists Bulletin, v. 43, p. 1–38.

Folk, R.L., 1962, Spectral subdivision of limestone types, *in* Ham, W.E., (ed.), Classification of carbonate rocks – a symposium: American Association of Petroleum Geologists Memoir 1, p. 62–84.

Table ES-2. Results of Petrographic Analysis for Rival Thin-Section Samples

Slide No.	Well	Depth	Class	Depositional Environment	Folk	Dunham
1	13700	6089.4	1	Strand plain	Pelsparite	Grainstone
2	13700	6094.5	3	Ramp	Biomicrite	Floatstone
3	13700	6099.5	3	Ramp	Biodismicrite	Floatstone
4	13700	6102.2	3	Ramp	Poorly washed dismicrite/biosparite	Mudstone/wackestone
5	13700	6105.2	1	Strand plain	Pelsparite	Grainstone
6	13700	6108.8	1	Ramp	Biosparite/pelsparite	Grainstone
7	13700	6112	2	Ramp	Biosparite	Packstone
8	13700	6115.5	3	Ramp	Sparite	Mudstone
9	13700	6120	2	Strand plain	Pelsparite	Grainstone
10	13700	6122	2	Strand plain	Oosparite	Grainstone
11	13700	6129	1 and 3	Back Ramp/strand plain	Micrite/oosparite	Micrite/grainstone
12	13700	6141	3	Strand plain/back ramp	Micrite/dismicrite	Mudstone
13	13700	6144.9	1	Strand plain	Oosparite/pelsparite	Grainstone
14	16409	6194	3	Strand plain, ramp	Pelsparite/micrite	Grainstone/mudstone
15	16409	6200	3	Ramp	Dismicrite	Mudstone
16	16409	6203.8	3	Ramp	Dismicrite	Mudstone
17	16409	6208	3	Ramp (storm?)	Biodismicrite	Floatstone
18	16409	6212.9	1	Strand plain	Oosparite	Grainstone
19	16409	6214.6	2	Deep ramp	Sparite	Mudstone
20	16409	6216	3	Deep ramp	Biodismicrite	Floatstone
21	16409	6217.3	3	Ramp (storm?)	Dismicrite/biosparite	Wackestone
22	16409	6220.3	3	Ramp	Sparite	Mudstone
23	16409	6223	2	Ramp	Poorly washed sparite	Mudstone
24	16409	6224.2	1	Strand plain	Pelsparite/oosparite	Grainstone
25	16409	6235	3	Back ramp	Dismicrite	Mudstone
26	16409	6237.2	1	Strand plain	Oosparite	Grainstone
27	16409	6243.2	1	Strand plain	Oosparite	Grainstone
28	16409	6248.8	3	Back ramp	Pelmicrite	Mudstone
Plug 1	16409	6219.2	3	Ramp (storm?)	Intramicrite	Packstone
Plug 2	16409	6219.5	3	Ramp	Intramicrite	Packstone
Plug 3	16409	6232.2	2	Deep ramp	Micrite	Mudstone
Plug 4	16409	6208.5	3	Back ramp	Micrite	Mudstone
Plug 5	16409	6201.0	2	Deep ramp	Micrite	Mudstone

RIVAL FIELD PETROGRAPHIC AND PHYSICAL ANALYSIS, OCTOBER 2011

INTRODUCTION

The Rival Field (Figure 1), located in Burke County, North Dakota, has been identified as a site amenable to carbon dioxide (CO_2) enhanced oil recovery (EOR) operations. The field is owned and operated by TAQA North, which acquired the field in 2008 from previous operator Primewest. The field produces oil and gas from the Midale and Rival Members of the Mission Canyon Formation and Charles Formation at a depth of approximately 6200 feet.

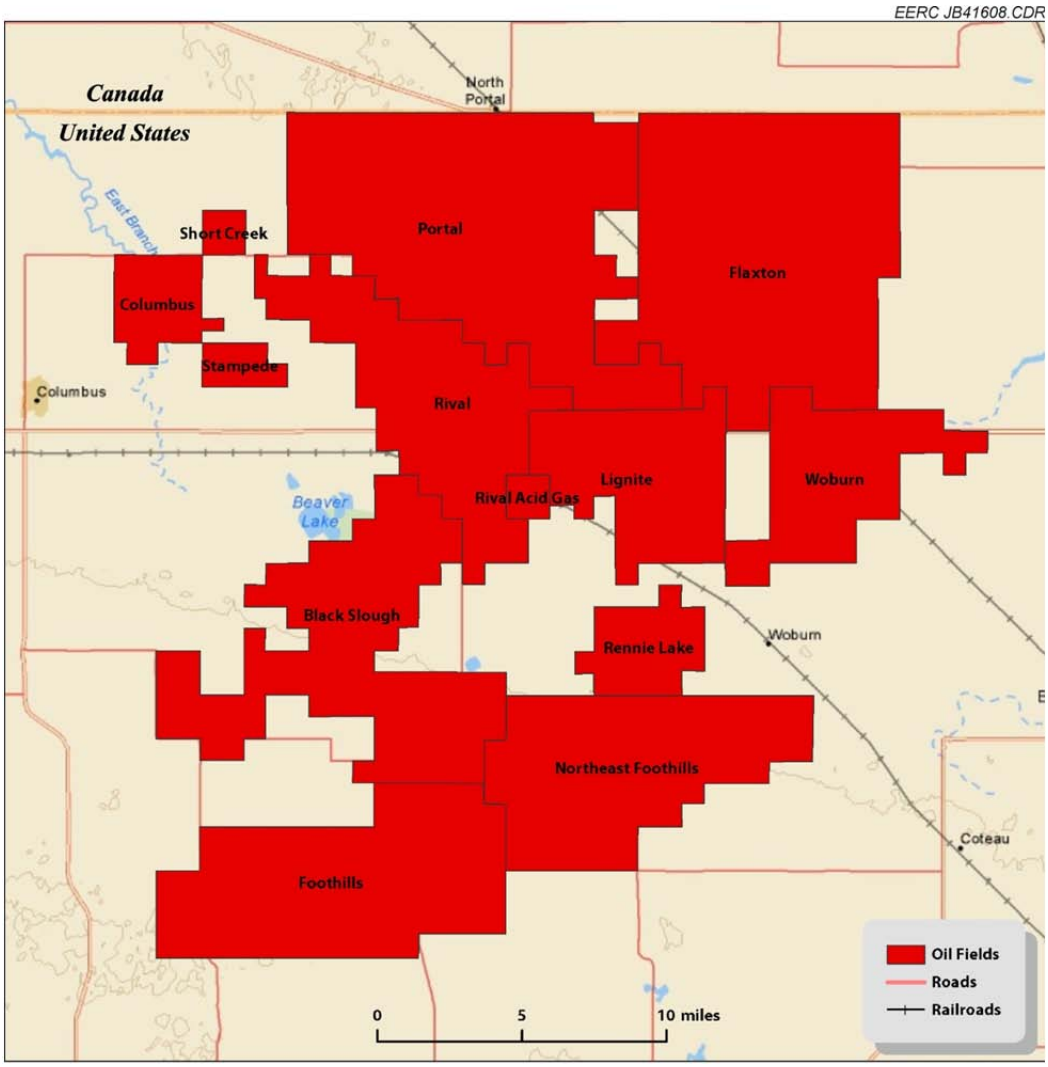

Figure 1. Map of the Rival and surrounding oil fields.

This study details the results of petrographic analysis performed on core specimens of the Madison Group Mission Canyon and Charles Formations from the Rival Field. The specimens were selected and collected in March 2011 by EERC personnel from the Wilson M. Laird Core and Sample Library housed at the University of North Dakota. Twenty-eight intervals were selected from two wells (North Dakota Industrial Commission [NDIC] Wells 16409 and 13700) for analysis, representing a variety of rock fabric ranging from reservoir to sealing formations. Samples were prepared and analyzed in-house by the Energy & Environmental Research Center (EERC) Applied Geology Laboratory (AGL).

Following initial thin-section preparation and analysis, five plug samples were acquired from NDIC Well 16409, with the goal of collecting pertinent sample properties (Figure 2). The samples were cut by AGL personnel using diamond-impregnated steel drill bits cooled by circulating water. Plug samples were received June 15, 2011. Plugs were cleaned of residual hydrocarbons using toluene and oven-dried prior to analysis. In all, plug samples were tested to measure:

- Bulk density
- Grain density
- Porosity
- Permeability to water
- Mineralogy
- Petrography

Plug analysis was performed to develop a basic understanding of the petrographic properties for rocks in the Rival Field, and these data will be used to form correlations between rock fabric and mineralogy to existing laboratory-derived data and geophysical well logs. In turn, data collected through plug testing supplement missing or incomplete historical data, specifically targeted at tight zones within the reservoir units and the intrareservoir shaley marl unit that separates the Midale and Rival Members. These data will be used in the formation of geostatistically populated geologic models.

THIN-SECTION PRODUCTION

Thin sections were created for each of the 28 selected petrographic samples and five plug samples according to standard AGL procedures. Slabs received were polished flat and affixed to glass slides using blue-dyed epoxy. Slabs were trimmed and ground using a diamond-impregnated steel saw and lapidary wheel, with water as the cutting fluid. Final polishing was performed by hand using wet silicon carbide sandpaper.

PLUG TESTING SUMMARY

Following petrographic analysis, five intervals were selected for plug analysis which were cut by EERC personnel at the Core Library using diamond-impregnated steel bits, with water as

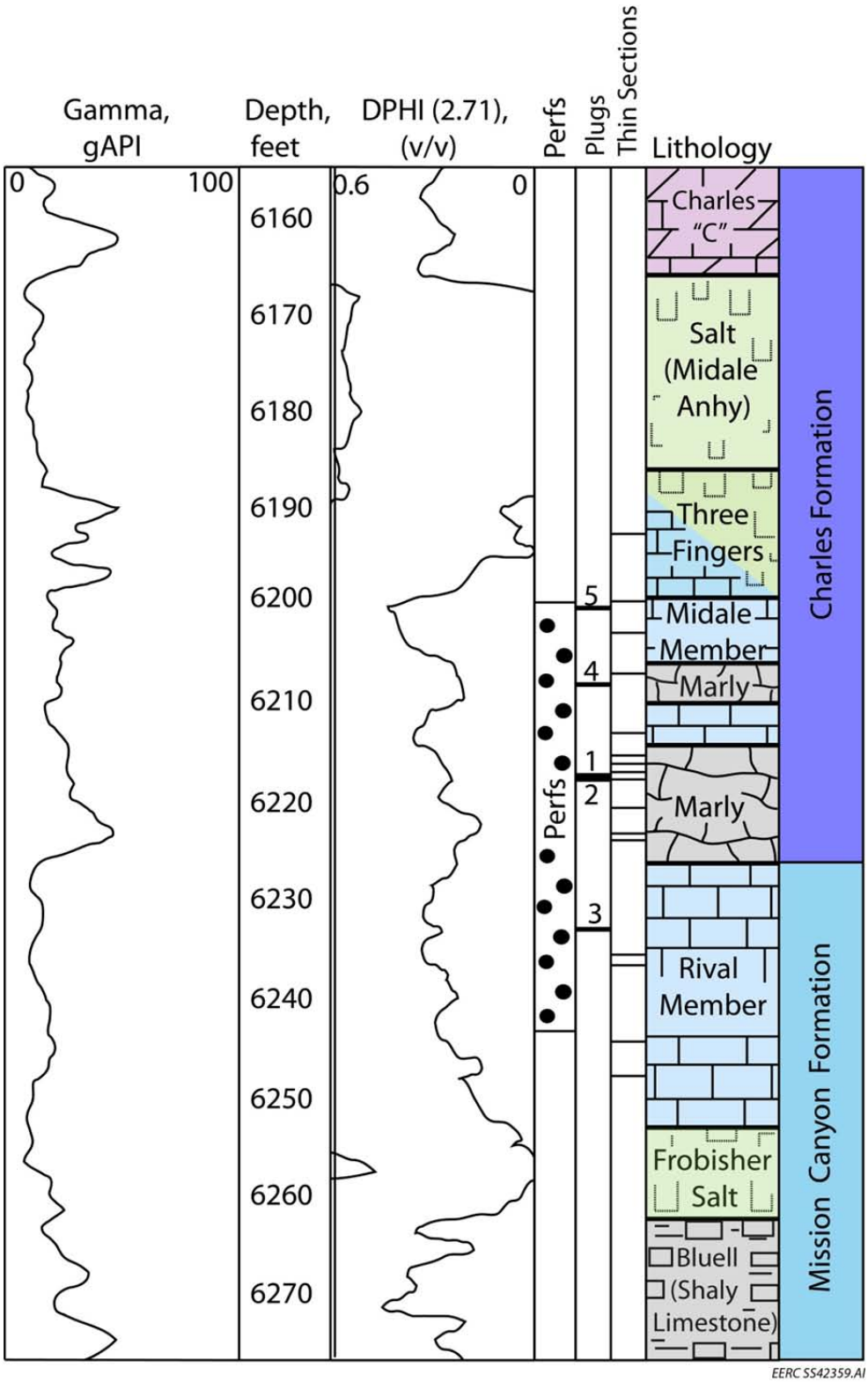

Figure 2. Diagram of samples locations from NDIC Well 16409 showing petrophysical well logs, well perforations, plug and thin-section sample depths, and reported facies from the NDIC well file.

cutting fluid. Plugs were cleaned of residual hydrocarbons by toluene submersion and evacuation followed by oven drying. Rough plug ends were trimmed parallel prior to testing.

Project workflow began with the clean, prepared plug samples which were thoroughly measured using calipers and a laboratory scale, including the calculation of bulk density. Remnant rough plug ends were ground into powder for x-ray diffraction analysis. Plugs were tested for permeability to water using a flexible wall permeameter running deaired water as the permeant under low (40 psi) confining pressure. Samples were dried and then tested for porosity and grain density using a gas pycnometer. Following analysis, thin sections were produced from one end of the plug using the methodology discussed previously.

RESULTS OF ANALYSIS

- Mineralogical assemblages and prevalence were determined and estimated utilizing a combination of plane-polarized, cross-polarized, and reflected light. Thorough descriptions are presented in Appendix A.

- Carbonate classifications were performed according to both the Folk and Dunham classification systems.

- Depositional environments were estimated by analyzing rock fabric, fossil size, disaggregation, and microstructure then defined according to descriptions presented in Facies Models 4 (James and Dalrymple, 2010) (Figures 3–5).

- Petrophysical classes were assigned according to Lucia (1995) (Figures 4 and 5).

- Photomicrographs were produced at 40× and 100× magnification, with plane- and cross-polarized light. Additional photographs depicting specific features were also collected (see Appendix A).

- The selected intervals largely fall into two scenarios: 1) micritic, fossiliferous, sometimes argillaceous mudstones that have experienced variable (sparry) dolomite recrystallization (Figure 6) and 2) porous ooid/pellet grainstone banks partially cemented with sparry dolomite cement (Figure 7). These fabrics are consistent with a standard warm-water neritic carbonate ramp experiencing fluctuating water depth.

- A range of porosity and permeability exist in the Rival unit, with water permeabilities in tested intervals ranging between 0.034 mD and 0.134 µD. Porosity in these intervals ranged from approximately 1% up to 17% (Table 1).

- Mineralogy is primarily carbonate, with samples ranging from clean calcite to high (60%) dolomite concentration. Minor phases present included clastic material (silt and clay), precipitated sulfate salts, and metal oxides (Table 3, Appendix B).

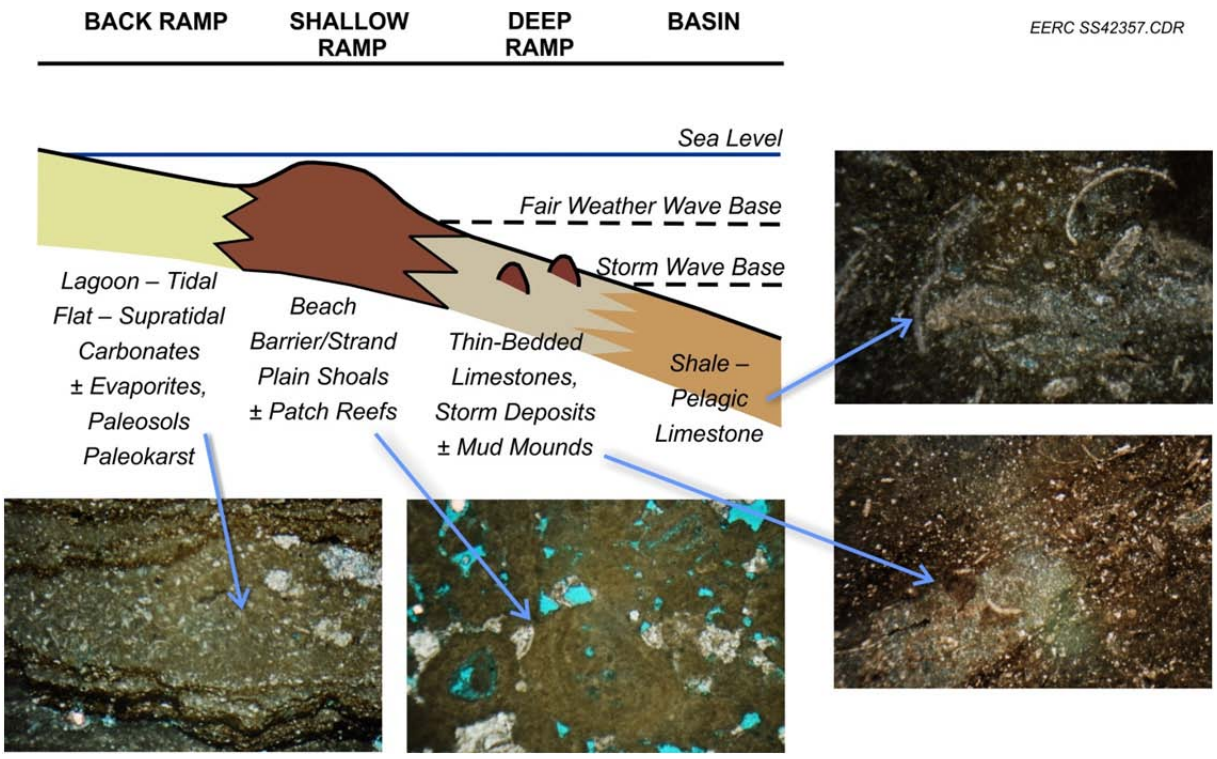

Figure 3. Depositional facies model of the Rival Field (from James and Dalrymple, 2010), with examples of thin sections from the Rival Field.

KEY FINDINGS

- Observed rocks represent a variety of depositional environments, but may be grouped into carbonate grainstone banks (reservoir rock) and argillaceous carbonate mudstones (nonreservoir rock).

- Observed facies, fossil assemblages, and microstructures are consistent with a warm-water neritic carbonate ramp environment.

- A fair degree of secondary dolomite recrystallization has occurred throughout the interval.

- Porosity in the Rival Field is present within carbonate grainstone banks that have loosely cemented by sparry dolomite.

- Less commonly observed vuggy mudstone banks may also represent viable reservoir rock, particularly in the presence of open microfractures. If unfractured, the tight nature of these samples may retain residual hydrocarbons.

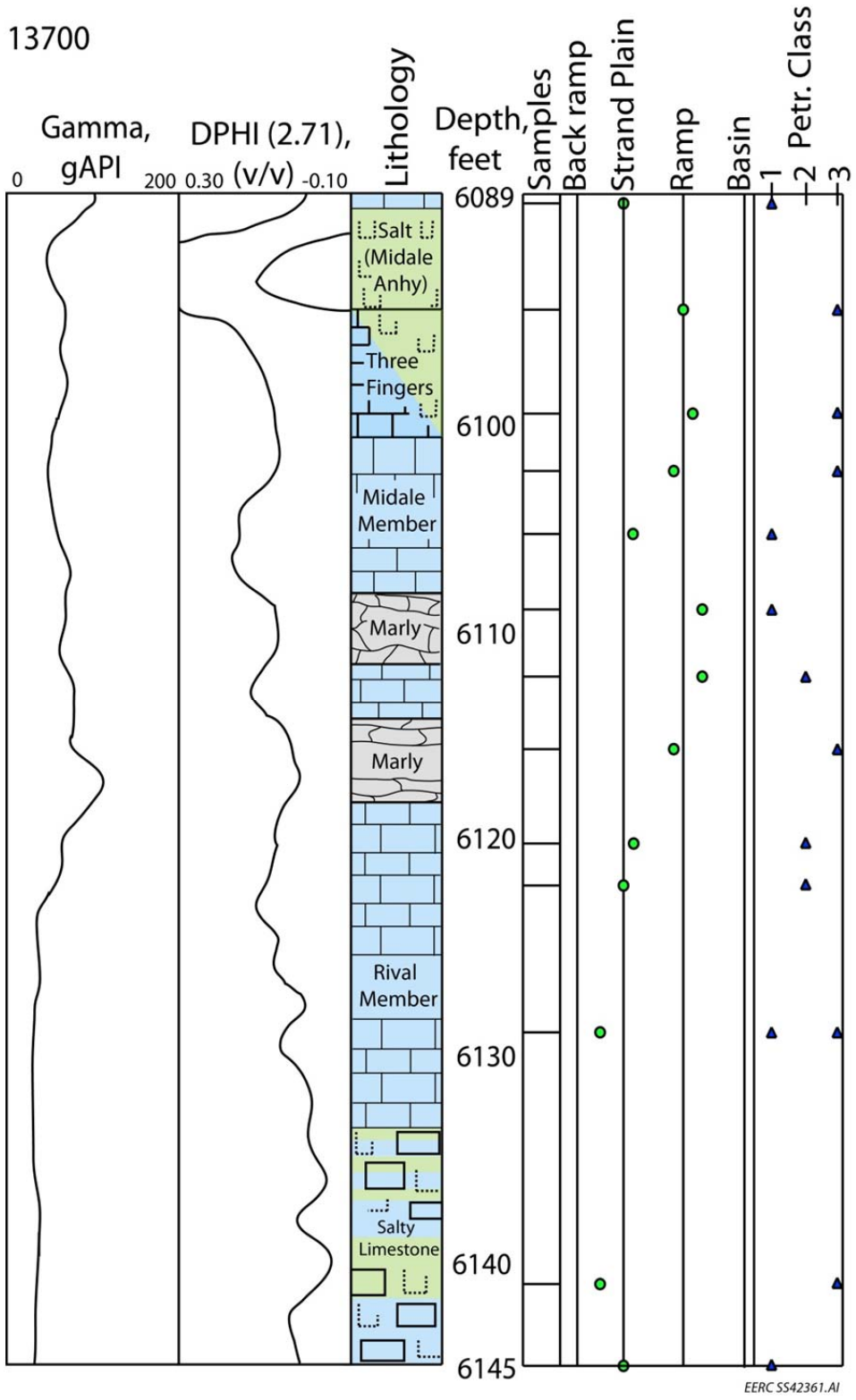

Figure 4. Depositional environment and petrophysical class of analyzed sections with well logs and interpreted lithology from NDIC Well File 13700.

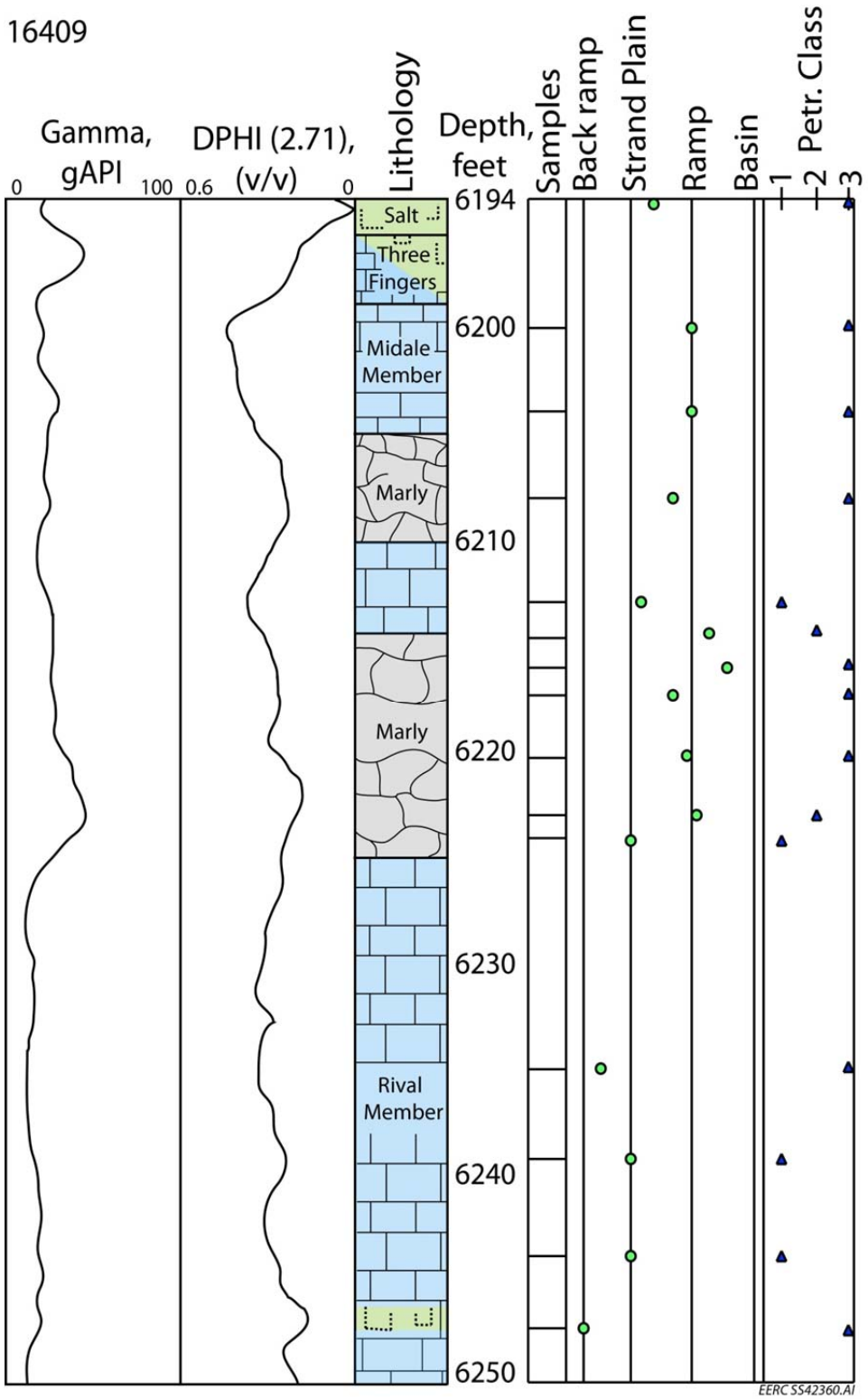

Figure 5. Depositional environment and petrophysical class of analyzed sections with well logs and interpreted lithology from NDIC Well File 16409.

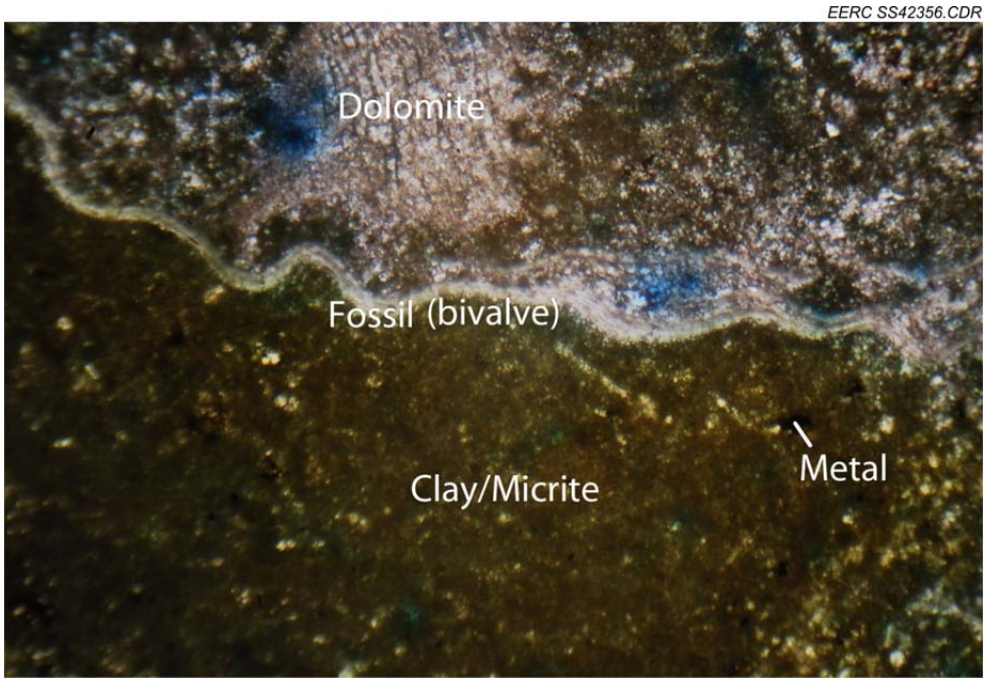

Figure 6. Type thin section representing tight mudstone (nonreservoir rock) – Well 16409, 6216', 40× magnification, plane-polarized light.

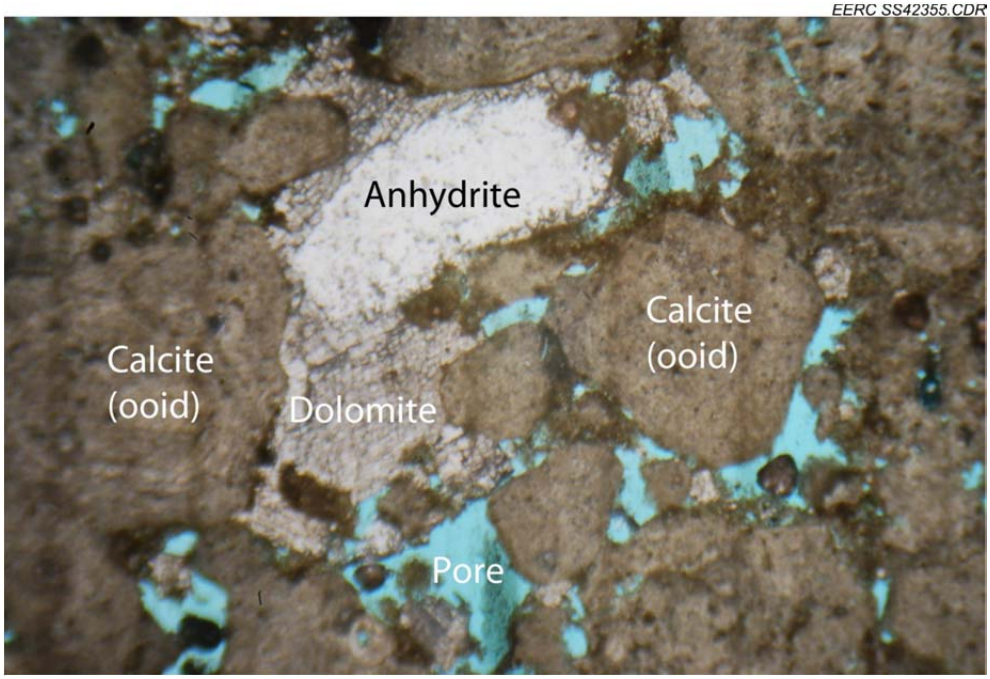

Figure 7. Type thin section representing porous grainstone (reservoir rock) – Well 13700, 6129', 40× magnification, plane-polarized light.

Table 1. Results of Petrographic Analysis for Rival Thin-Section Samples

Slide No.	Well	Depth	Class	Depositional Environment	Folk	Dunham
1	13700	6089.4	1	Strand plain	Pelsparite	Grainstone
2	13700	6094.5	3	Ramp	Biomicrite	Floatstone
3	13700	6099.5	3	Ramp	Biodismicrite	Floatstone
4	13700	6102.2	3	Ramp	Poorly washed dismicrite/biosparite	Mudstone/wackestone
5	13700	6105.2	1	Strand plain	pelsparite	Grainstone
6	13700	6108.8	1	Ramp	Biosparite/pelsparite	Grainstone
7	13700	6112	2	Ramp	Biosparite	Packstone
8	13700	6115.5	3	Ramp	Sparite	Mudstone
9	13700	6120	2	Strand plain	Pelsparite	Grainstone
10	13700	6122	2	Strand plain	Oosparite	Grainstone
11	13700	6129	1 and 3	Back ramp/strand plain	Micrite/oosparite	Micrite/grainstone
12	13700	6141	3	Strand plain/back ramp	Micrite/dismicrite	Mudstone
13	13700	6144.9	1	Strand plain	Oosparite/pelsparite	Grainstone
14	16409	6194	3	Strand plain, ramp	Pelsparite/micrite	Grainstone/mudstone
15	16409	6200	3	Ramp	Dismicrite	Mudstone
16	16409	6203.8	3	Ramp	Dismicrite	Mudstone
17	16409	6208	3	Ramp (storm)	Biodismicrite	Floatstone
18	16409	6212.9	1	Strand plain	Oosparite	Grainstone
19	16409	6214.6	2	Deep ramp	Sparite	Mudstone
20	16409	6216	3	Deep ramp	Biodismicrite	Floatstone
21	16409	6217.3	3	Ramp (storm)	Dismicrite/biosparite	Wackestone
22	16409	6220.3	3	Ramp	Sparite	Mudstone
23	16409	6223	2	Ramp	Poorly washed sparite	Mudstone
24	16409	6224.2	1	Strand plain	Pelsparite/oosparite	Grainstone
25	16409	6235	3	Back ramp	Dismicrite	Mudstone
26	16409	6237.2	1	Strand plain	Oosparite	Grainstone
27	16409	6243.2	1	Strand plain	Oosparite	Grainstone
28	16409	6248.8	3	Back ramp	Pelmicrite	Mudstone
Plug 1	16409	6219.2	3	Ramp (storm)	Intramicrite	Packstone
Plug 2	16409	6219.5	3	Ramp	Intramicrite	Packstone
Plug 3	16409	6232.2	2	Deep ramp	Micrite	Mudstone
Plug 4	16409	6208.5	3	Back ramp	Micrite	Mudstone
Plug 5	16409	6201.0	2	Deep ramp	Micrite	Mudstone

Table 2. Results of Rival Plug Sample Porosity, Permeability, and Density Testing

Sample	Depth, ft	Porosity, %	Bulk Density, g/cm³	Grain Density, g/cm³	Permeability to Water, mD
1 (vertical)	6219.2	1.05	2.45	2.45	0.000134
2 (horizontal)	6219.5	1.28	2.63	2.66	0.000426
3 (horizontal)	6232.2	11.51	2.38	2.66	0.034
4 (horizontal)	6208.5	16.79	2.29	2.68	0.021
5 (horizontal)	6201.0	17.44	2.30	2.70	0.00176

Table 3. Results of Rival Plug Sample Mineralogy by X-Ray Diffraction

Sample	Depth	Quartz	Feldspars	Pyrite	Dolomite	Calcite	Gypsum	Clay*	Iron Oxide	Amorphous
1	6219.2	4.39	ND**	0.31	5.24	67.07	1.68	ND	ND	21.3
2	6219.5	3.88	ND	0.29	12.10	56.86	3.33	1.74	0.40	21.3
3	6232.2	1.55	ND	ND	ND	83.89	2.54	ND	ND	12.0
4	6208.5	2.49	ND	0.82	36.88	46.36	3.58	1.36	ND	7.52
5	6201.0	9.13	6.4	1.63	59.49	21.75	ND	ND	ND	1.55

***** Amount of clay is likely underestimated to some degree because of amorphous behavior.

** None detected.

- Intrareservoir tight, marly carbonates have very low-porosity and permeability characteristics. This is due to a solid, well-cemented mix of lithic fragments (primarily limestone), micrite mud, and cement. It is unclear if these marl-type lithologies were deposited along the ramp from 1) detrital material coming from the shallow shelf and strand plain with occasional storm deposits; 2) in the back ramp setting, receiving higher overall energy and clastic influx from the continent and shallow marine settings; or 3) despite visual similarities, the lithology may be deposited in either environment, as is the current interpretation, supported by fine-scale fluctuations in mineralogy and rock properties.

- Porosity and permeability have a poor relationship in Rival rocks. Permeability (at least in the tight zones that were tested) is expected to be strongly tied to rock fabric.

REFERENCES

Dunham, R.J., 1962, Classification of carbonate rocks according to depositional texture, *in* Ham, W.E. (ed.), Classification of carbonate rocks: American Association of Petroleum Geologists Memoir, p. 108–121.

Folk, R.L., 1959, Practical petrographic classification of limestones: American Association of Petroleum Geologists Bulletin, v. 43, p. 1–38.

Folk, R.L., 1962, Spectral subdivision of limestone types, *in* Ham, W.E., (ed.), Classification of carbonate rocks – a symposium: American Association of Petroleum Geologists Memoir 1, p. 62–84.

James, N.P., and Dalrymple, R.W. 2010, Facies Models 4: Geological Association of Canada Geotext 6.

Lucia, F.J., 1995, Rock fabric/petrophysical classification of carbonate pore space for reservoir characterization: American Association of Petroleum Geologists Bulletin, v. 79, no. 9, p. 1275–1300.

APPENDIX A

PETROGRAPHIC DESCRIPTIONS AND PHOTOMICROGRAPHS

This page left blank intentionally.

SLIDE 1: WELL 13700, DEPTH 6089.4, CLASS 1, STRAND PLAIN

Assemblage	Percentage	Comments
Carbonate Mud Pellets	70%	
Fossils	Trace	Small bivalves and large unidentified tubular
Sparite Cement	25%	Dolomite ~10% filled vugs.
Metal	Trace	Pyrite

This sample is dominated by pellet grains with sparry dolomitized cement (Folk: pelsparite, Dunham: grainstone). No porosity was observed in the sample, although some microporosity may exist in dolomite cement-filled vugs, which are present in approximately 10% of the sample. A bedding contact is present in the sample. A trace amount of small bivalve fossils is present as well as larger, tubular fossils or trace fossils that are unidentified, possibly burrows.

EERC SS42282.CDR

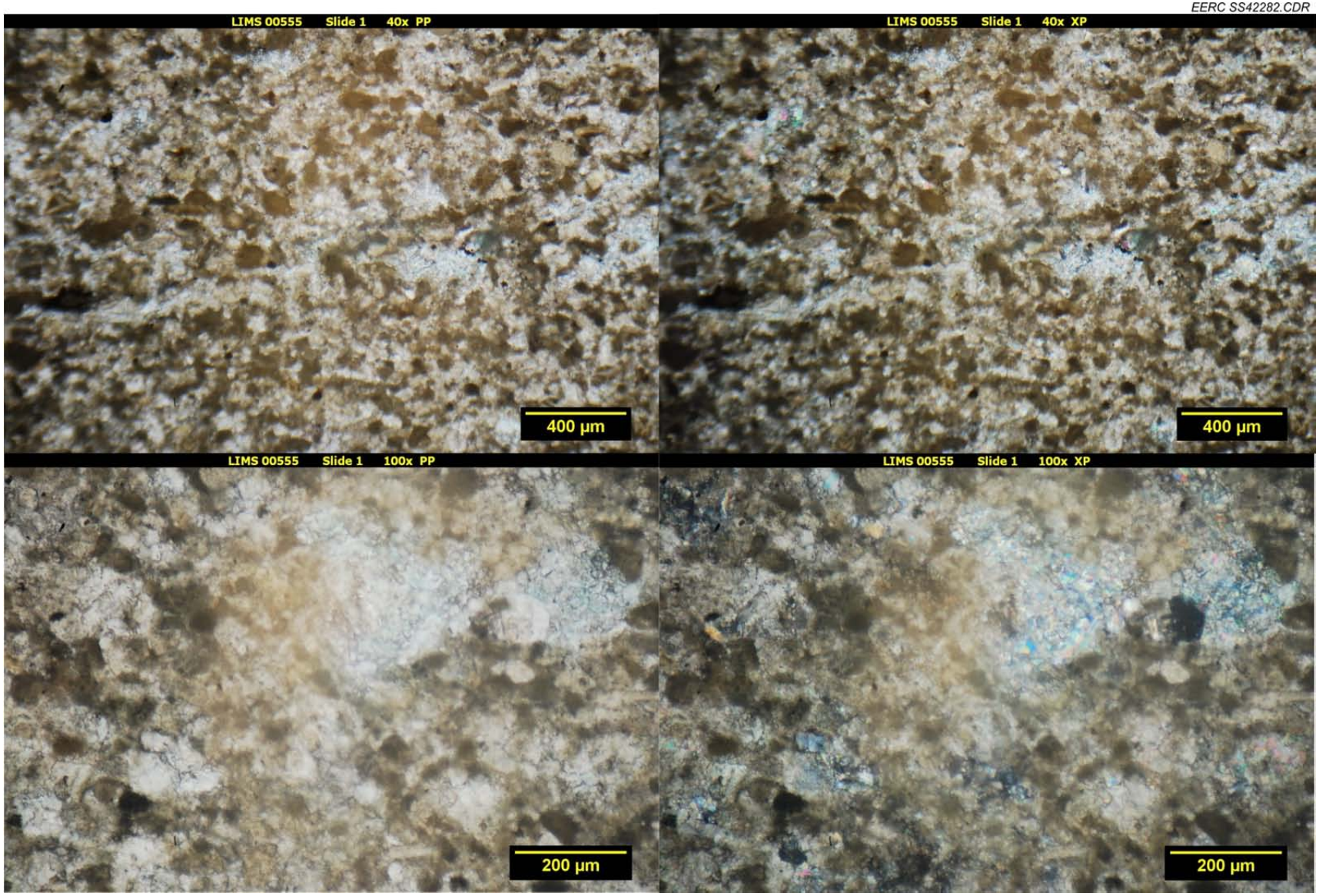

SLIDE 2: WELL 13700, DEPTH 6094.5, CLASS 3, RAMP

Assemblage	Percentage	Comments
Micrite Mud	85%	
Sparite	10%	Recrystallized, fine-grained
Fossils	5%	Disaggregated pieces, some ostracod
Metal	Trace	Anhedral to subhedral, pyrite

Slide 2 contains large portions of carbonate mud, with fine-grained dolomite recrystallization in some areas. Disaggregated fossil material is present, with rare intact ostracods. No porosity is visible in the sample. Pyrite exists in small quantities (Folk: biomicrite, Dunham: floatstone).

EERC SS42283.CDR

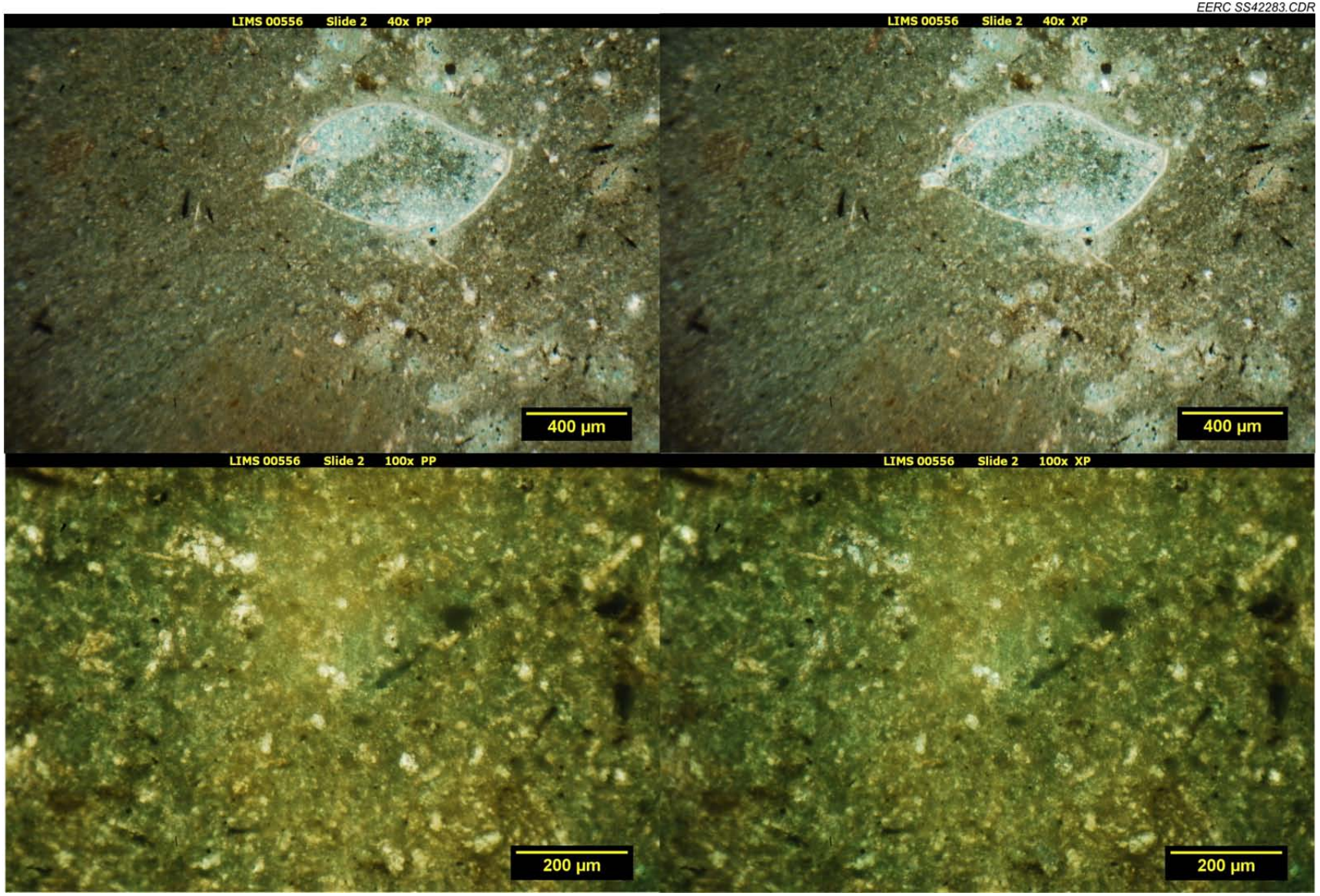

SLIDE 3: WELL 13700, DEPTH 6099.5, CLASS 3, RAMP

Assemblage	Percentage	Comments
Micrite Mud	50%	
Sparite	35%	Fine-grained, dolomite
Fossils	10%	Disaggregated, bivalve, gastropod, ostracod
Porosity	5%	Pinpoint vugs
Metal	Trace	Pyrite
Clay	Trace	Dispersed

This sample contains a mixture of micrite mud and fine-grained sparite as the groundmass, which supports disaggregated fossil fragments. A small amount of porosity is present as pinpoint vugs. Metal and clay are present throughout the sample, however, not in significant amounts (Folk: biodismicrite, Dunham: floatstone).

EERC SS42284.CDR

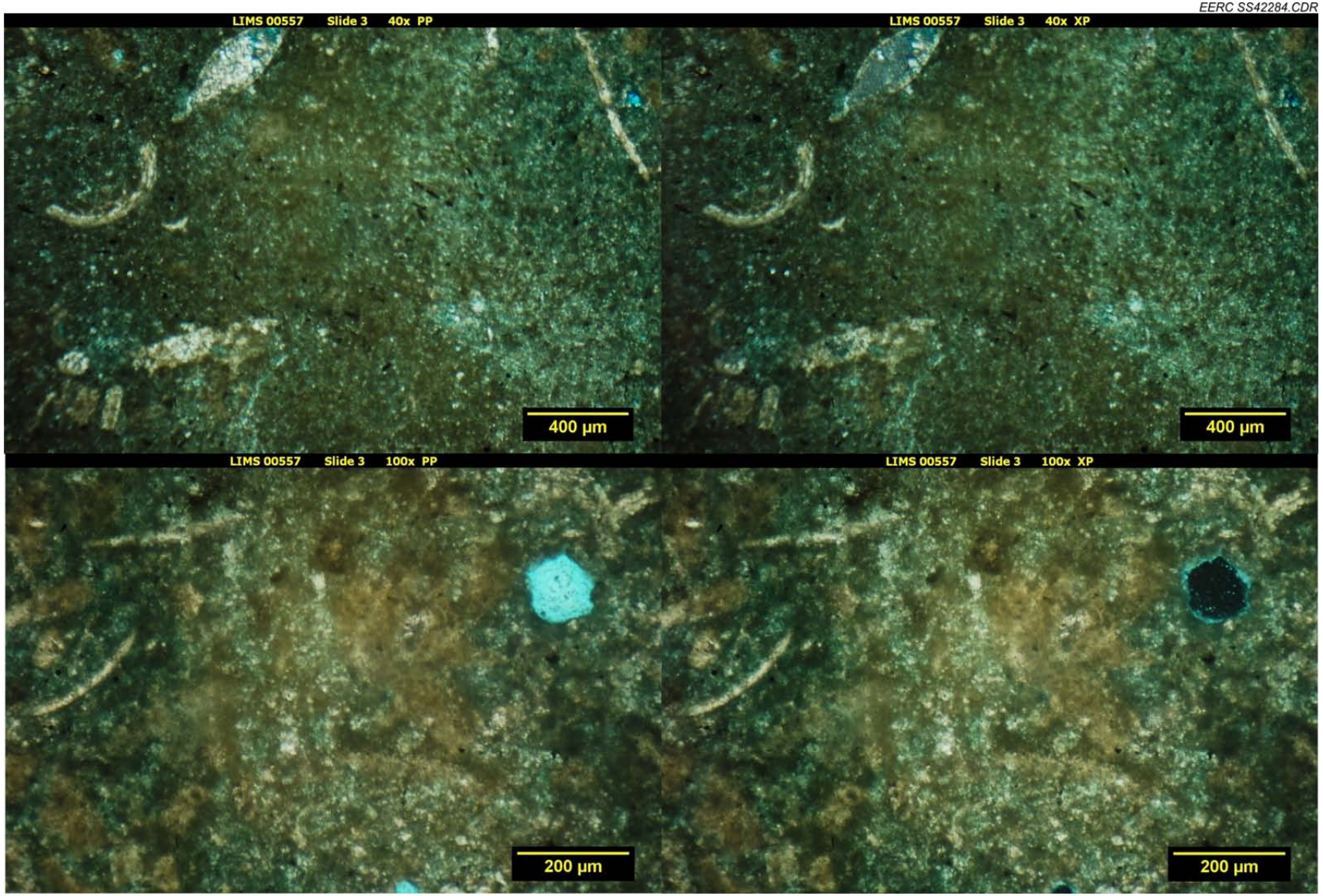

SLIDE 4: WELL 13700, DEPTH 6102.2, CLASS 3, RAMP

Assemblage	Percentage	Comments
Micrite Mud	35%	Mottled
Fossils	5%	Bivalves
Porosity	10%	Pinpoint vugs – mesoporosity
Dolomite Recrystallization Zones	10%	
Metal	Trace	Pyrite
Sparite Cement	40%	Dolomite

This slide has a mixture of sparry cement and micrite mud, which are approximately in equal proportions, but in their own zones of the sample. In addition to sparry cement, a large dolomite recrystallization zone is present over a portion of the sample. Bivalve fossils are present, and porosity exists as pinpoint vugs, representing approximately 10% of the sample (Folk: poorly washed dismicrite/ biosparite, Dunham: mudstone/wackestone).

EERC SS42285.CDR

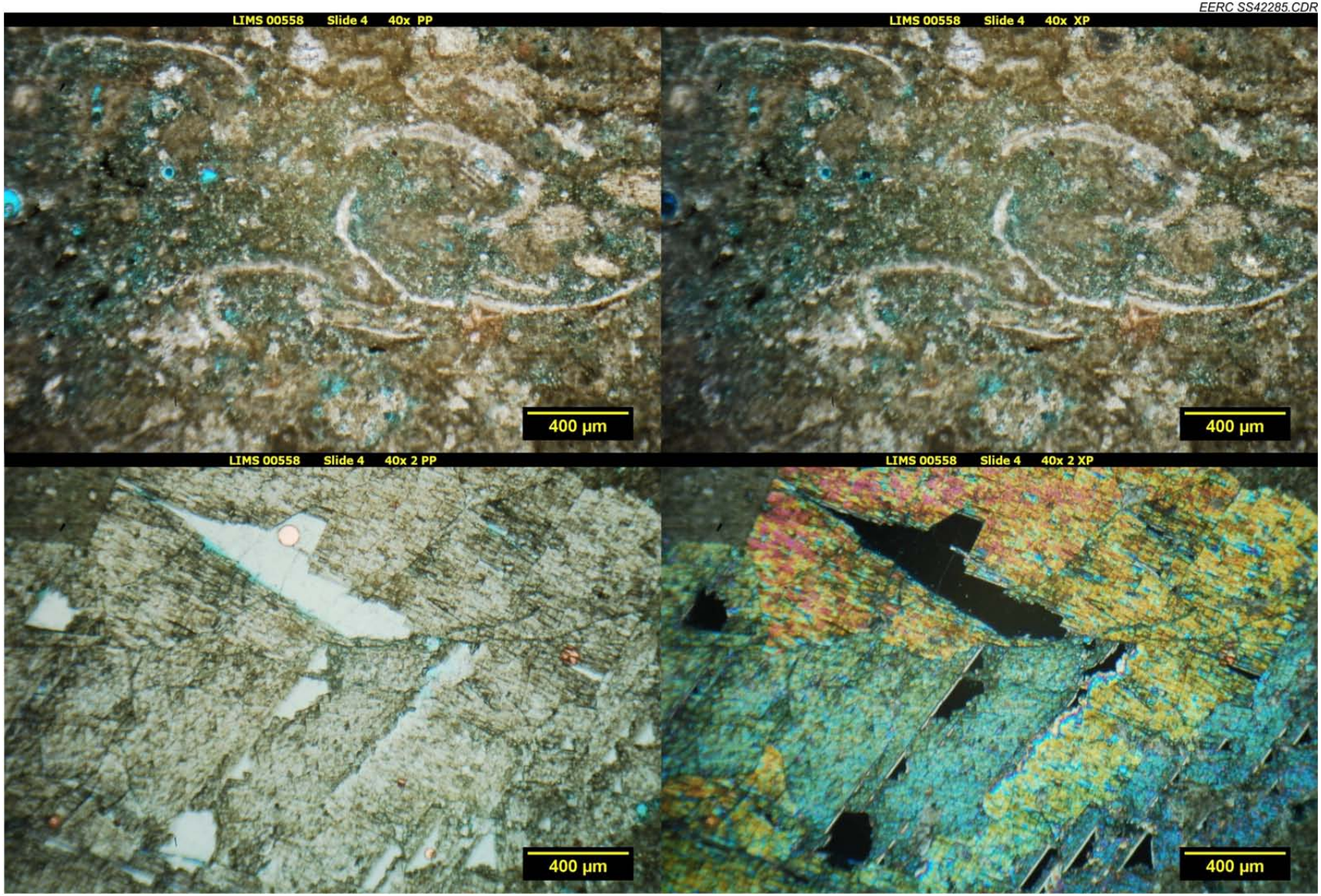

SLIDE 5: WELL 13700, DEPTH 6105.2, CLASS 1, STRAND PLAIN

Assemblage	Percentage	Comments
Carbonate Mud Pellets	70%	
Sparite Cement	10%	Dolomite
Fossils	Trace	Bivalve
Metal	Trace	Pyrite, mostly small, one large grain
Porosity	15%	5% meso, 10% micro

Slide 5 contains a significant portion of porosity as opposed to the previous samples; however, a large portion of it is microporosity. This sample contains a significant portion of pellets bounded by sparry cement (Folk: pelsparite, Dunham: grainstone), although the sample is not completely cemented. Trace bivalve fossils are present as well as dispersed metal (pyrite), which is typically small grain size, with the exception of one fairly large grain.

EERC SS42287.CDR

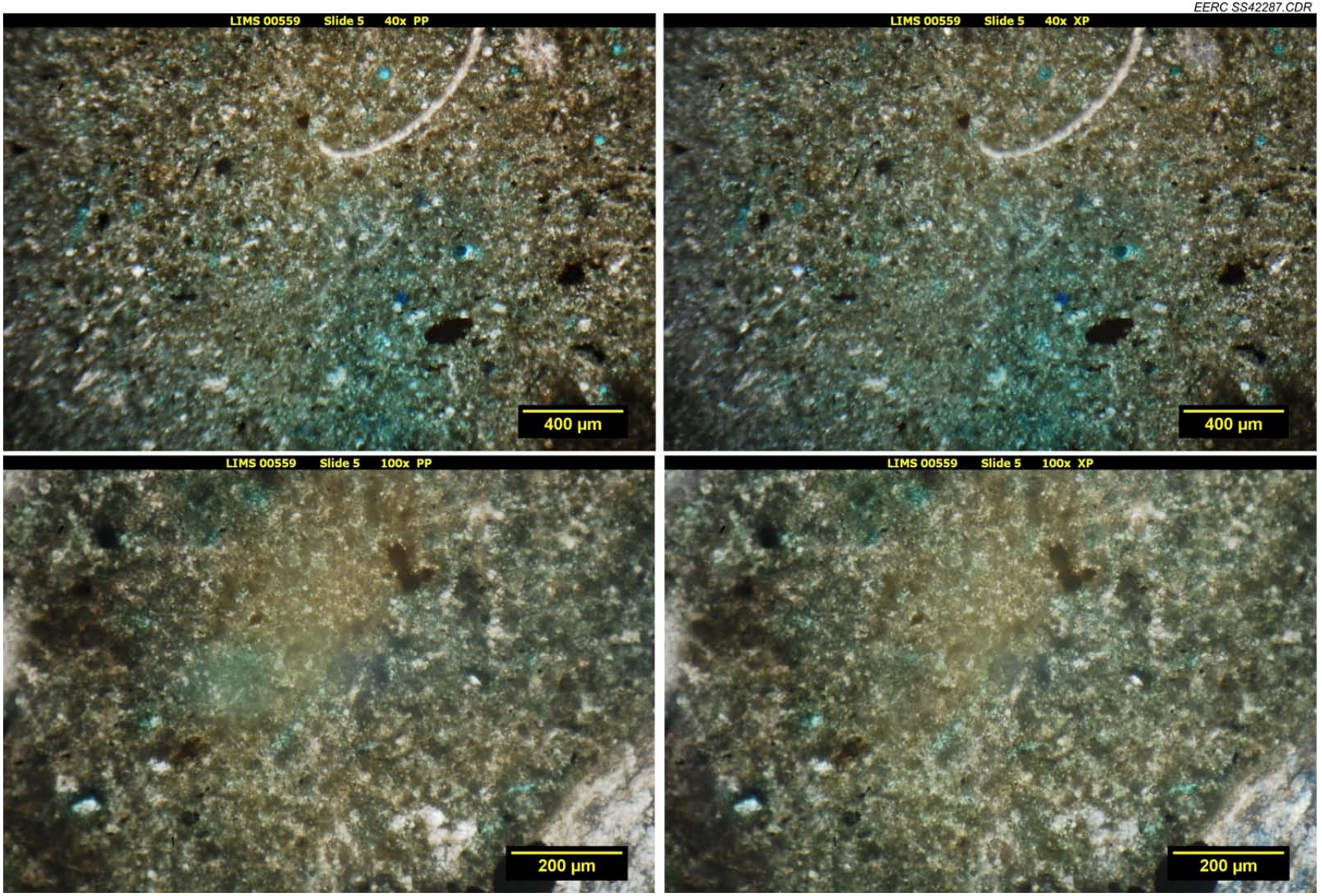

SLIDE 6: WELL 13700, DEPTH 6108.8, CLASS 1, RAMP

Assemblage	Percentage	Comments
Sparry Cement	40%	Including recrystallized zones, dolomite
Clay	10%	Zonal, pore filling
Fossils	10%	Bivalve
Sparite + Pellets	15%	
Porosity	25%	10% macro, 10% meso, 5% micro

This sample has much higher porosity and contains a range of pore sizes. The sample is highly heterogeneous, consisting of minor bedding and zonal recrystallization. Three distinct fabrics were encountered: recrystallized sparite zones, argillaceous carbonate zones, and a partially recrystallized pellet fabric. Bivalve fossils in this sample were larger than previous samples (Folk: biosparite/pelsparite, Dunham: grainstone).

EERC SS42288.CDR

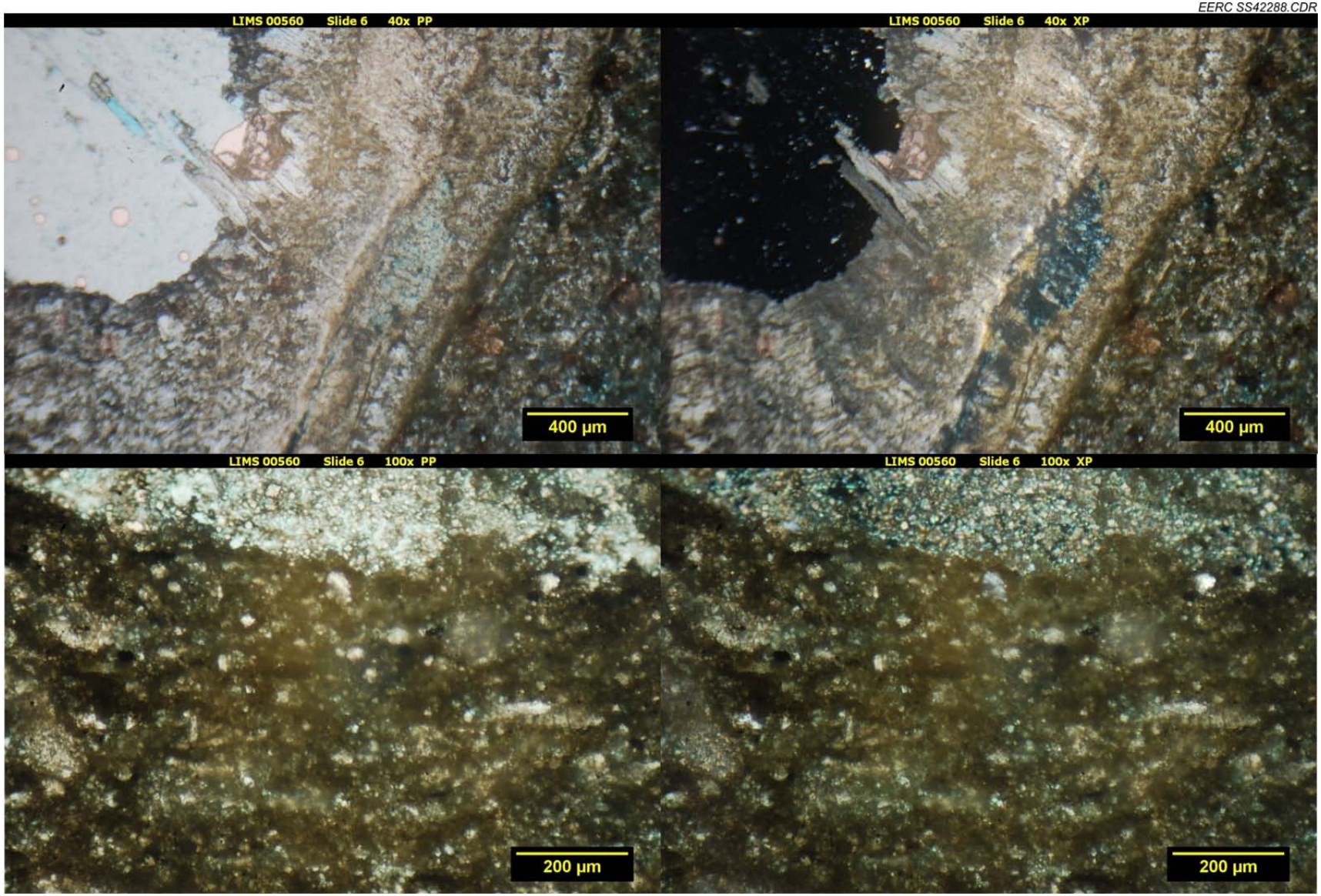

SLIDE 7: WELL 13700, DEPTH 6112.0, CLASS 2, RAMP

Assemblage	Percentage	Comments
Fossils	20%	Bivalve and unidentified tubular
Porosity	5%	Mostly microporosity
Clay	10%	Dispersed
Sparite	50%	Some large recrystallization (10%), most microsparite (40%), dolomitized
Micrite Mud	15%	

This sample had a larger proportion of fossils than other samples. The sample is thinly bedded and dominated by fine-grained sparry cement. A small amount of clay is present in the sample, and porosity is present, although mostly microporosity. Several large voids exist that appear to be dissolved fossils. The sample may contain rare ooids (Folk: biosparite, Dunham: packstone).

EERC SS42289.CDR

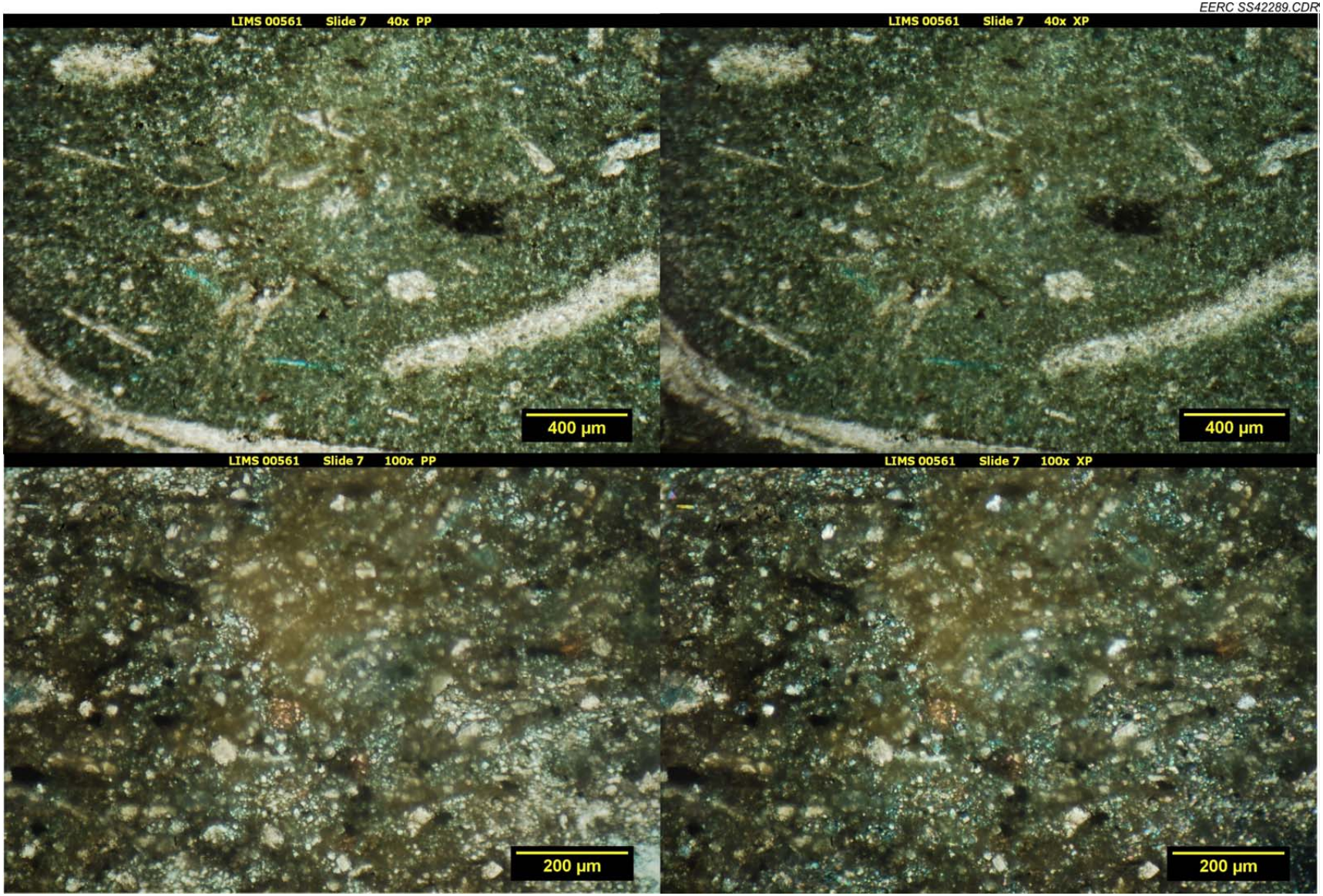

SLIDE 8: WELL 13700, DEPTH 6115.5, CLASS 3, RAMP

Assemblage	Percentage	Comments
Sparite	80%	Dolomite
Porosity	15%	5% macro – dissolved fossils, 10% meso
Pyrite	5%	Appears to be bedding
Fossils	Trace	Bivalve

Sample 8 was an uninteresting homogeneous, porous sparite rock. Large pores appeared to be dissolved fossils, while the majority of porosity was present as gaps between sparry recrystallization. A small amount of bivalve fossils are present as well as some pore-filling pyrite zones (Folk: sparite, Dunham: mudstone).

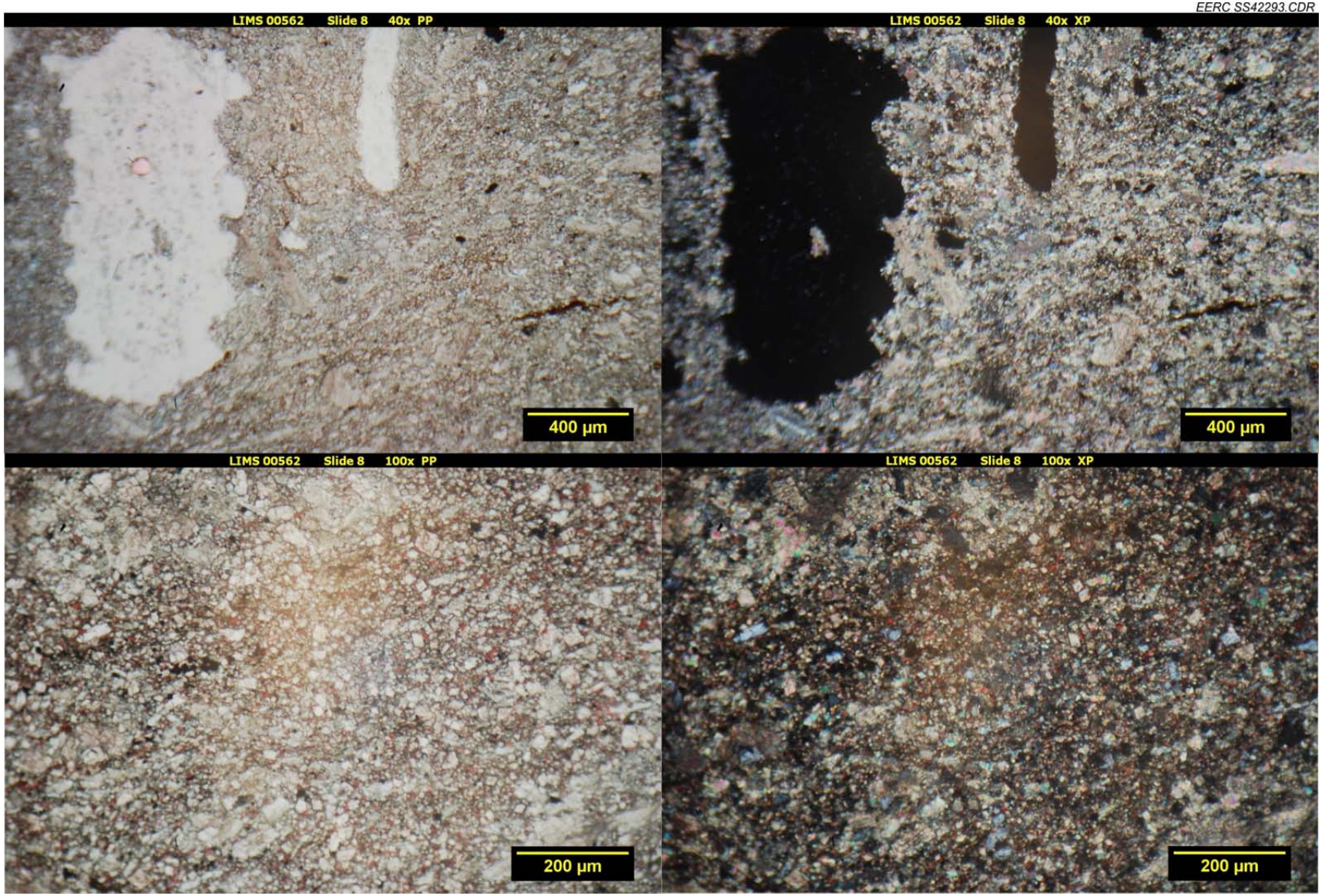
EERC SS42293.CDR
LIMS 00562 Slide 8 40x PP
400 µm
LIMS 00562 Slide 8 40x XP
400 µm
LIMS 00562 Slide 8 100x PP
200 µm
LIMS 00562 Slide 8 100x XP
200 µm

SLIDE 9: WELL 13700, DEPTH 6120.0, CLASS 2, STRAND PLAIN

Assemblage	Percentage	Comments
Micrite Pellets	60%	Possibly muddy ooids
Sparite Cement	30%	Dolomite
Porosity	10%	Mostly meso, some macro

This sample consists of sparite-cemented pellets (Folk: pelsparite, Dunham: grainstone). The sample has been heavily cemented; however, approximately 10% porosity remains between the large pellet (muddy ooid) grains. This sample is microbedded and very clean, with no observed clay, metal, or fossils.

EERC SS42291.CDR

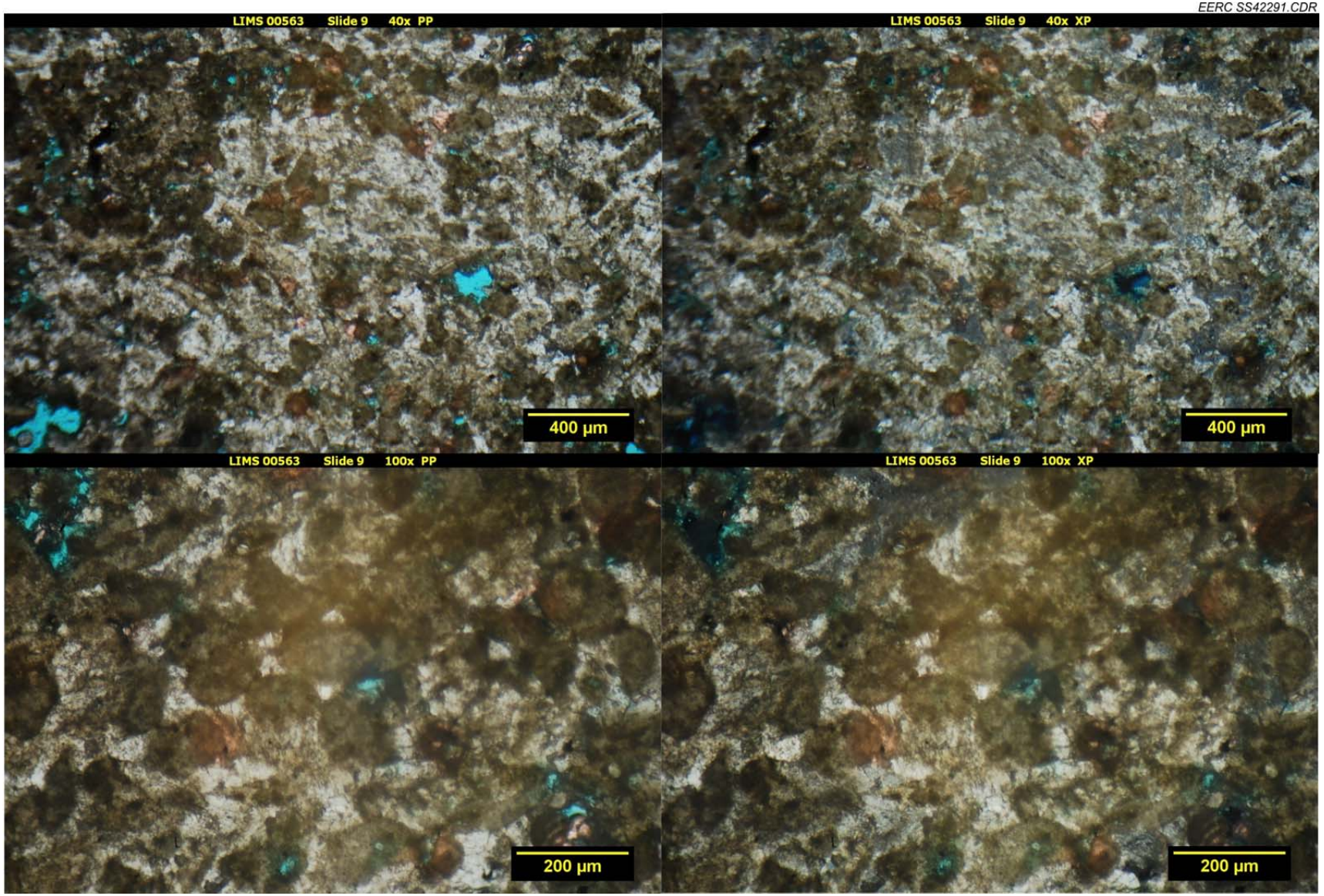

SLIDE 10: WELL 13700, DEPTH 6122.0, CLASS 2, STRAND PLAIN

Assemblage	Percentage	Comments
Micrite Pellets	70%	Possibly muddy ooids
Sparite Cement	20%	5% of which is recrystallized zones, dolomitized
Porosity	10%	Mesoporosity size

Slide 10 is a prominent pelsarite (oosparite – Folk) or grainstone (Dunham), consisting of a large number of muddy pellets or ooids bonded together by sparite cement. Approximately 10% porosity remains in the sample. No metal or fossils were observed in this sample. Pellets are similar to the last sample, being much larger than the early pellet-containing fossils.

EERC SS42292.CDR

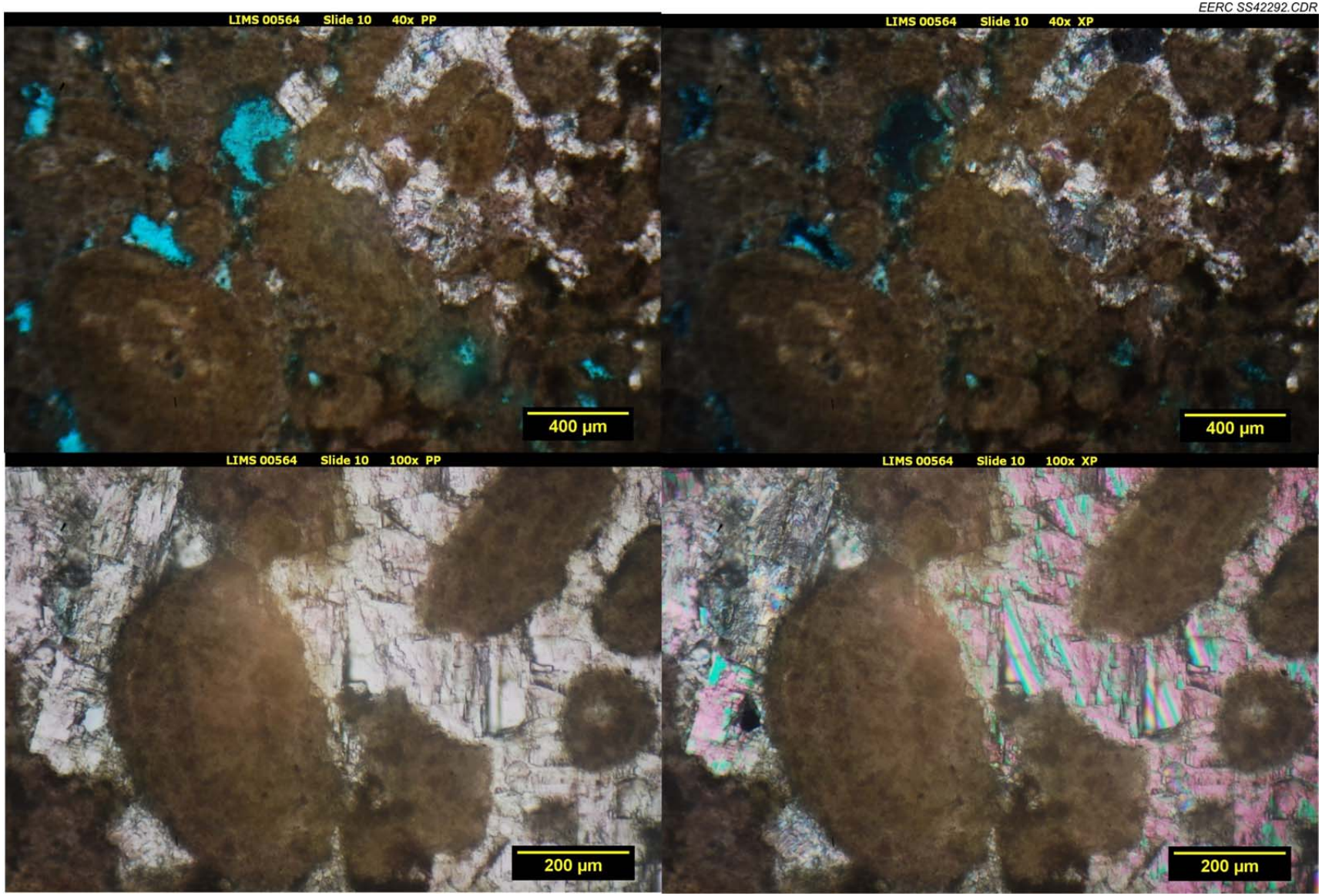

SLIDE 11: WELL 13700, DEPTH 6129.0, CLASSES 1 AND 3, BACK RAMP/STRAND PLAIN

Assemblage	Percentage	Comments
Micrite Mud	65%	
Porosity	10%	Micro–meso, pinpoint vugs
Siderite	25%	

Assemblage	Percentage	Comments
Ooids	60%	
Porosity	15%	
Micrite Mud	15%	
Salt	5%	Anhydrite pore filling
Sparite	5%	Dolomite

Two facies in individual but poorly defined beds are present in Slide 11. The first is a micrite mudstone (Folk–Dunham) that contains significant siderite and poorly developed porosity. The mud appears clean, with no fossils, metal, or clay present.

The second facies is an ooid grainstone (Dunham, oosparite – Folk) that has significant porosity and some (carbonate) muddy zones. Some pores contain salt, likely anhydrite. Sparite cement is present that has most likely been dolomitized. Again, no fossils, clay, or metal were observed in the sample.

EERC SS42295.CDR

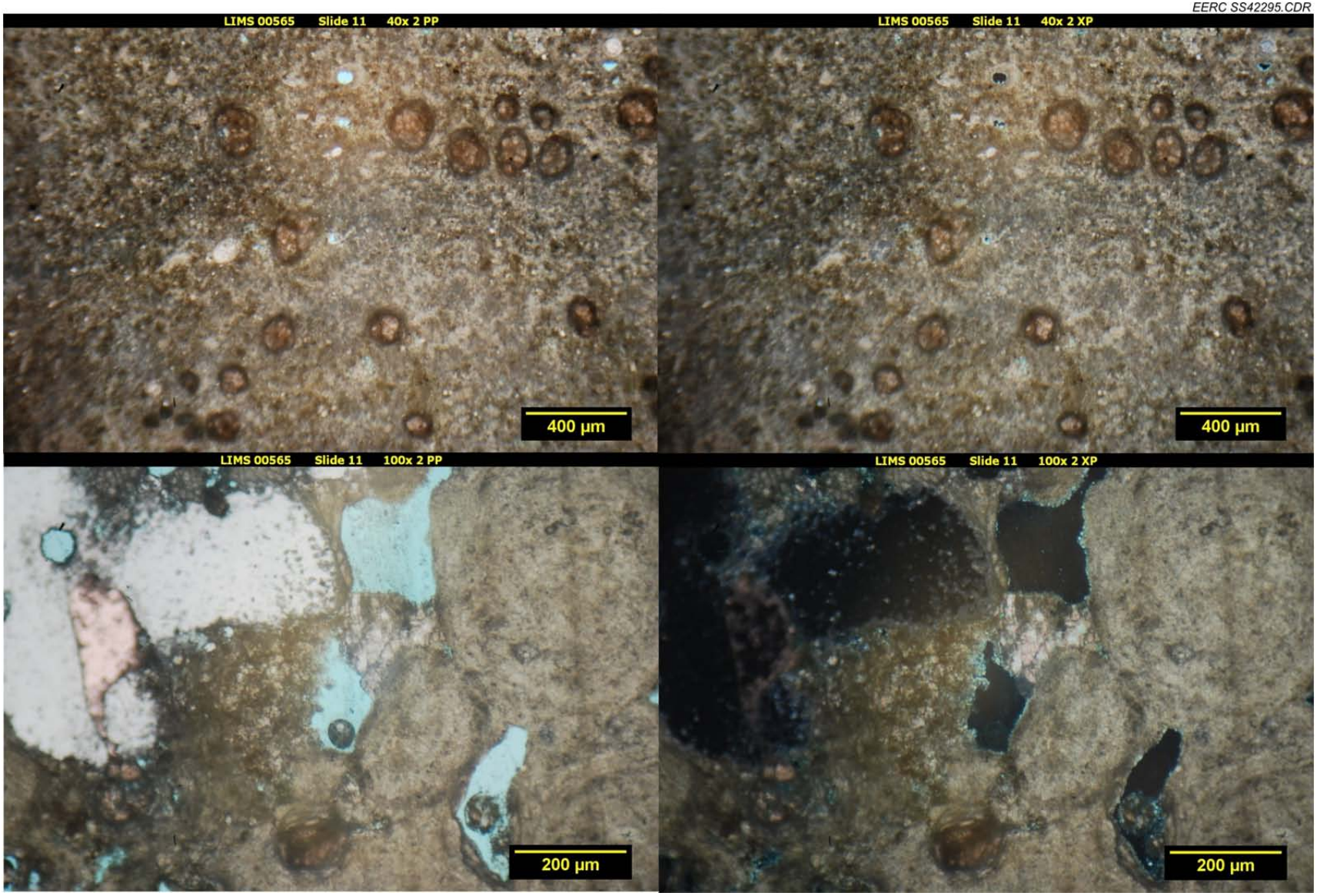

EERC SS42294.CDR

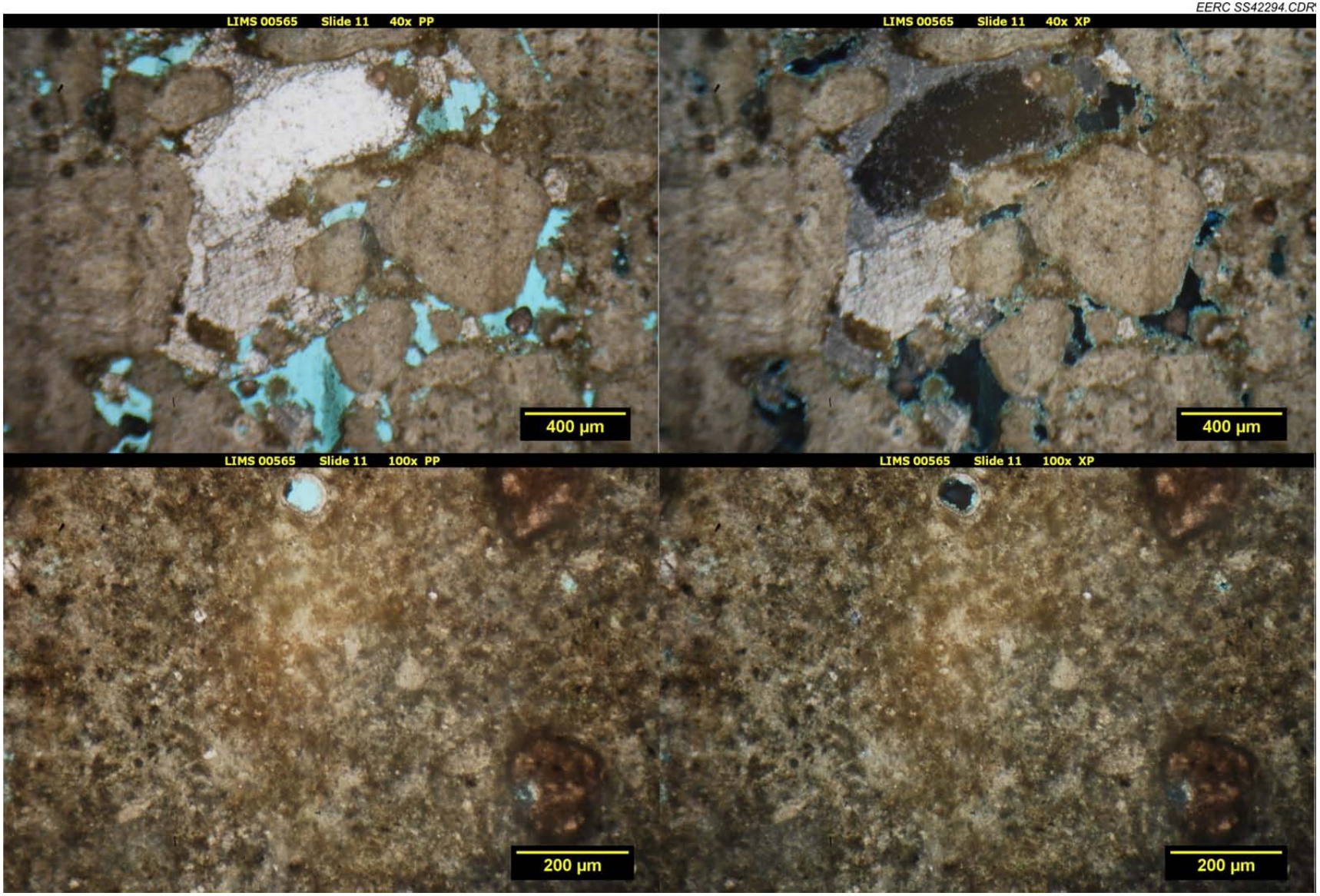

SLIDE 12: WELL 13700, DEPTH 6141.0, CLASS 3, STRAND PLAIN/BACK RAMP

Assemblage	Percentage	Comments
Micrite Mud	75%	
Sparite	10%	Dolomite recrystallization
Porosity	10%	Microporous
Carbonate Mud Pellets	5%	
Pyrite	Trace	In stylolites

Much of this sample is micrite mud, with some recrystallized sparitic zones. A portion of microporosity is retained in the sample, as well as a few pellets, which form microbanklike structures. Two stylolites are present in the section and appear to be filled with metal, likely pyrite (Folk: micrite/dismicrite, Dunham: mudstone).

EERC SS42296.CDR

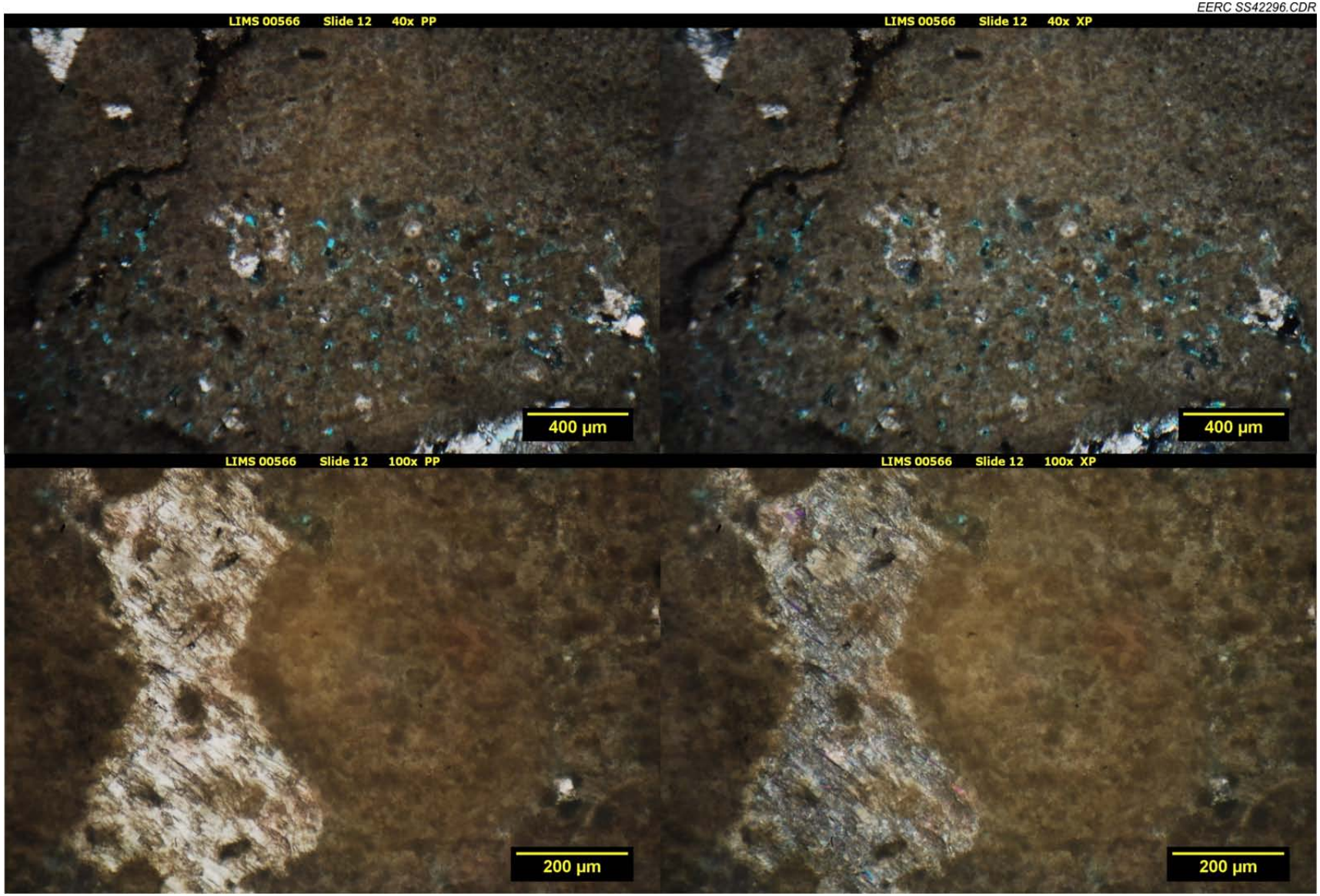

SLIDE 13: WELL 13700, DEPTH 6144.9, CLASS 1, STRAND PLAIN

Assemblage	Percentage	Comments
Muddy Ooids	60%	Large pellets
Sparite	15%	Dolomite
Pyrite	Trace	In stylolites
Micrite	15%	In mudstone bed
Porosity	10%	Mesoporosity

Slide 13 is a slightly porous grainstone similar to Slides 9 and 10. Muddy ooids (or large pellets) make up the majority of the sample, cemented together by sparite (Folk: oosparite/pelsparite, Dunham: grainstone). A pyrite-filled stylolite cuts across the sample, as does a mudstone bed, which constitutes approximately 15% of the sample.

EERC SS42297.CDR

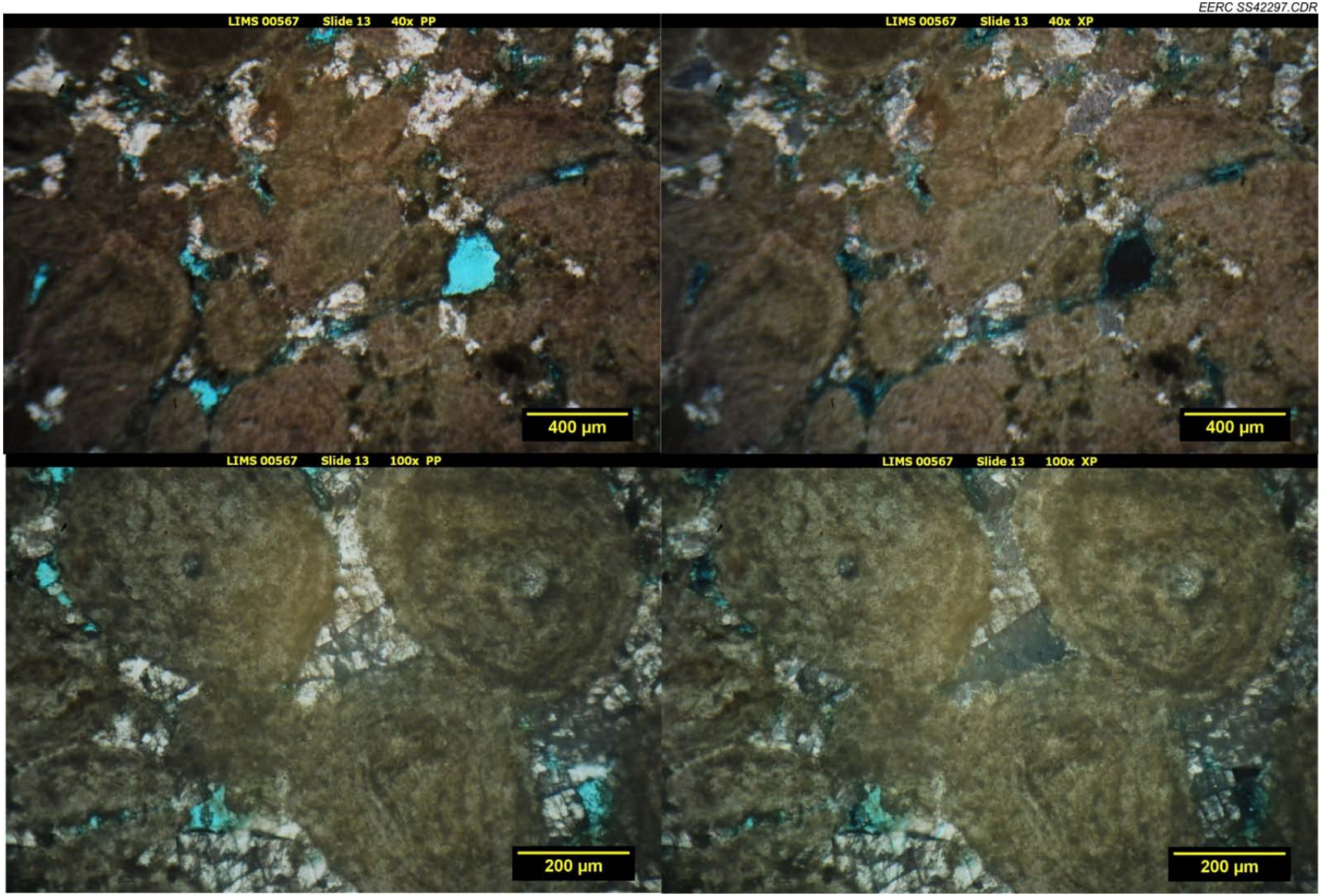

SLIDE 14: WELL 16409, DEPTH 6194.0, CLASS 3, STRAND PLAIN, APPROACHING RAMP

Assemblage	Percentage	Comments
Micrite Mud	70%	
Sparite Cement	15%	Dolomite
Porosity	5%	Mostly micro, some meso
Pyrite	5%	Stylolite filling
Fossils	5%	Bivalves

Prominent stylolites cut across the sample and are filled with metal (pyrite). The sample itself contains a majority of micrite mud, with a small amount of fossil bivalves. Sparite exists in the sample as recrystallized zones and mineral cement. Two different fabrics are present in the sample, muddy beds, which are nearly all laminated carbonate mud, and muddy pellet-rich beds, with sparite cements (Folk: pelsparite/micrite, Dunham: grainstone/mudstone).

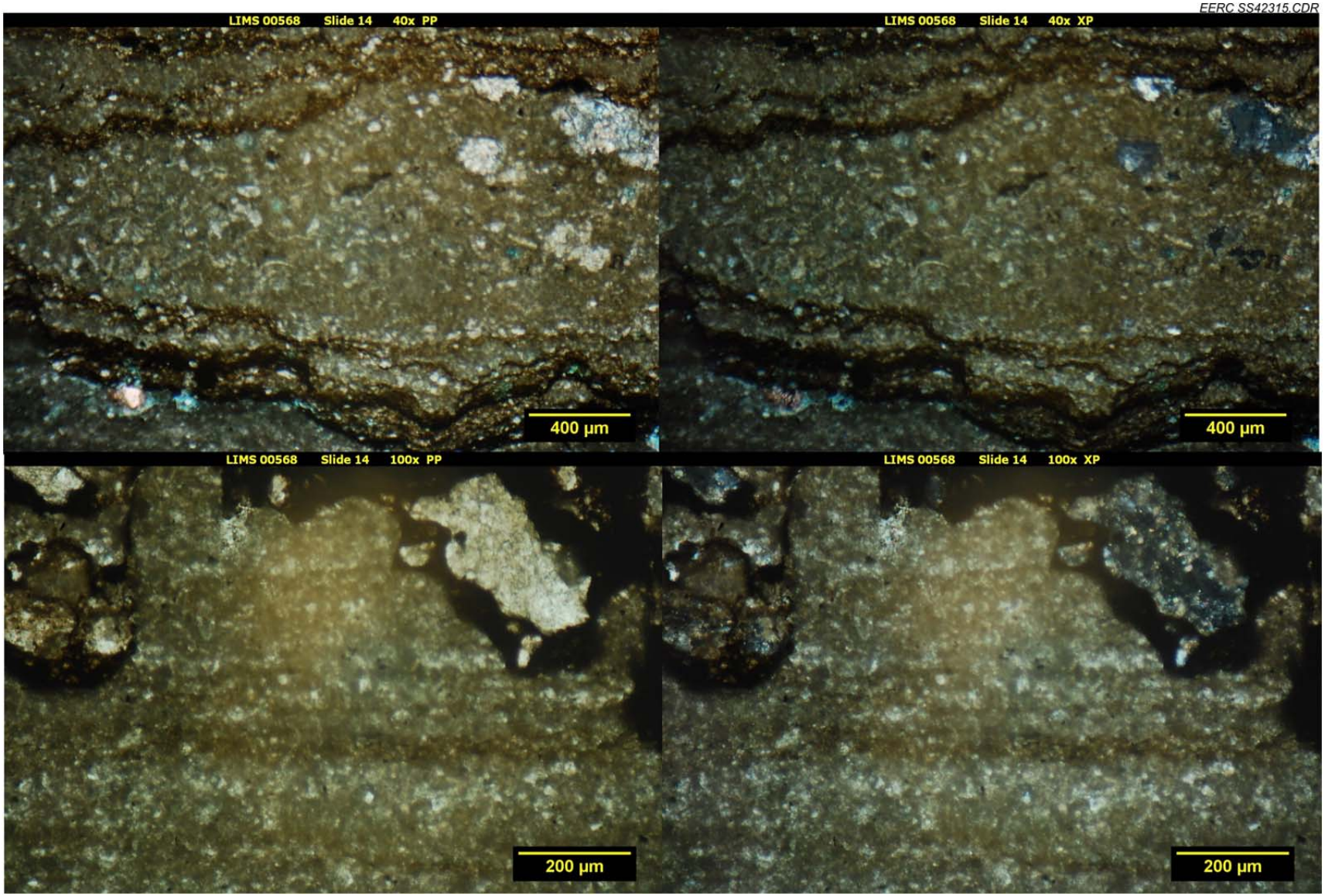
EERC SS42315.CDR
LIMS 00568 Slide 14 40x PP
400 µm
LIMS 00568 Slide 14 40x XP
400 µm
LIMS 00568 Slide 14 100x PP
200 µm
LIMS 00568 Slide 14 100x XP
200 µm

SLIDE 15: WELL 16409, DEPTH 6200.0, CLASS 3, RAMP

Assemblage	Percentage	Comments
Sparite	45%	Fine-grained, dolomite
Pyrite	10%	
Anhydrite	Trace	Anhedral
Micrite	45%	
Fossils	Trace	Bivalve

Sample 15 contains approximately equal quantities of micrite and sparite. The sample has a small proportion of tiny bivalve fossils. No porosity was observed. Pyrite metal is dispersed as small lenticular psuedolaminations throughout the sample. Several anhydrite crystals were observed in the sample, devoid of crystal habits (Folk: poorly washed dismicrite, Dunham: mudstone).

EERC SS42314.CDR

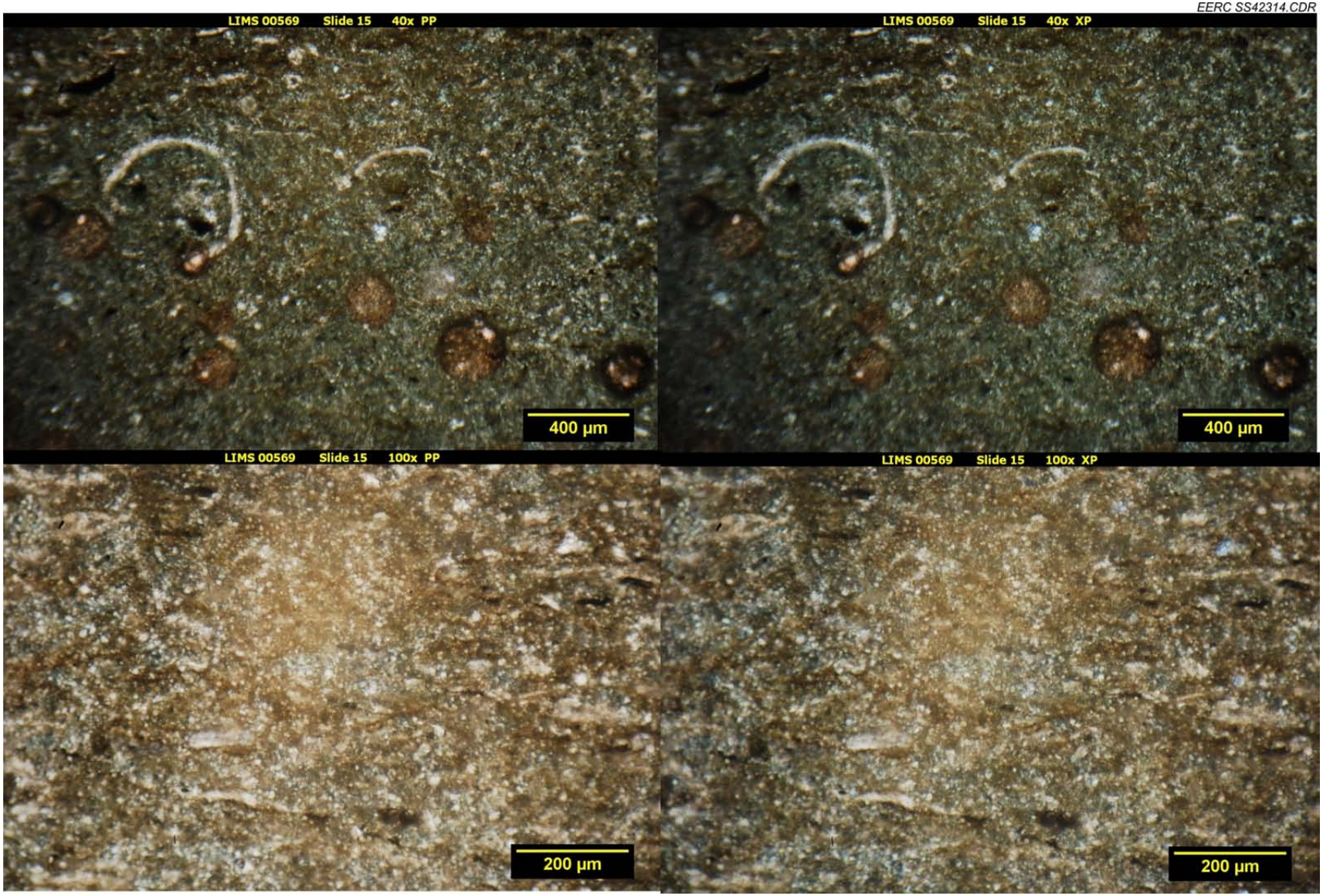

SLIDE 16: WELL 16409, DEPTH 6203.8, CLASS 3, RAMP

Assemblage	Percentage	Comments
Sparite	45%	Microsparite and recrystallized zones
Micrite Mud	30%	
Clay	15%	
Fossils	10%	Disaggregated
Porosity	Trace	Microporosity

This sample is loosely bedded and contains variable clay, mud, and sparite amongst the zones. Beds are of variable thickness. Fossils are present throughout the sample, although slightly higher concentrations appear to be in some beds. No metals were observed in this sample. The sample contains very little porosity (Folk: dismicrite, Dunham: mudstone).

EERC SS42300.CDR

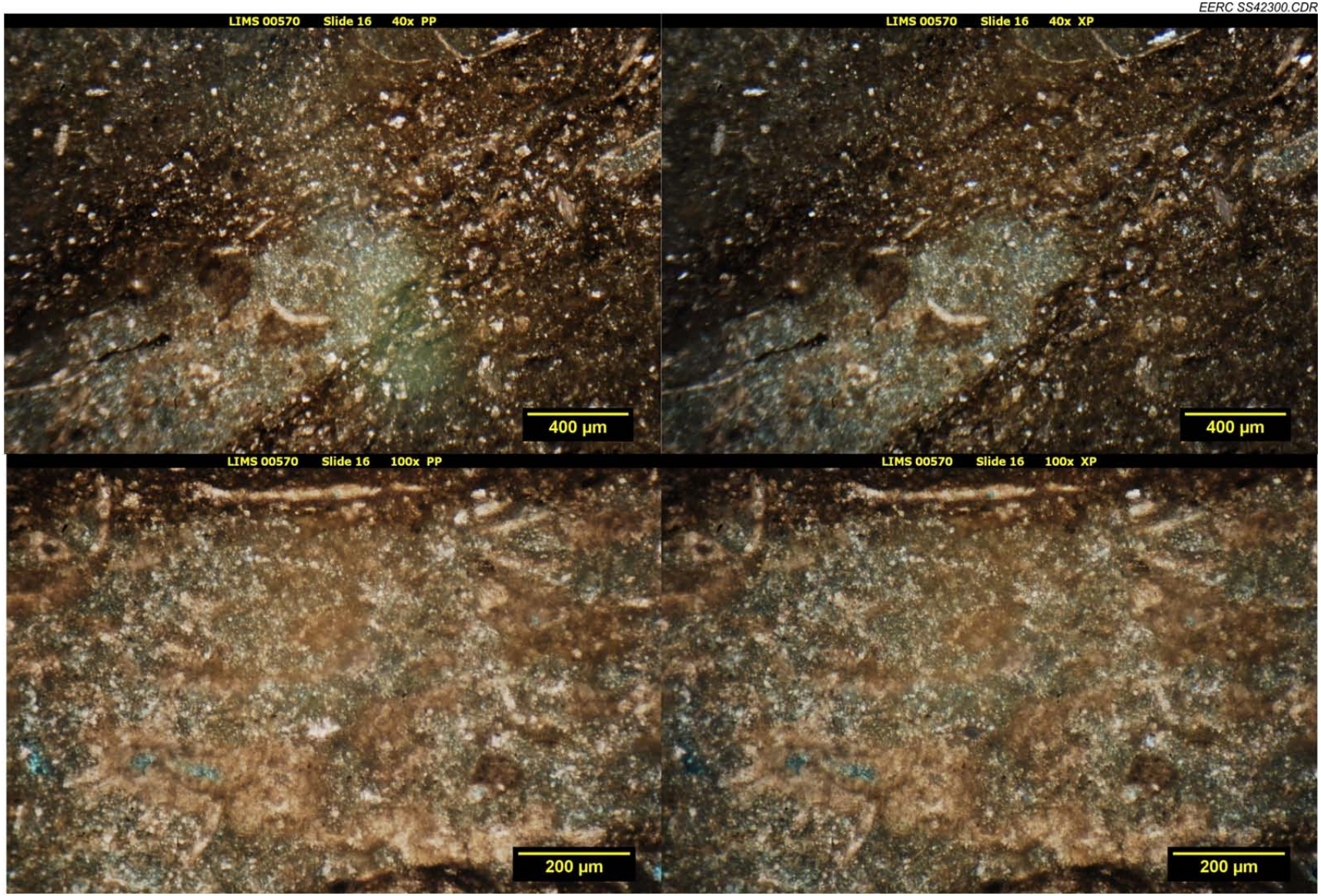

SLIDE 17: WELL 16409, DEPTH 6208.0, CLASS 3, RAMP (STORM DEPOSIT)

Assemblage	Percentage	Comments
Micrite Mud	50%	
Sparite	20%	Fine grained, with the exception of rare massive recrystallization
Clay	15%	Dispersed
Fossils	10%	Disaggregated
Porosity	5%	Shelter

Slide 17 is a very disorganized, mottled biodismicrite (Folk)/floatstone (Dunham). The sample is mottled, and fossil orientation is in different directions. Sample groundmass is mixed micrite and fine-grained sparite, with dispersed clay. A small amount of porosity is preserved in the sample. Several small stylolites are present in the sample. A significant portion of the sample has experienced secondary dolomite growth.

EERC SS42299.CDR

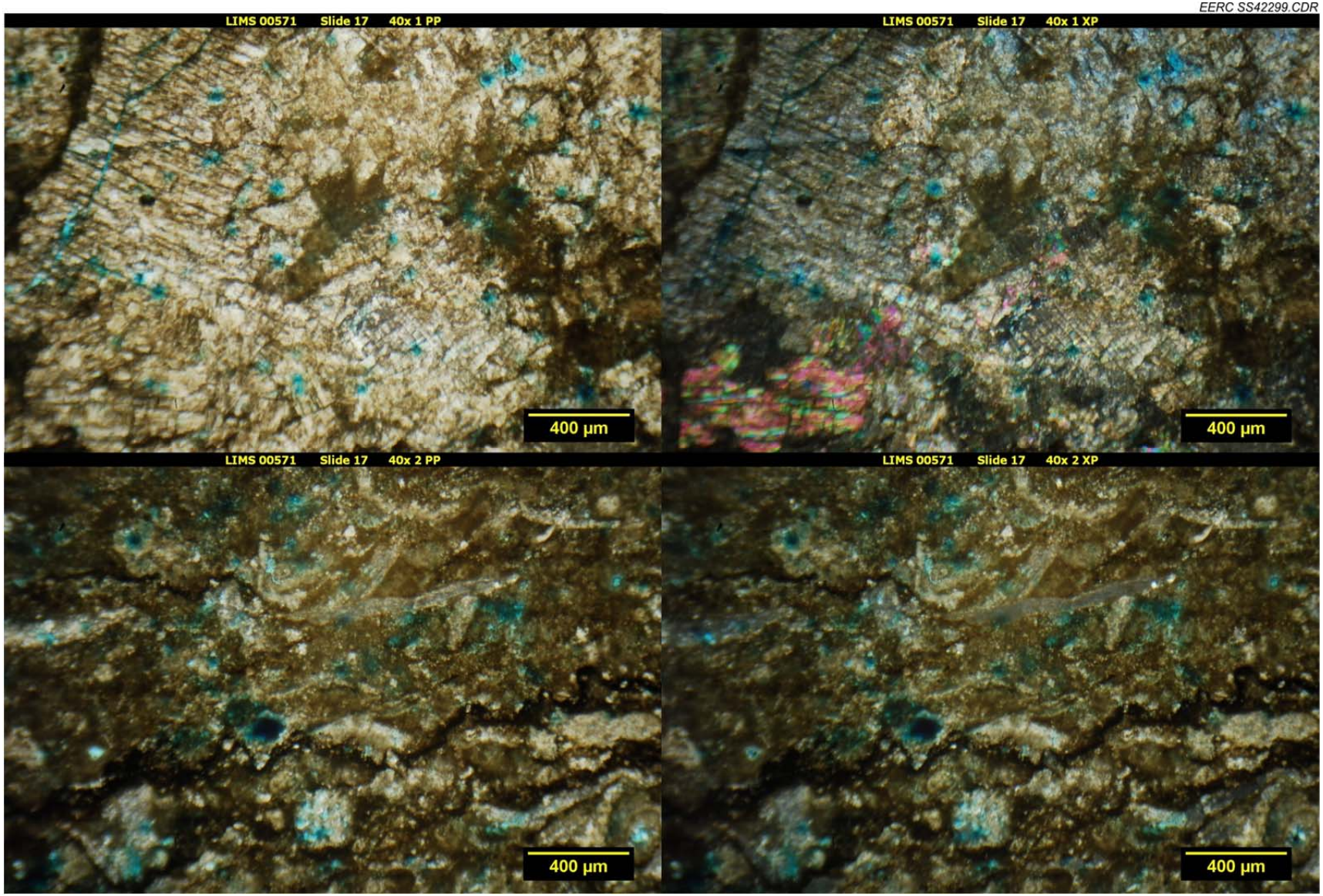

SLIDE 18: WELL 16409, DEPTH 6212.9, CLASS 1, STRAND PLAIN

Assemblage	Percentage	Comments
Muddy Ooids	65%	Possibly large pellets
Porosity	15%	Macro- to mesoporosity
Metal	10%	Pyrite, acting as cement
Sparite	10%	Dolomite

This porous sample contains muddy ooids cemented together by dolomite and, in some areas, metal (Folk: oosparite, Dunham: grainstone). Porosity is intragranular and macro- to mesoporosity in size. Some areas have nearly choked themselves off with cement, while other regions appear fairly clear.

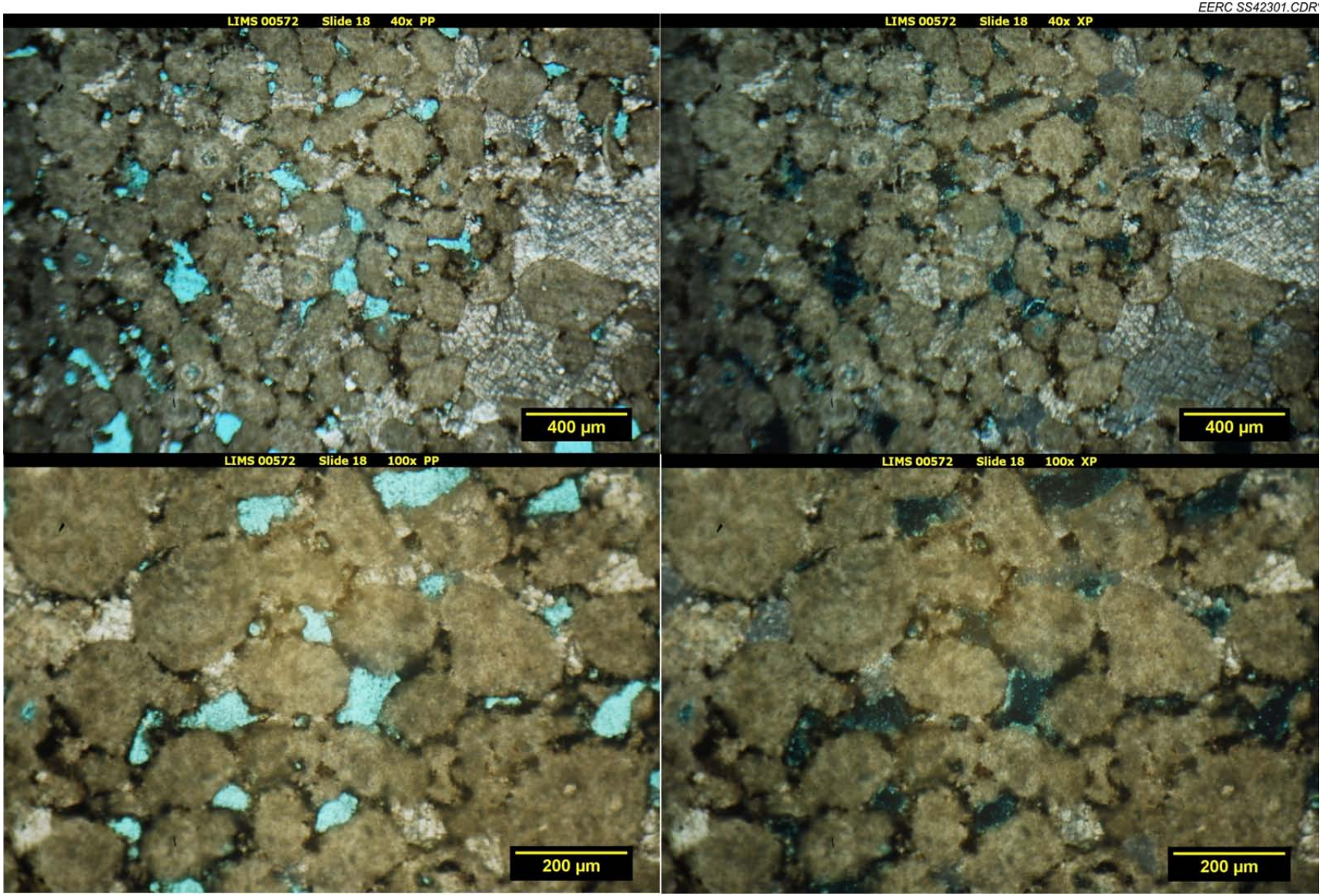
EERC SS42301.CDR
LIMS 00572 Slide 18 40x PP
400 µm
LIMS 00572 Slide 18 40x XP
400 µm
LIMS 00572 Slide 18 100x PP
200 µm
LIMS 00572 Slide 18 100x XP
200 µm

SLIDE 19: WELL 16409, DEPTH 6214.6, CLASS 2, DEEP RAMP

Assemblage	Percentage	Comments
Sparite	80%	Fine-grained dolomite
Porosity	10%	Mostly micro, trace meso
Clay	10%	Dispersed
Metal	Trace	Pyrite
Fossils	Trace	Bivalve

Slide 19 contains a large amount of fine-grained sparite. Portions of the sample are argillaceous, containing dispersed clay and anhedral pyrite grains. The sample is porous, although most appears to be microporosity confined to aggregated sparry zones. The sample has no visible microstructure (Folk: sparite, Dunham: mudstone).

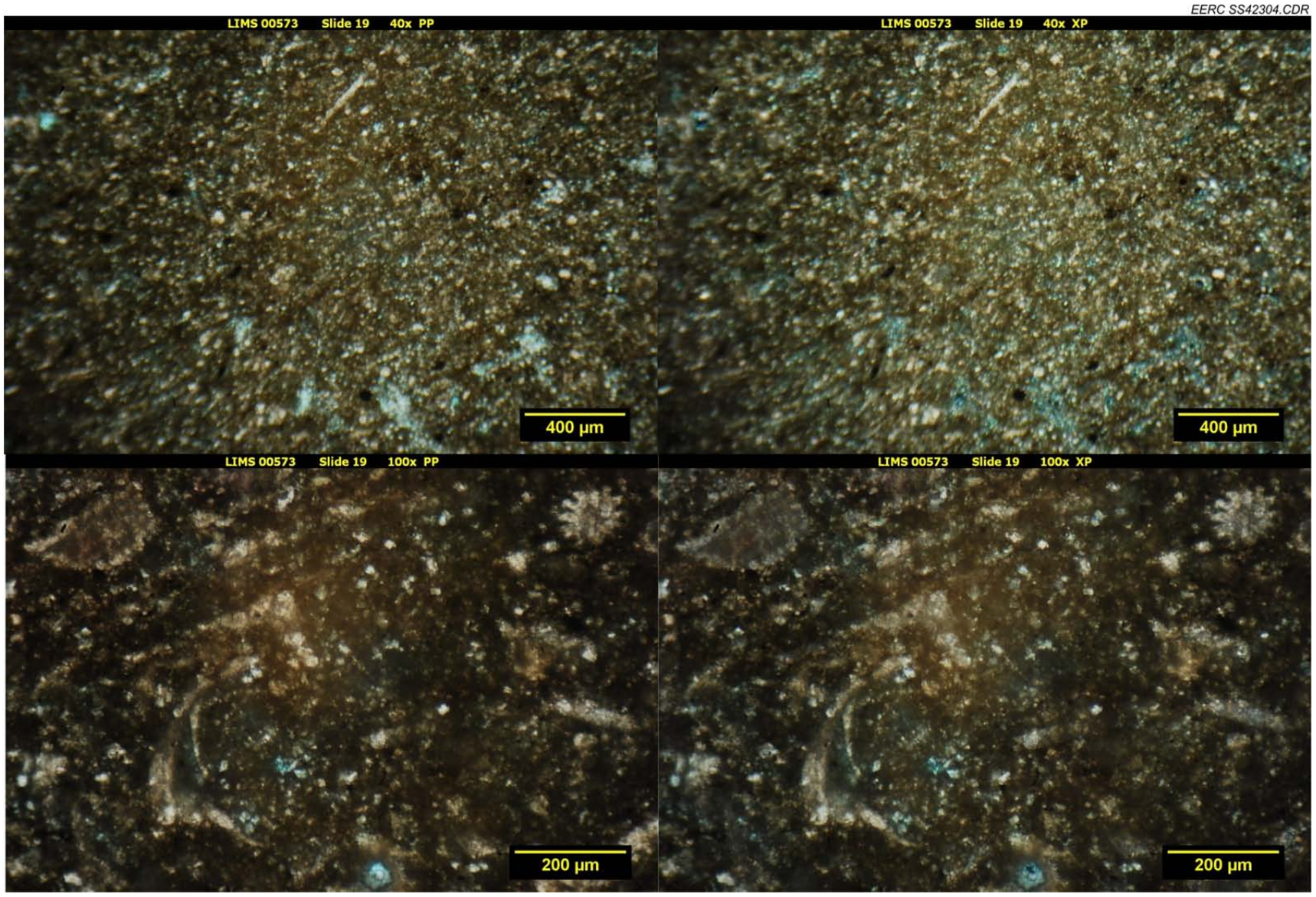
EERC SS42304.CDR
LIMS 00573 Slide 19 40x PP
400 µm
LIMS 00573 Slide 19 40x XP
400 µm
LIMS 00573 Slide 19 100x PP
200 µm
LIMS 00573 Slide 19 100x XP
200 µm

SLIDE 20: WELL 16409, DEPTH 6216.0, CLASS 3, DEEP RAMP

Assemblage	Percentage	Comments
Micrite Mud	40%	
Clay	25%	Dispersed, zonal
Sparite	20%	Fine-grained
Fossils	10%	Bivalve (clam) cephlapod
Porosity	5%	Pinpoint vug

Slide 20 contains a higher portion of micrite mud, but retains a small percentage of sparry dolomite within the fabric. Zonal clay is dispersed throughout the sample. Scattered fossil remnants are present in the sample, including large, thin, rippled shells (clam). A small amount of porosity is present as pinpoint vugs (Folk: biodismicrite, Dunham: floatstone).

EERC SS42303.CDR

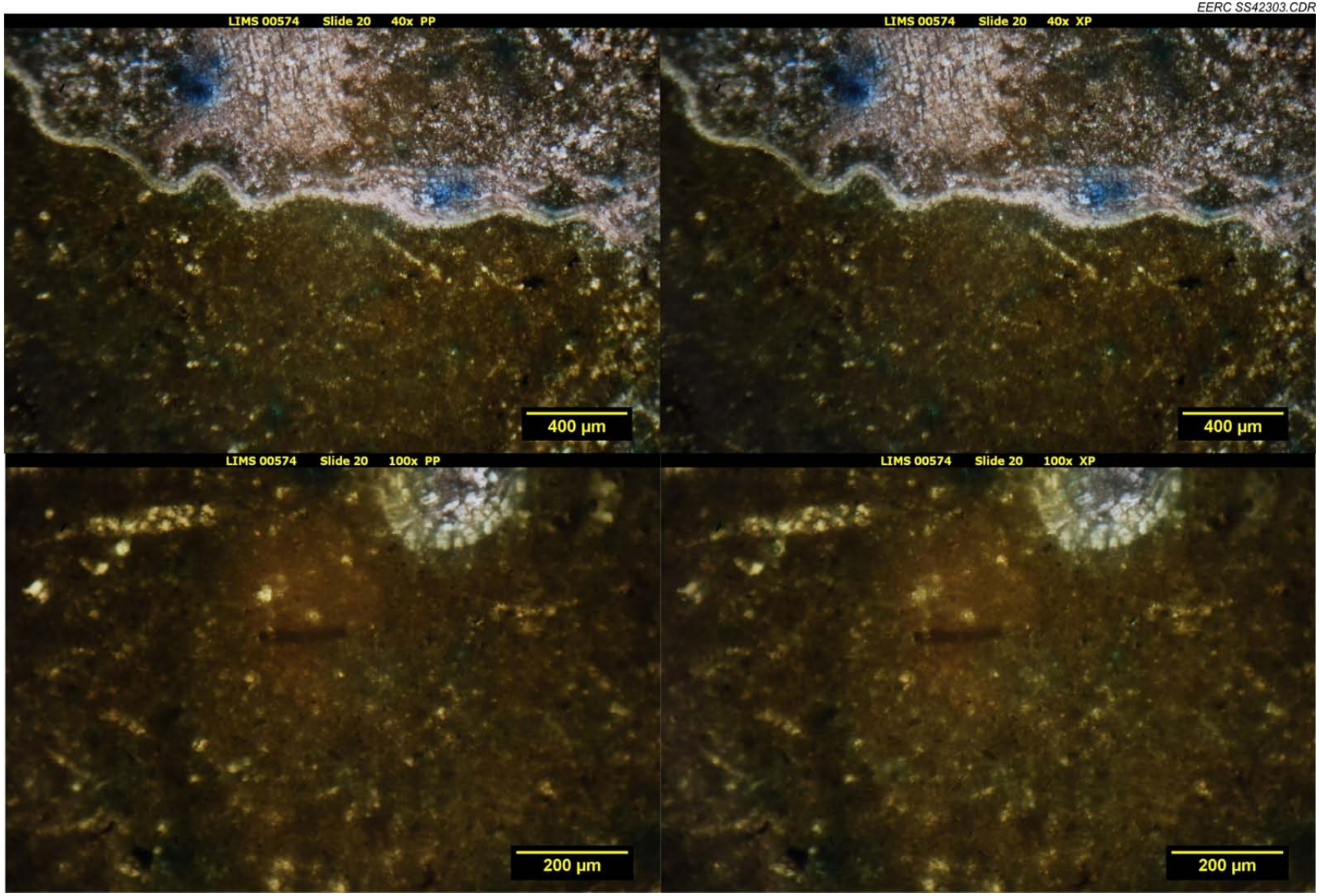

SLIDE 21: WELL 16409, DEPTH 6217.3, CLASS 3, RAMP (STORM DEPOSIT)

Assemblage	Percentage	Comments
Micrite Mud	40%	
Sparite	35%	Fine-grained, dolomite
Clay	15%	Dispersed
Fossil Fragments	10%	Disaggregated
Ooids	Trace	
Metal	Trace	Pyrite, coarse, subhedral

Sample 21 represents a higher energy sample, where fossils became disaggregated and sediments were mixed and blended. The sample also contains trace ooids and considerable clay. The sample contains little microstructure, but is heavily mottled. Micrite and sparite areas are zoned throughout the sample (Folk: poorly washed dismicrite/biosparite, Dunham: wackestone).

EERC SS42352.CDR

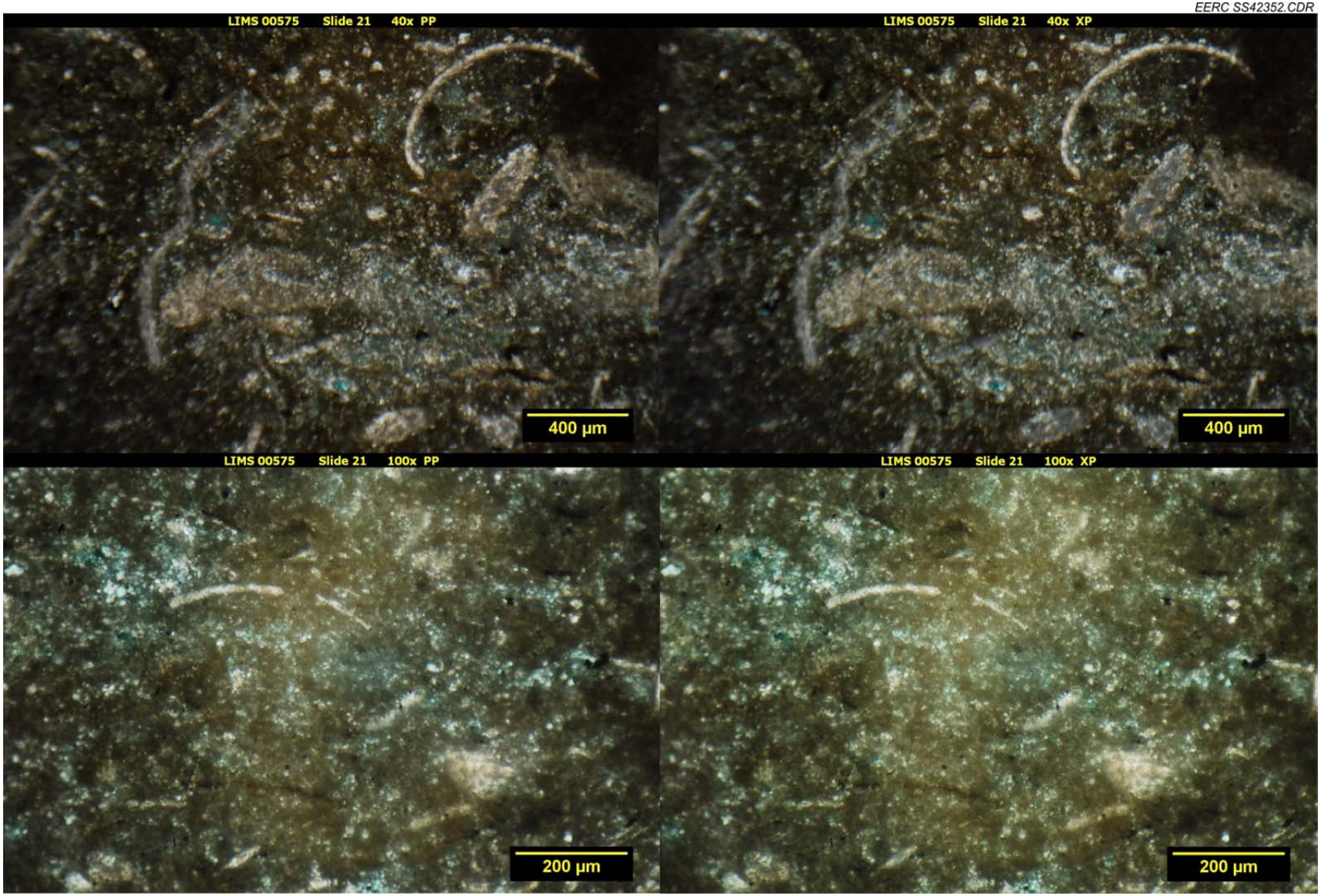

SLIDE 22: WELL 16409, DEPTH 6220.3, CLASS 3, RAMP

Assemblage	Percentage	Comments
Sparite	85%	Fine-grained, dolomite
Porosity	10%	Pinpoint vugs, meso/macroporosity
Fossils	Trace	Bivalves
Metal	5%	Pyritic
Concretions	Trace	Siderite

Slide 22 is loosely bedded/laminated and porous, containing numerous pinpoint vugs. The sample is largely fine-grained sparite (Folk: sparite, Dunham: mudstone). Beds range from solid sparite with metal microlaminations to more aggregated and porous.

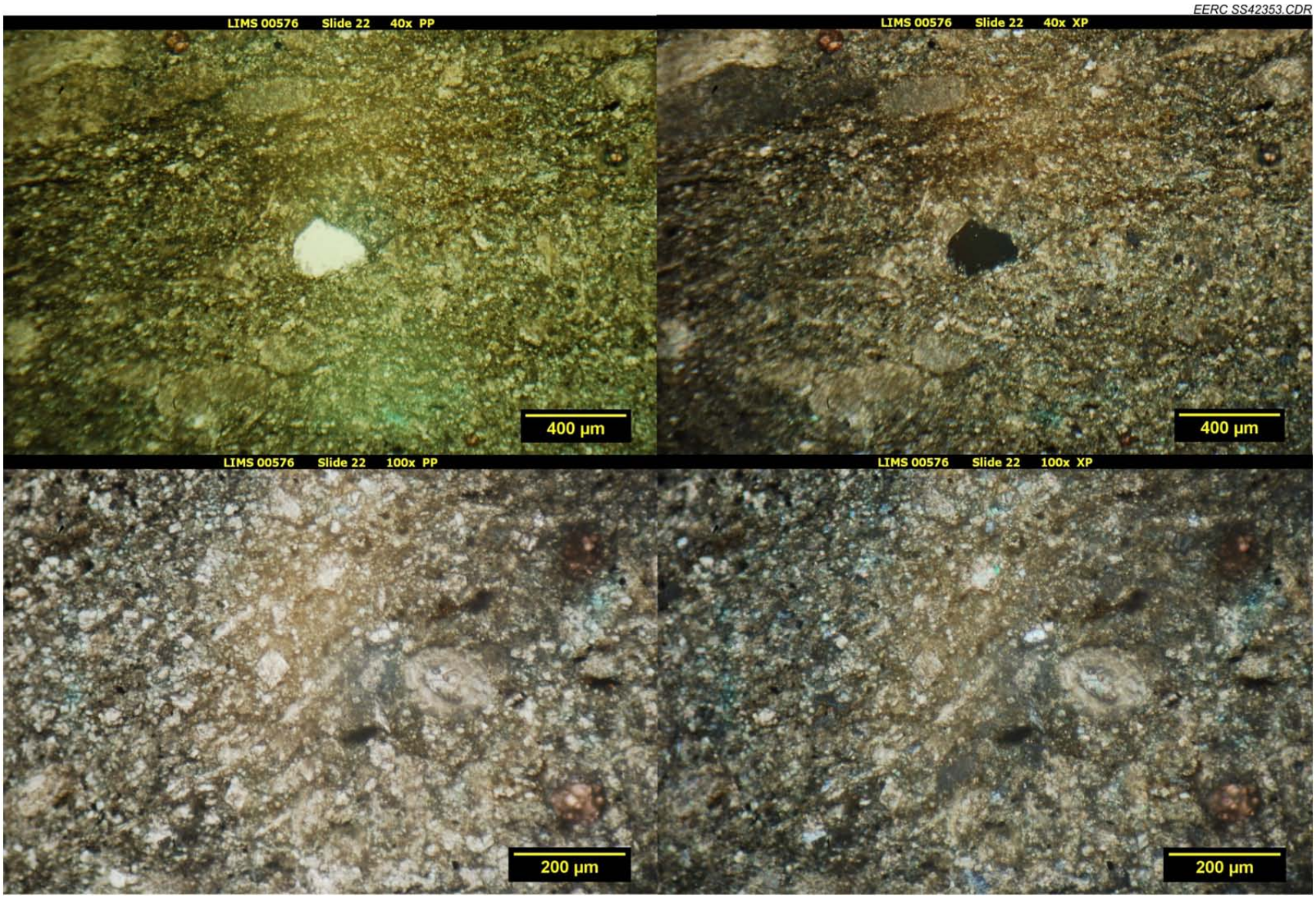
EERC SS42353.CDR
LIMS 00576 Slide 22 40x PP
400 µm
LIMS 00576 Slide 22 40x XP
400 µm
LIMS 00576 Slide 22 100x PP
200 µm
LIMS 00576 Slide 22 100x XP
200 µm

SLIDE 23: WELL 16409, DEPTH 6223.0, CLASS 2, RAMP

Assemblage	Percentage	Comments
Sparite	50%	Fine-grained, dolomite
Micrite Mud	30%	
Porosity	10%	Pinpoint vuggy
Clay	5%	Dispersed
Fossils	5%	Bivalves

This porous sample is a fairly well sorted mixture of fine-grained sparite and micrite mud. The sample has a minor amount of argillaceous material and fossils. No microstructures are present, and the sample contains less metal than other intervals (Folk: poorly washed sparite, Dunham: mudstone).

EERC SS42316.CDR

SLIDE 24: WELL 16409, DEPTH 6224.2, CLASS 1, STRAND PLAIN

Assemblage	Percentage	Comments
Pellets	60%	Micritic, possibly muddy ooids
Sparite	25%	Coarse-grained, dolomite
Porosity	15%	Up to macro in size

Slide 24 contains a large concentration of muddy pellets/structureless muddy ooids. The sample is porous and contains macro and mesoporosity sizes. The grains are cemented with dolomitic sparite, which comprises approximately 25% of the sample. No metal or biologic evidence is present in the slide (Folk: pelsparite/oosparite, Dunham: grainstone).

EERC SS42311.CDR

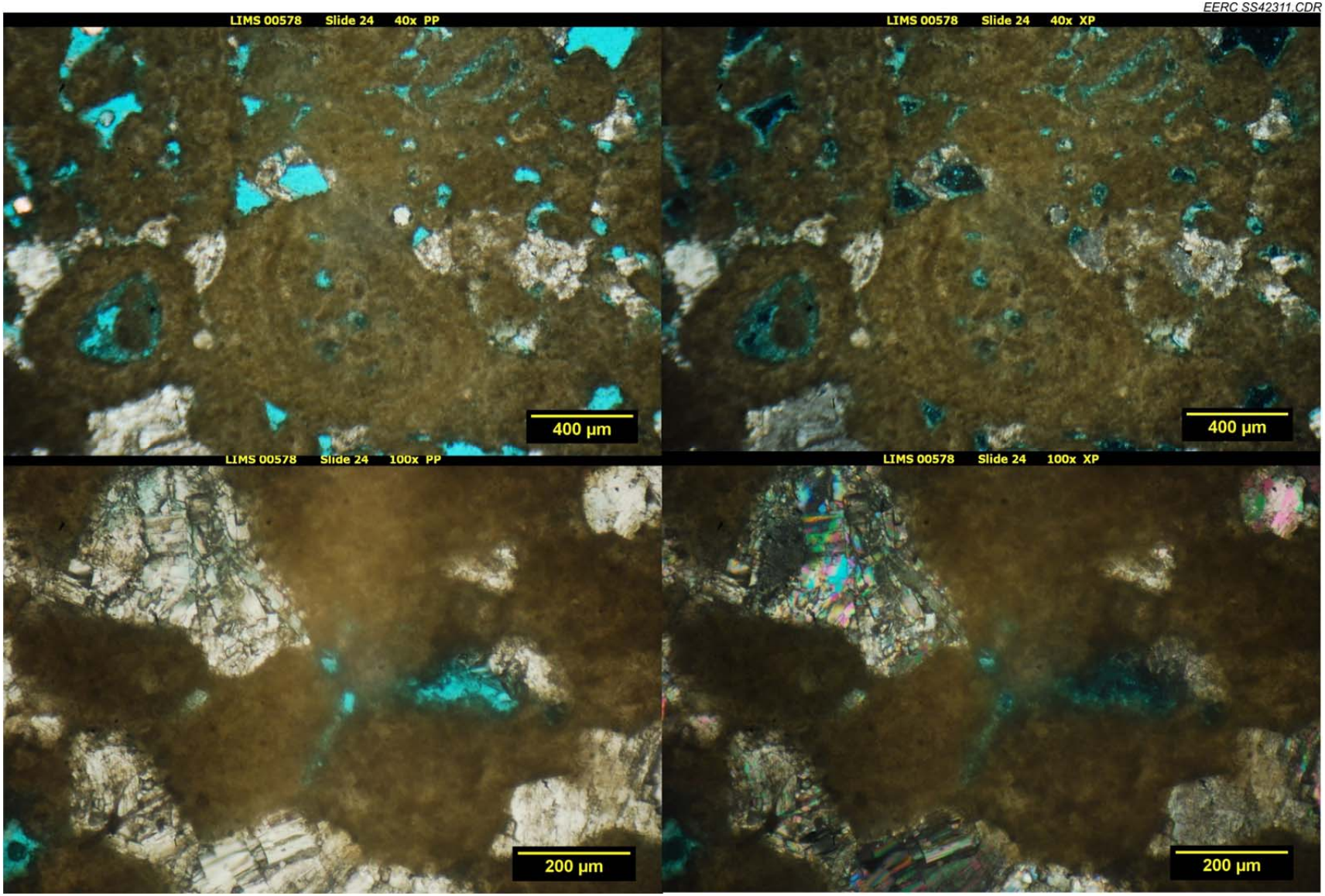

SLIDE 25: WELL 16409, DEPTH 6235.0, CLASS 3, BACK RAMP

Assemblage	Percentage	Comments
Micrite Mud	65%	
Sparite	20%	Recrystallized dolomite
Porosity	15%	Vuggy/pinpoint vugs, burrows
Siderite	Trace	Concretions

No microstructure or sorting is present in Slide 25. The sample is clean, with no observed clay, metal, or fossil material. The sample contains linear porosity, which may be indicative of burrows or some form of biologic activity. Zones of the sample have been recrystallized by sparry dolomite (Folk: dismicrite, Dunham: mudstone).

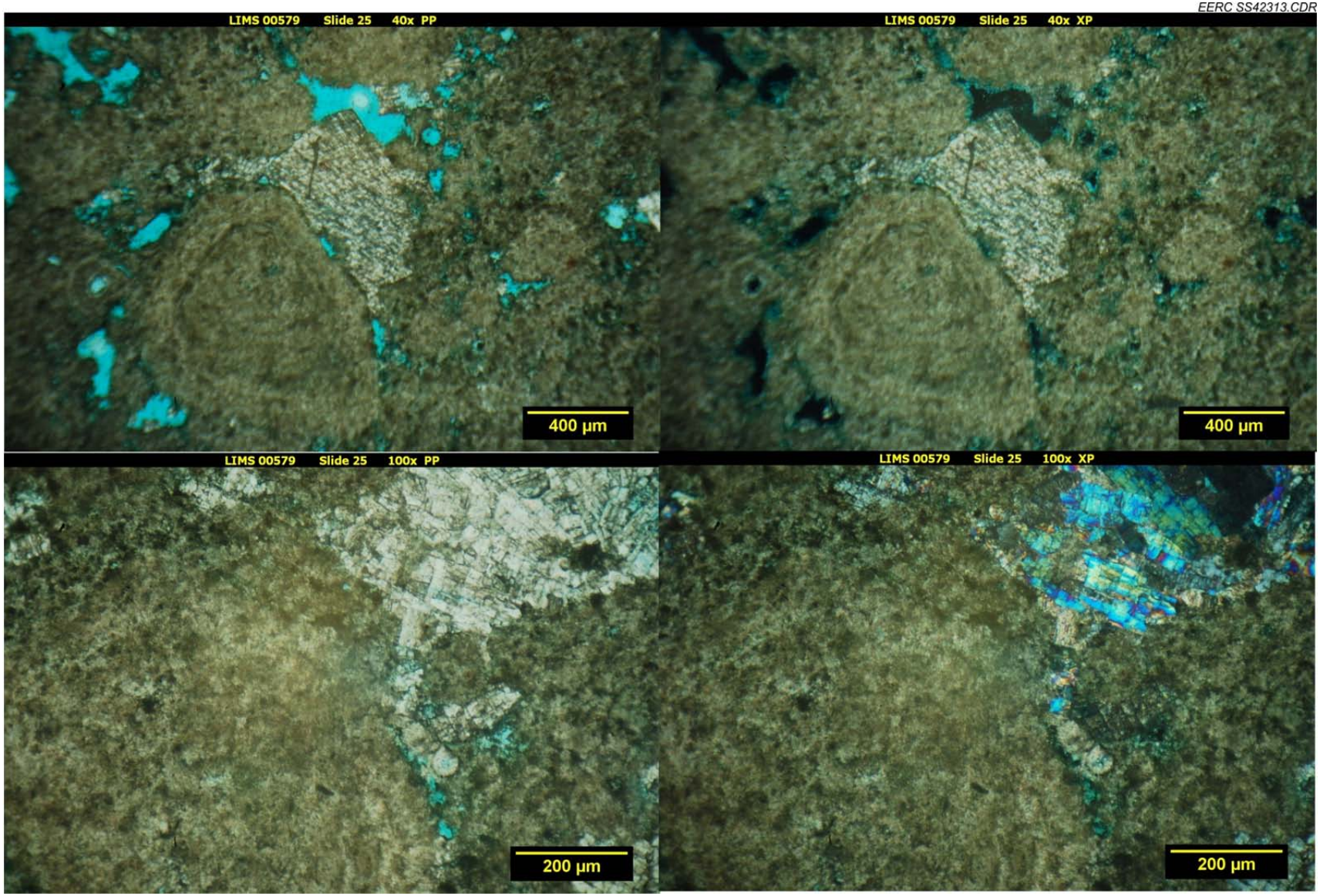
EERC SS42313.CDR
LIMS 00579 Slide 25 40x PP
400 µm
LIMS 00579 Slide 25 40x XP
400 µm
LIMS 00579 Slide 25 100x PP
200 µm
LIMS 00579 Slide 25 100x XP
200 µm

SLIDE 26: WELL 16409, DEPTH 6237.2, CLASS 1, STRAND PLAIN

Assemblage	Percentage	Comments
Ooids	65%	Muddy
Sparite	25%	Dolomite, coarse-grained
Porosity	10%	Macroporosity

Slide 26 is a well-cemented, poorly sorted, loosely packed oosparite (Folk)/grainstone (Dunham) in which only a fraction of the porosity is preserved. No fossils or metal were observed in the section. Some ooid grains in the sample are coarse-grained. No microstructure or bedding was observed.

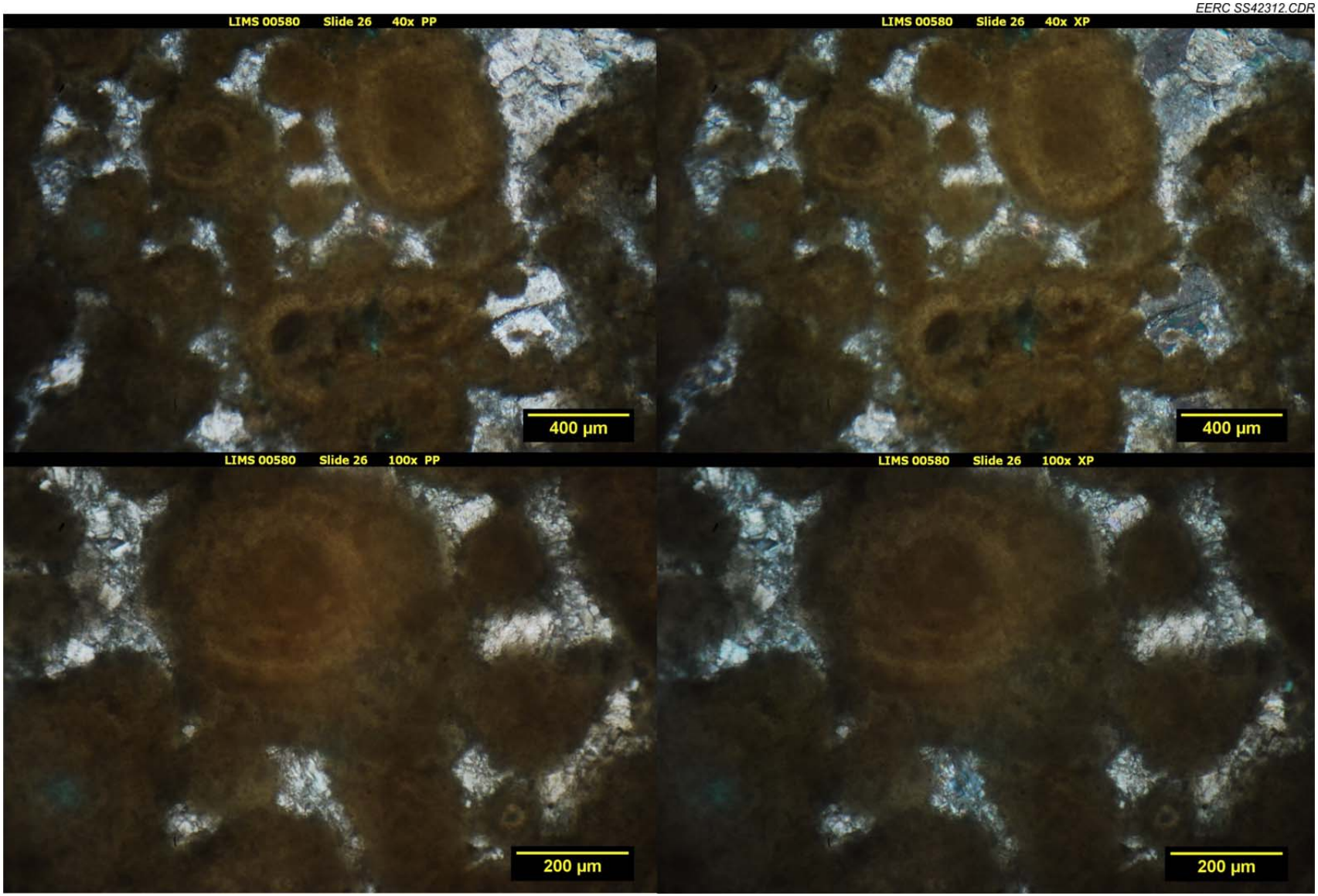
EERC SS42312.CDR
LIMS 00580 Slide 26 40x PP
400 µm
LIMS 00580 Slide 26 40x XP
400 µm
LIMS 00580 Slide 26 100x PP
200 µm
LIMS 00580 Slide 26 100x XP
200 µm

SLIDE 27: WELL 16409, DEPTH 6243.2, CLASS 1, STRAND PLAIN

Assemblage	Percentage	Comments
Ooids	65%	Trace pellets/pellet-sized ooids
Porosity	25%	Mostly macro
Sparite	10%	Dolomite

Slide 27 had a high concentration of poorly sorted ooids and possible pellets and contained significant large porosity. Sparry cement is present but loose (Folk: oosparite, Dunham: grainstone).

EERC SS42302.CDR

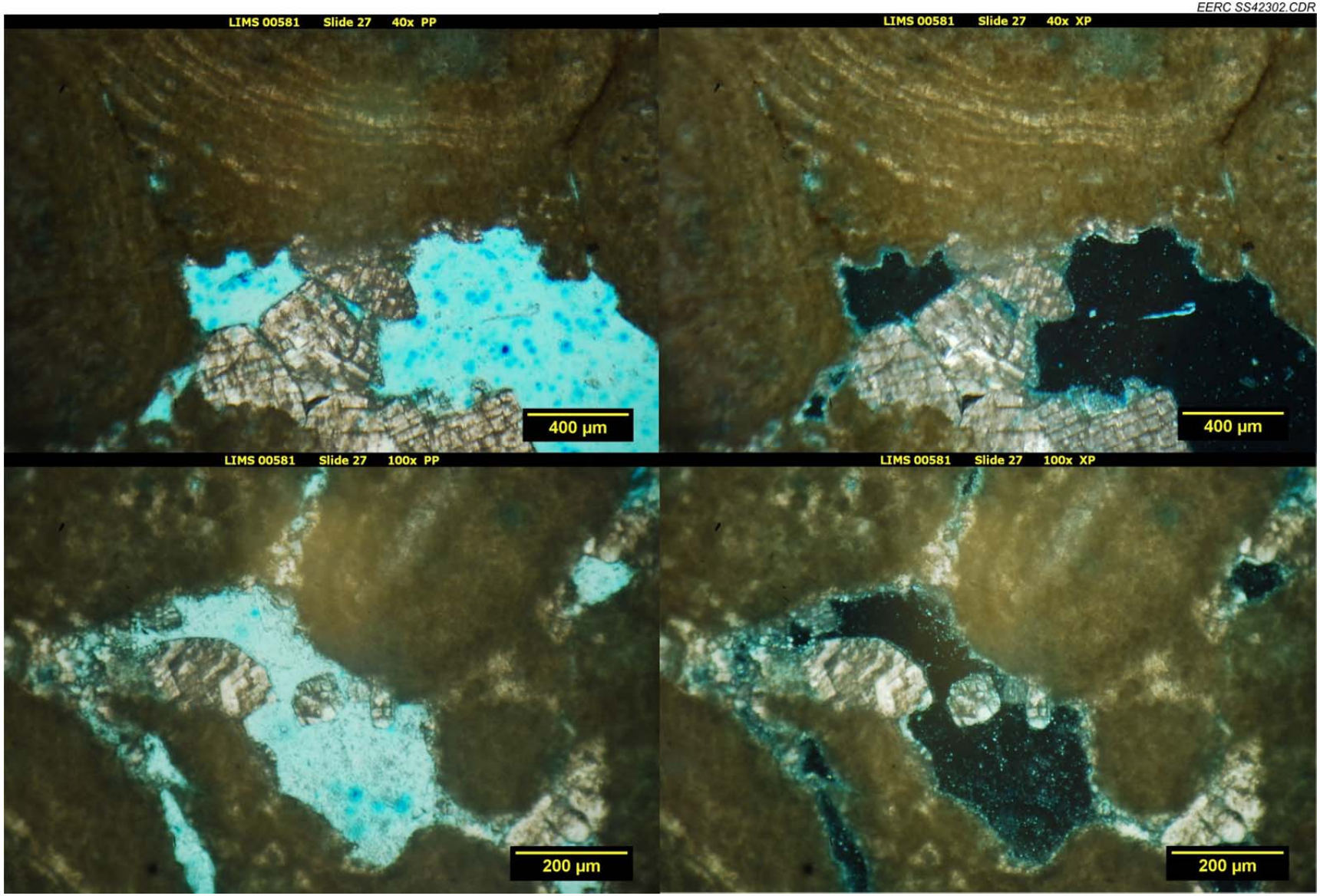

SLIDE 28: WELL 16409, DEPTH 6248.8, CLASS 3, BACK RAMP

Assemblage	Percentage	Comments
Micrite Mud	70%	
Sparite	10%	Recrystallized, dolomite
Muddy Pellets	20%	Very fine grained
Porosity	Trace	Micro–mesoporosity
Siderite	Trace	Nodular

Slide 28 is a pelmicrite (Folk)/mudstone (Dunham) that contains a large portion of micrite mud. A small portion of the sample has experienced dolomitic recrystallization. Small pockets of very fine grained pellets are present; however, the sample is almost devoid of porosity. No microstructure is present, other than zonal mixed mud and pellets. No metal or fossils were observed in the sample.

EERC SS42305.CDR

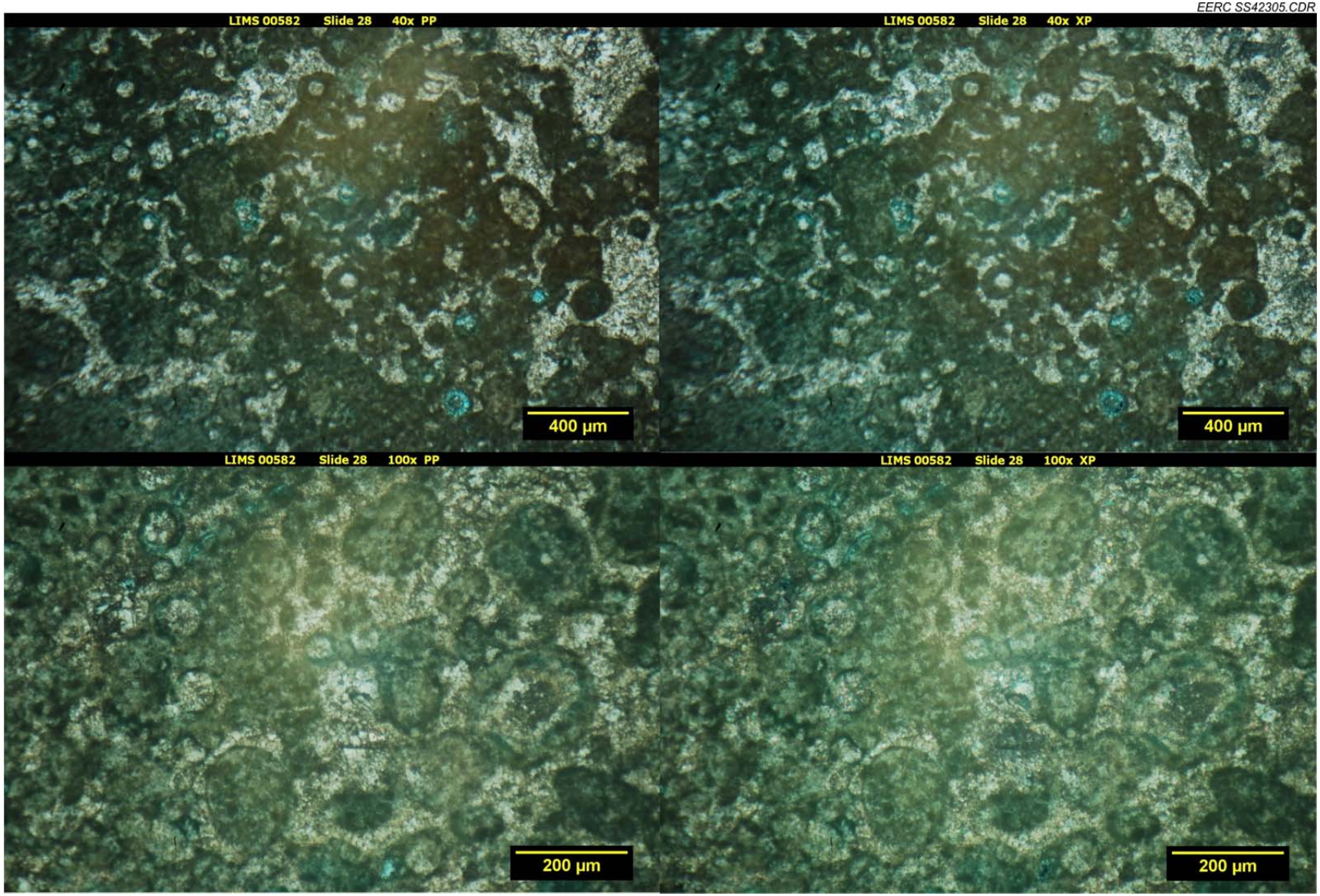

PLUG 1 – SLIDE 29: WELL 16409, DEPTH 6219.2, CLASS 3, RAMP

Assemblage	Percentage	Comments
Interclasts	35%	Limestone
Micrite Mud	30%	
Sparite	25%	Dolomite, recrystallized
Fossils	10%	Fragmented
Porosity	Trace	Meso – shelter
Organics	Trace	

This plug sample is a tight intramicrite (Folk) packstone (Dunham) that has a small amount of porosity preserved through fossil sheltering. The rock contains a high concentration of limestone interclasts and disaggregated, fragmented fossil remnants. Micrite cement contains fine-grained sparry dolomite as well as larger recrystallized dolomite zones. This sample likely represents a storm deposit, as no bedding or sedimentary structure was observed.

EERC SS42306.CDR

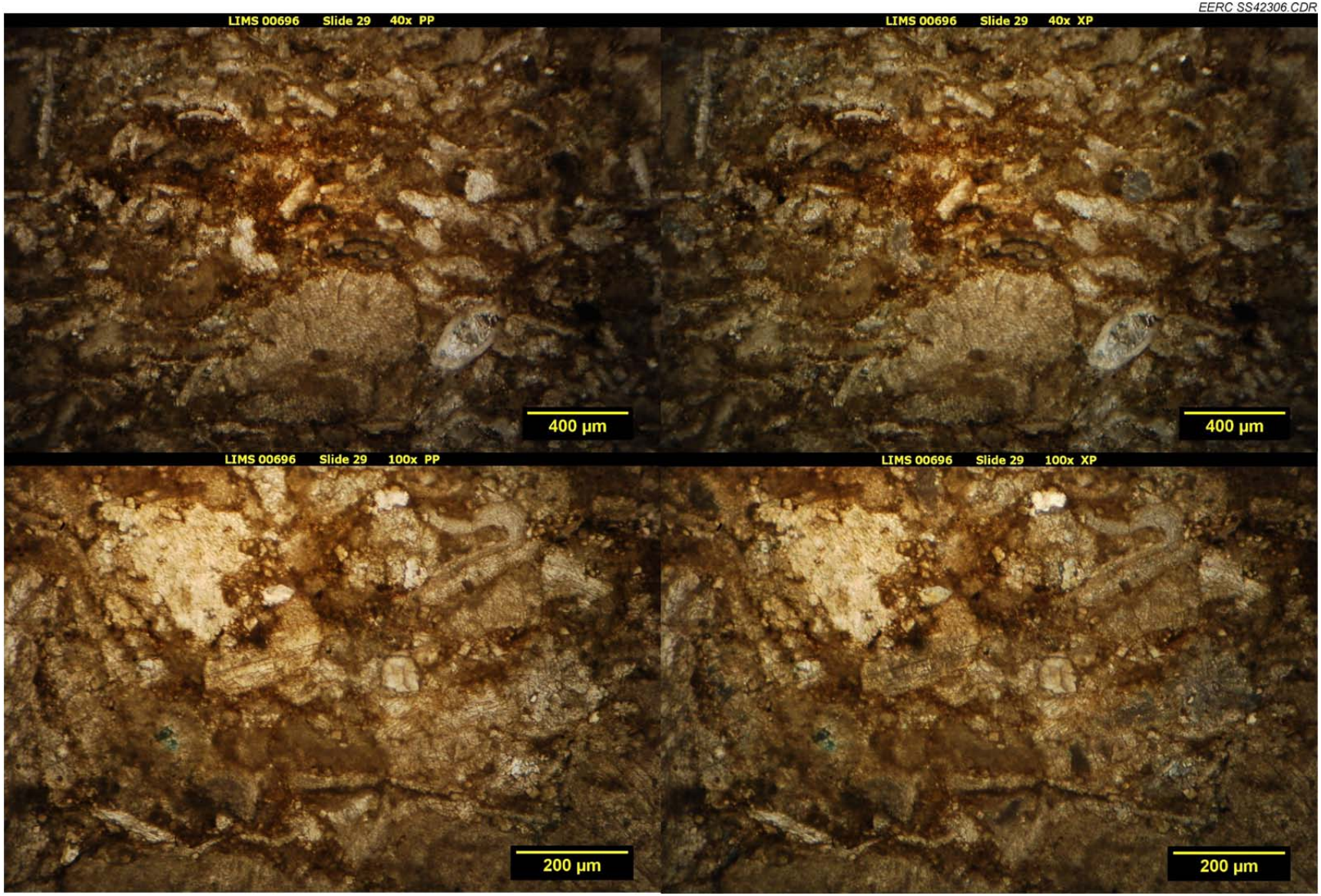

PLUG 2 – SLIDE 30: WELL 16409, DEPTH 6219.5, CLASS 3, RAMP

Assemblage	Percentage	Comments
Interclasts	30%	Limestone
Micrite Mud	30%	
Sparite	30%	Dolomite, recrystallized
Fossils	10%	Fragmented

The slide created from Plug 2 was slightly argillaceous limestone comprising approximately equal portions of limestone interclasts, micrite, and dolomite recrystallized zones. The rock is an intramicrite (Folk) packstone (Dunham), with no visible porosity. The sample is loosely bedded, with slight alterations between packstone and rare floatstone beds. A small amount of aragonite may be present in this section.

EERC SS42307.CDR

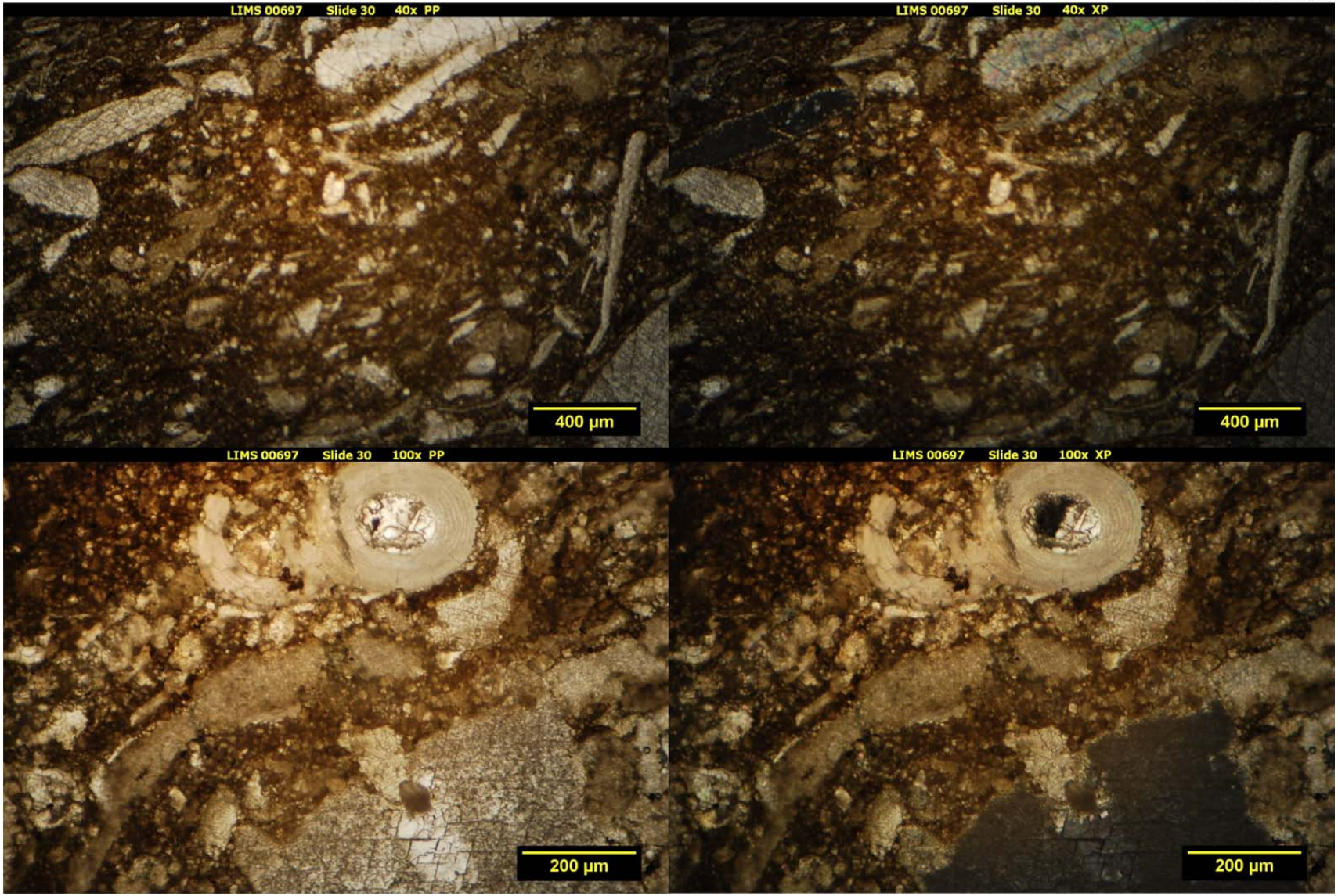

PLUG 3 – SLIDE 31: WELL 16409, DEPTH 6232.2, CLASS 2, DEEP RAMP

Assemblage	Percentage	Comments
Micrite Mud	80%	
Porosity	10%	Vuggy and microfracture
Sparite	5%	Dolomite, recrystallization
Fossils	5%	Bivalve, intact

This sample is a vuggy, stylolitic micrite mudstone (Folk–Dunham) with fine, primarily vertical microfractures. Most fractures have been healed; however, open fractures are also present. The sample is very clean, with no observable clay.

EERC SS42308.CDR

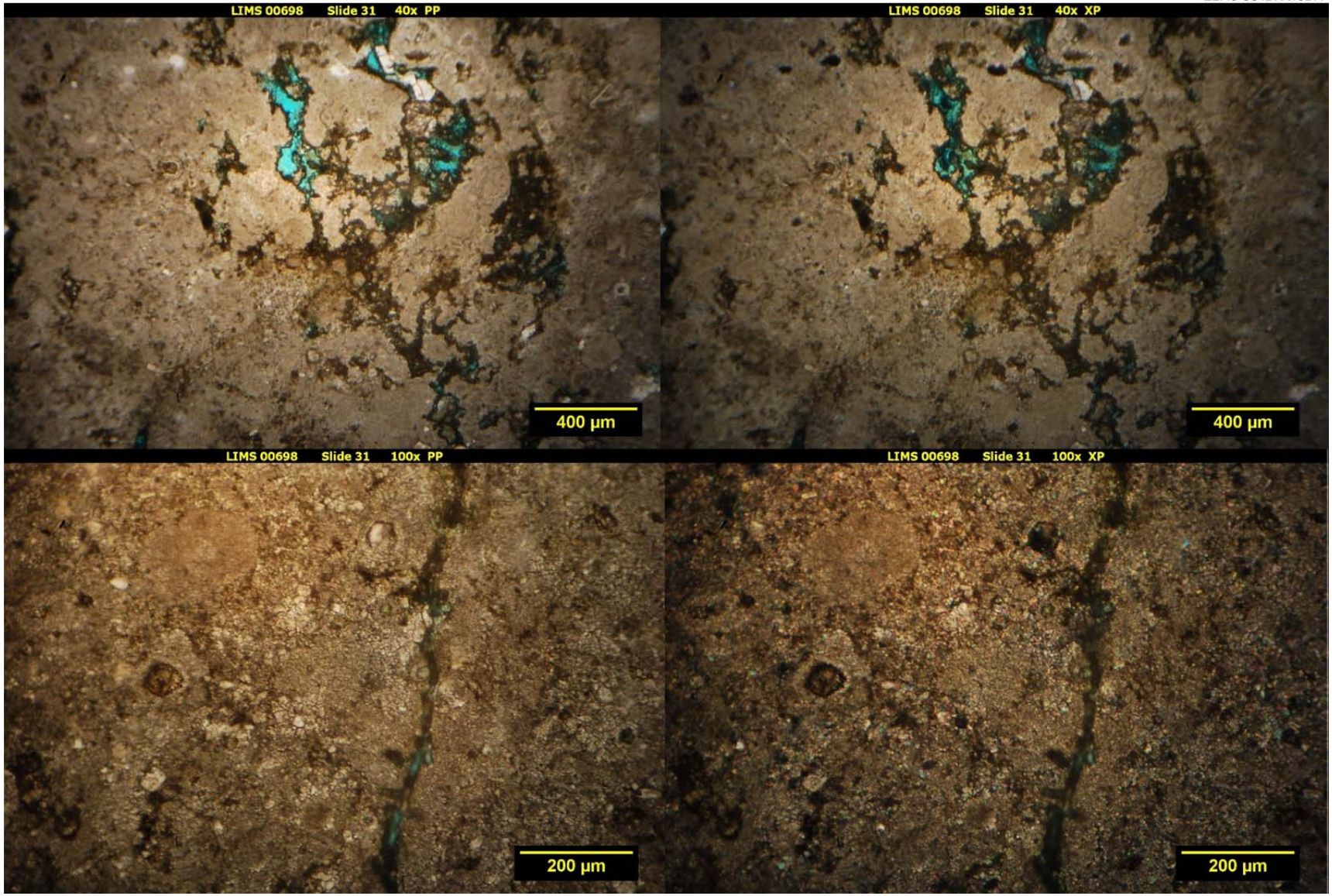

PLUG 4 – SLIDE 32: WELL 16409, DEPTH 6208.5, CLASS 3, BACK RAMP

Assemblage	Percentage	Comments
Micrite Mud	60%	
Interclasts	25%	Limestone
Salt	5%	Gypsum, pore filling
Clay	5%	Structural
Sparite	5%	Dolomite, recrystallized
Organics	Trace	
Fossils	Trace	Thin, disaggregated
Porosity	Trace	Vuggy

The slide made from Plug 4 is a micrite mudstone (Folk–Dunham) that shows little microstructure or particle orientation. Rare porosity is preserved as small vugs, with sulfate salts filling once-existing pore spaces. The sample is clean, with the exception of small clay fragments. This sample is thought to represent a lagoonal deposit because of salt content and the presence of thin, disaggregated fossils. Micrite in this sample is likely dolomitized.

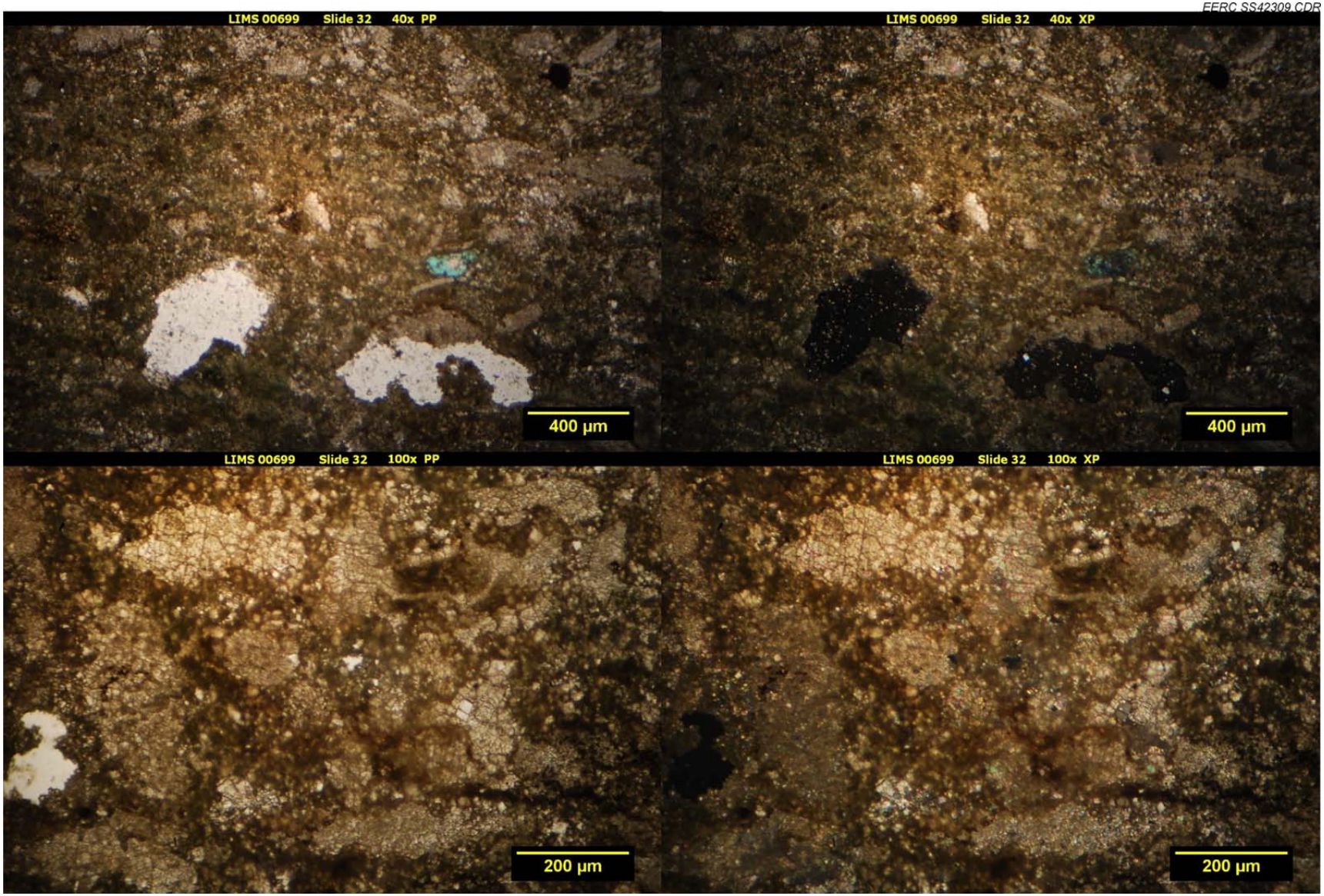
LIMS 00699 Slide 32 40x PP
400 µm
LIMS 00699 Slide 32 40x XP
400 µm
LIMS 00699 Slide 32 100x PP
200 µm
LIMS 00699 Slide 32 100x XP
200 µm

PLUG 5 – SLIDE 33: WELL 16409, DEPTH 6201.0, CLASS 2, DEEP RAMP

Assemblage	Percentage	Comments
Micrite Mud	60%	
Porosity	15%	Vuggy, meso–macro
Sparite	15%	Fine-grained secondary dolomite
Clay	10%	Laminations and dispersed
Organics	Trace	

This plug sample comprises primarily micrite mudstone (Folk–Dunham) with a significant amount of vuggy porosity. The sample is slightly argillaceous and contains thin stringers and weak clayey laminations. Some vuggy porosity is the result of dissolved fossil molds, and no fossil remains were observed in the sample. Micrite sample mass contains fine-grained secondary dolomite grains.

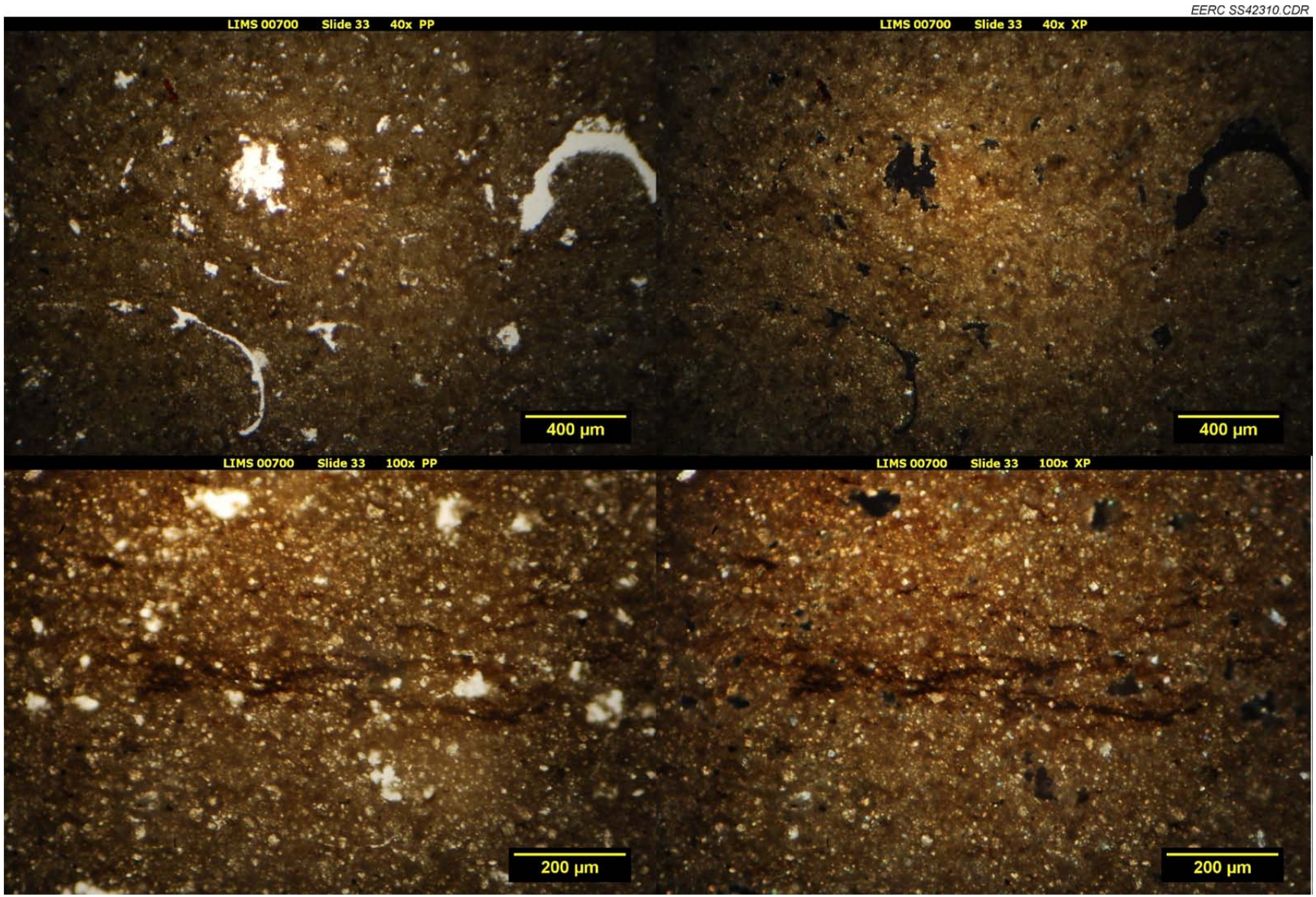
EERC SS42310.CDR
LIMS 00700 Slide 33 40x PP
400 µm
LIMS 00700 Slide 33 40x XP
400 µm
LIMS 00700 Slide 33 100x PP
200 µm
LIMS 00700 Slide 33 100x XP
200 µm

Dolomite Recrystallization Examples

Dolomite recrystallization is prevalent throughout the examined intervals. While the photomicrographs provide plentiful examples of fine-grained sparry dolomite and coarse dolomite cement, completely recrystallized zones were neglected, as they 1) only represent a small portion of the rock fabric and 2) provide little insight into the rock fabric, petrographic class, and/or depositional environment classification, as products are purely diagenetic. As such, two examples of dolomite recrystallization from Wells 4 and 17 are illustrated here, showing 1) subhedral (and porous) dolomite (Slide 4) and 2) more chaotic anhedral dolomite (Slide 17).

EERC SS42286.CDR

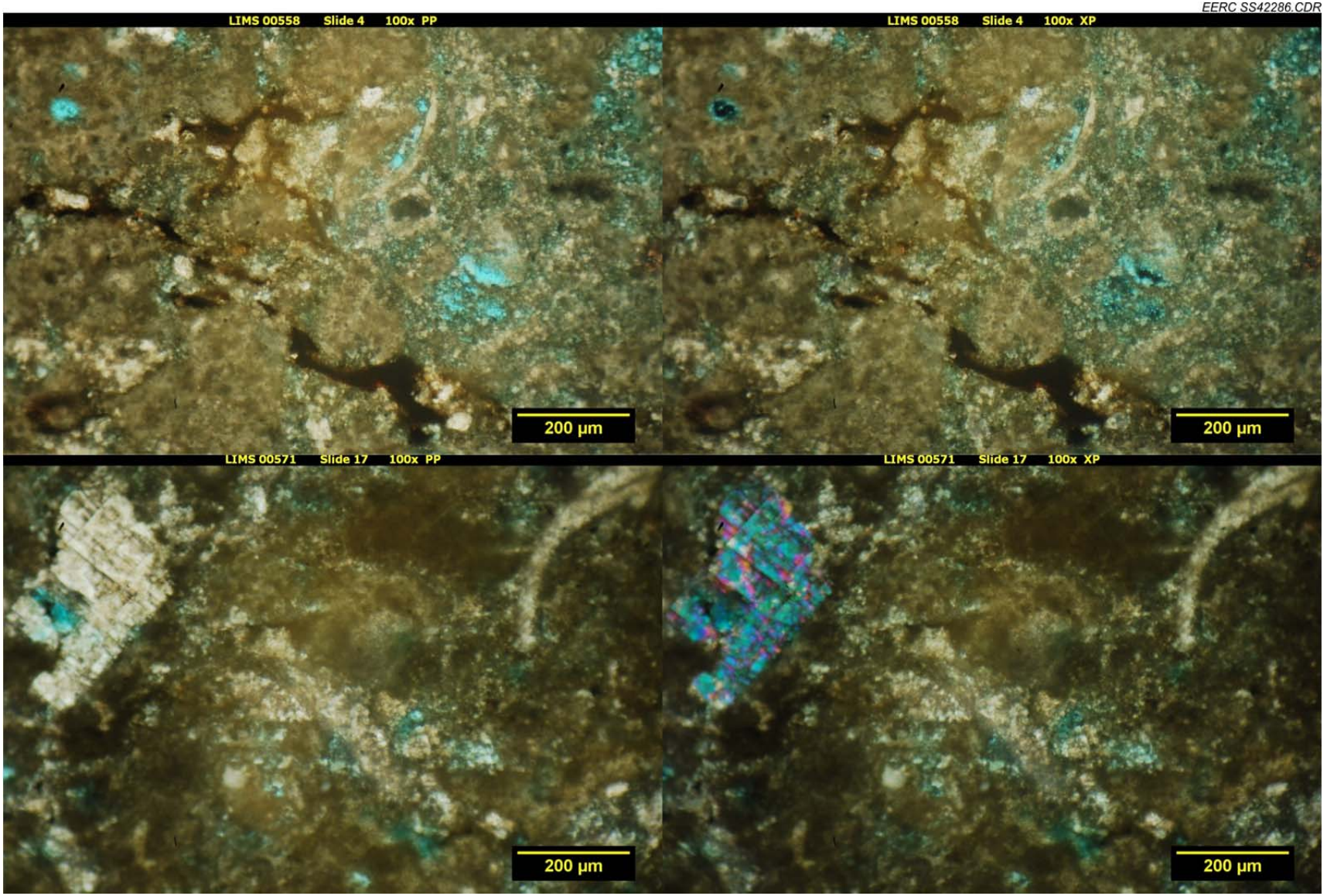

APPENDIX B

SUPPORTING WORKFLOWS AND FIGURES

SUPPORTING WORKFLOWS AND FIGURES

GLOSSARY OF PETROPHYSICAL TERMS

Total Porosity

With a wireline well data vintage of nearly 50 years, there has been much innovation in logging techniques. Porosity logs are a fine example of this innovation; there have been three major deployments of porosity-logging tools since the 1950s. The neutron–gamma (NEUT) curve was run from 1957 to 1989 but is most commonly seen in vintages of the 1960s to early 1970s (Schlumberger, 1991). Acoustically derived porosity was first deployed in the mid-1970s. Current porosity-logging techniques involve using both neutron and density curves. Since there is more confidence in the newer logging techniques, the neutron–density porosity curve was deemed high priority, followed by acoustic and NEUT. Merging all porosity curves into one total porosity curve yielded 207 wells with porosity in the study area. In some cases, there were overlapping neutron porosity (NPHI) and sonic porosity (SPHI) curves for the same wells. Precedence was taken as follows: NPHI > SPHI > NEUT.

A transform was created from a crossplot to convert NEUT counts to porosity percent using a crossplot of core porosity vs. counts. Best results were a slope of:

Total Porosity = (−0.0001456447 * NEUT + 0.3216842)

The acoustic wireline log (DT) was converted into SPHI. The Wyllie approach was used and calibrated to core analysis porosity values. SPHI is found in 135 wells across the study area. DT matrix equals 44 and DT fluid equals 189 (water), with a 1.1 compaction correction. Total dissolved solids (TDS) for the reservoir is approximately 175,000 ppm.

Neutron–density porosity was used if available. 101 wells in the study area have NPHI wireline logs. Density porosity (DPHI) was calculated from the density curve and appropriate matrix mineralogy. Dolomite was used for the Midale Member and limestone for the Rival Member. The final porosity value for the neutron–density porosity curve was calculated by adding both the NPHI and DPHI divided by 2 for the 19 wells that have density curves. This method helps average the higher values recorded by the NPHI curve and the lower values of the DPHI curve. If no density curve was available, then the NPHI value was used.

Shale Volume

Volume of shale (VSH) was calculated in petrophysical software using a gamma ray (GR) matrix and maximum value. This, in turn, was used to determine effective porosity (GR matrix equals 10, GR shale equals 70). VSH is found in 240 wells.

Effective Porosity

Effective porosity equals total porosity * (1 – VSH). After applying shale correction to total porosity, 200 wells remained with an effective porosity curve. Effective porosity comprises two main components: bulk volume movable and bulk volume irreducible.

Net-to-Gross

Net-to-gross is essentially another way to represent porosity. It is defined by effective porosity divided by total porosity.

Permeability

To calculate the petrophysical formulae for permeability, Tixier, Timur, and Coates all rely on irreducible water saturation as a variable. This variable is presumed to be 0.2–0.27 from relative permeability curves in the Rival Member, but no values are provided for the Midale Member. Calculations with the relative permeability values "as is" were exceptionally high; thus core permeability was used for further petrophysical interpretation. Core permeability is available in 80 wells. A cloud transform is applied during petrophysical modeling utilizing the core analysis values (this concept is covered in the Transforms section).

Water Saturation

The Archie equation was used to define water saturation for the wireline log suite (Equation 1). Several variables are needed for this equation: porosity, formation water resistivity, observed bulk resistivity, cementation factor, and saturation factor. Effective porosity calculated from petrophysical analysis was used for the porosity variable. Formation water resistivity was determined from Schlumberger's Resistivity of NaCl Water Solutions lookup table, where reservoir TDS and temperature are the inputs. One averaged value for both TDS and temperature was used to calculate a single formation water resistivity value. 175,000 ppm and a temperature of 166°F yielded an R_w value of 0.026. This value was cross-referenced with literature on the Rival Field which reported a value of 0.025 (Laird, 1960). Bulk resistivity was determined from petrophysical analysis by merging several different deep resistivity curves from different logging methods into one representative curve for 185 wells. Both the cementation factor and saturation exponents were not resolved from multimineral analysis, thus the default value of 2 was used. Upon running the Archie equation, 153 wells have calculated wireline water saturation values. The mean value was 0.79 and considered too high, according to published literature (Laird, 1960). Thus core analysis water saturation (mean of 0.49) was upscaled into the 3-D model and cokriged with Archie water saturation values to produce a cloud correlation between core and wireline data.

$$S_w = [\ (a / \Phi^m)*(R_w / R_t)\ ]^{(1/n)} \qquad \text{[Eq. 1]}$$

Where:
S_w = water saturation
Φ = porosity

R_w = formation water resistivity
R_t = observed bulk resistivity
a = a constant (value of 1)
m = cementation factor (value of 2)
n = saturation exponent (value of 2)

DATA ANALYSIS

Variograms were computed for the major, minor, and vertical directions for Zones 2, 3, and 4 for the following properties: effective porosity, permeability, water saturation, and net-to-gross. Since effective porosity and permeability are related throughout carbonate facies, they were given the same variogram. The effective porosity variogram was more robust as it had over 200 data points, while core permeability was limited to 80. Thus all variogram variables were identical for both effective porosity and permeability in Zones 2, 3, and 4. Zones 3 and 4 are shown in Figures B-1 and B-2, where cyclicity is shown among the data points. Both variograms for these zones were picked on the second full cycle, as the first was incomplete.

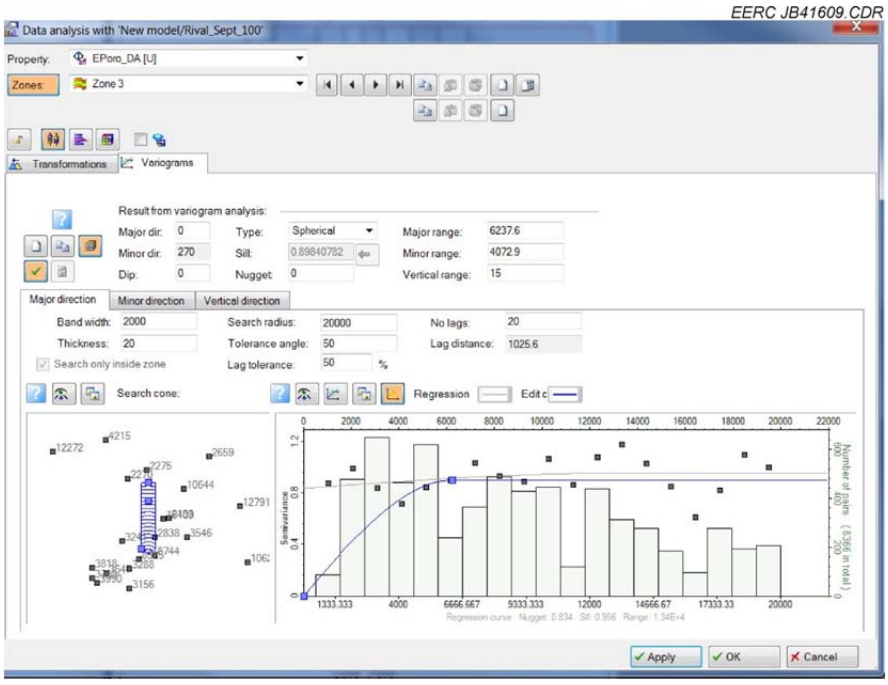

Figure B-1. This variogram defined for effective porosity was also utilized for permeability in Zone 3 (Midale). The sill reached approximately 0.9.

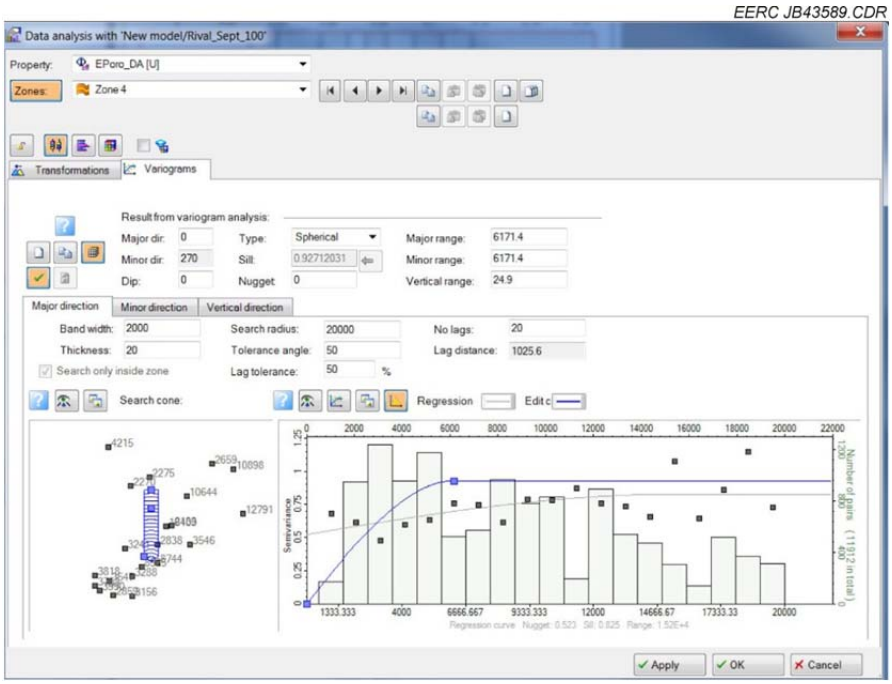

Figure B-2. This variogram defined for effective porosity was also utilized for permeability in Zone 4 (Rival). The sill reached approximately 0.9.

TRANSFORMS

Porosity-to-permeability transforms were set up for Zones 3 (Midale) and 4 (Rival). The cloud transforms, also known as bivariate distribution, were based on crossplots of core porosity vs. core permeability. Four bins were selected in the Midale zone (Figure B-3) and 10 bins in the Rival zone (Figure B-4) along the x-axis of the crossplot, with an equal number of points in each bin. The bins separate the data for correlation purposes, thus the minimum and maximum calculated property values can change across bins. This cloud transform technique allows for a more dynamic porosity–permeability relationship by allowing calculated values to be both greater and less than the correlated value.

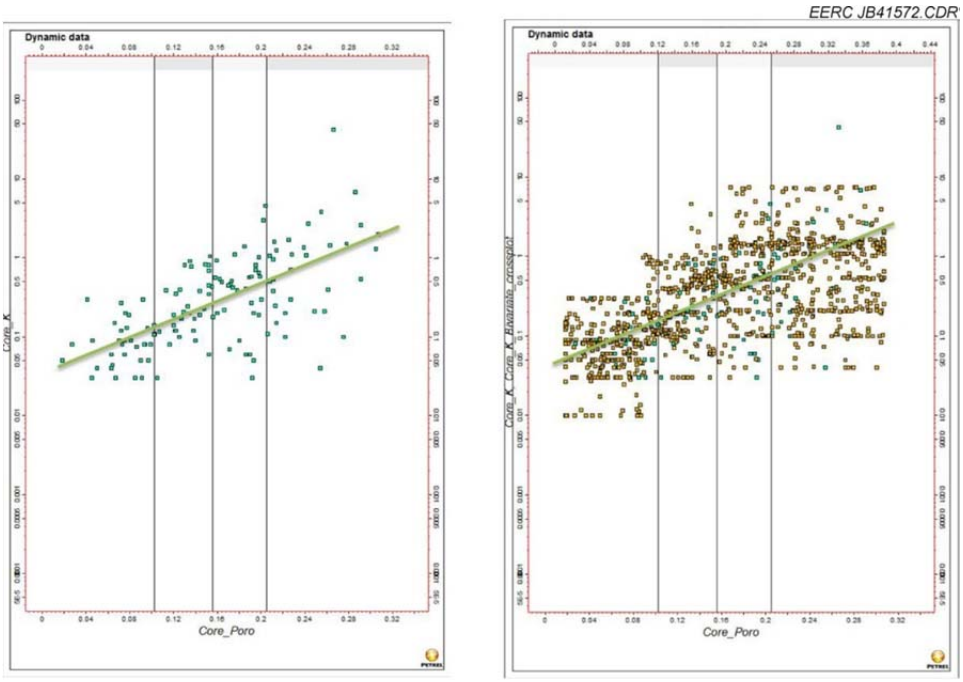

Figure B-3. Cloud transform in the Midale zone for permeability values derived from a core porosity vs. core permeability crossplot. This transform was an excellent fit, with an equal number of property points scattered in a cloud around the correlation line.

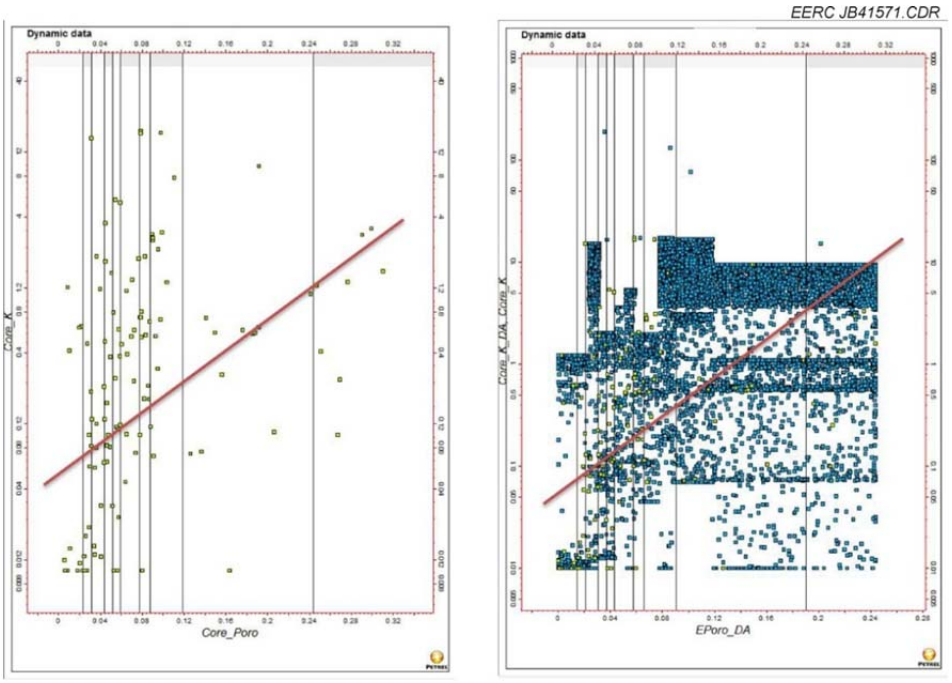

Figure B-4. Cloud transform in the Rival zone for permeability values derived from a core porosity vs. core permeability crossplot. This transform is a poor to fair fit.

A water saturation transform in the form of cokriging was used for Zones 3 and 4. This workflow involves upscaling the core analysis data with more certainty and the Archie data with less uncertainty into the model. Both data sets were given variograms through the data analysis process, before petrophysical modeling. The Archie water saturation data were simulated with Gaussian random function simulation (GRFS) to create a value for each grid cell in the model. Next, the core water saturation data were simulated with GRFS, and a cokriging workflow was used. This process involved choosing both the secondary variable and collocated cokriging properties to be the Archie water saturation.

Cokriging uses a linear regression similar to both ordinary and universal kriging techniques and is dependent on covariance values. In traditional cokriging, the variogram and covariance can cause interference between the two data sets; thus collocated cokriging was used to minimize this effect. Collocated cokriging reduces the chance of overestimation by creating low and high bounds dependent of the secondary variable on a cell-by-cell basis rather than relying on covariance between the two data sets. In this case, bounds were estimated from the correlation between Archie water saturation and core water saturation, removing values that were previously overestimated (Figure B-5).

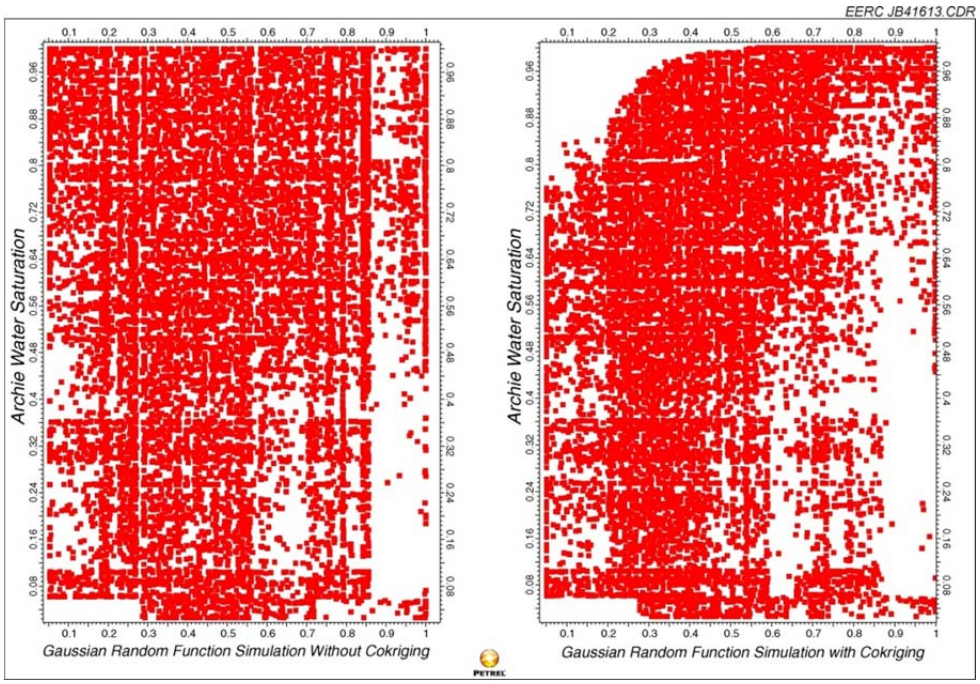

Figure B-5. Crossplots of Archie water saturation vs. core water saturation; both property values are from the 3-D geologic model: Values derived from GRFS without cokriging (left) and values derived from GRFS with cokriging (right).

3-D GEOLOGIC MODEL FIGURES

Fence diagrams and cross sections were created to better view the 3-D geologic model (Figure B-6). The following properties are shown: depositional facies, effective porosity, permeability, water saturation (Archie), water saturation (cokriged), and net-to-gross (porosity). Zones 1–5 are all shown. Zones 1 and 2 represent the nonpermeable seals on the reservoir; thus they will be displayed as a single value (solid color). All diagrams are shown with 50× vertical scale change.

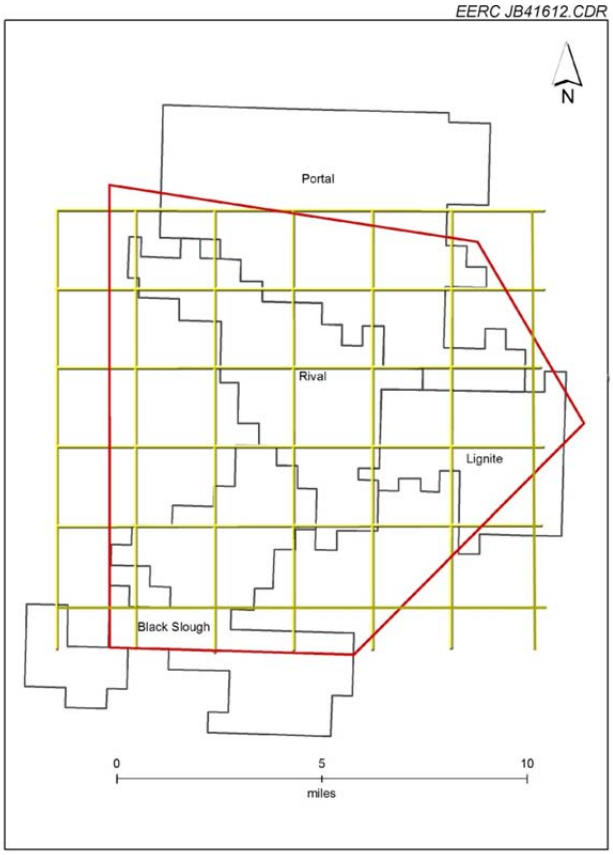

Figure B-6. Layout of fence diagrams as seen from map view.

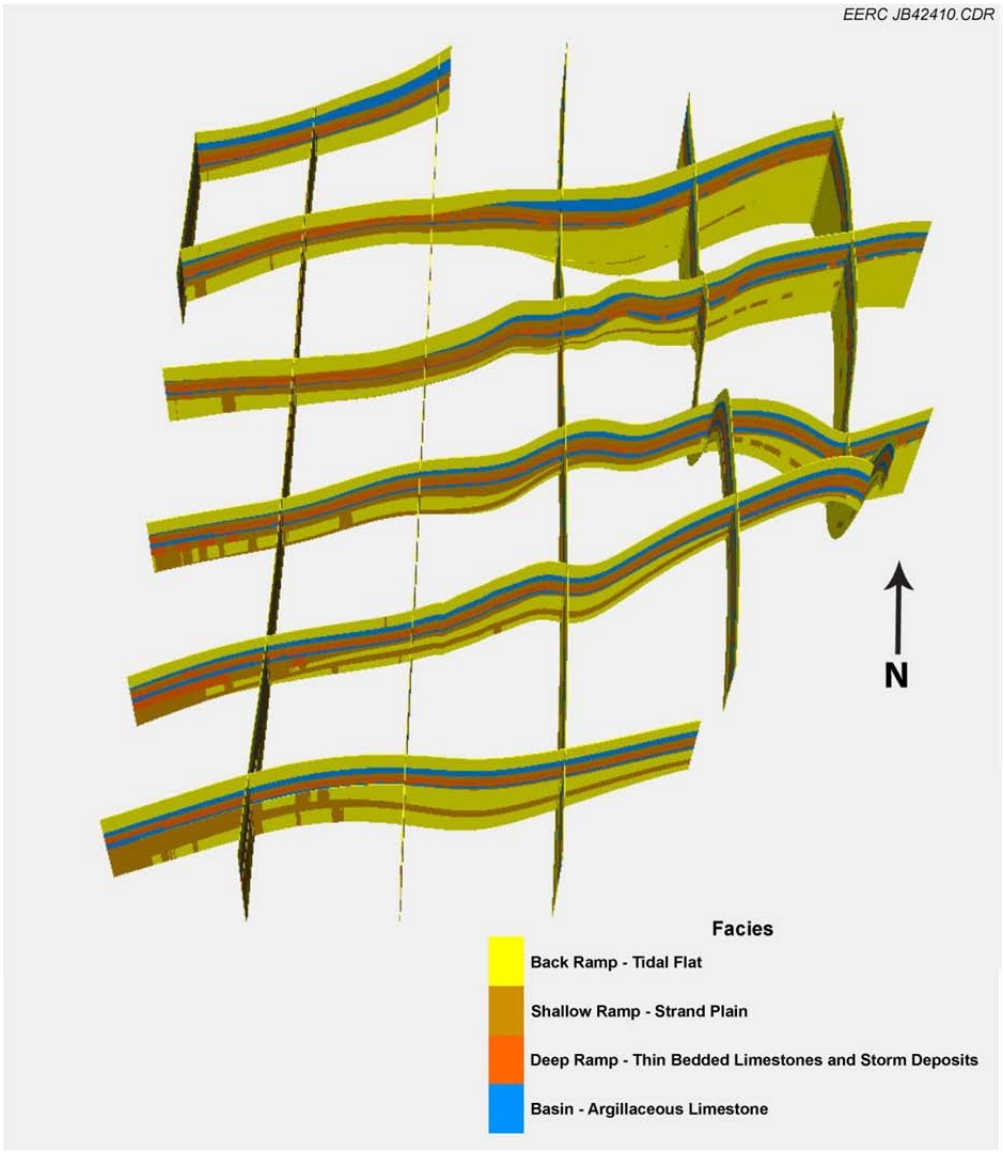

Figure B-7. Fence diagram of the depositional facies model clipped to the study area boundary. Data were imported from Applied Geology Laboratory (AGL) petrophysical analysis and extrapolated across the entire field. Facies were populated with truncated Gaussian simulation (TGS) with trends (see Figure B-6 for a map view layout).

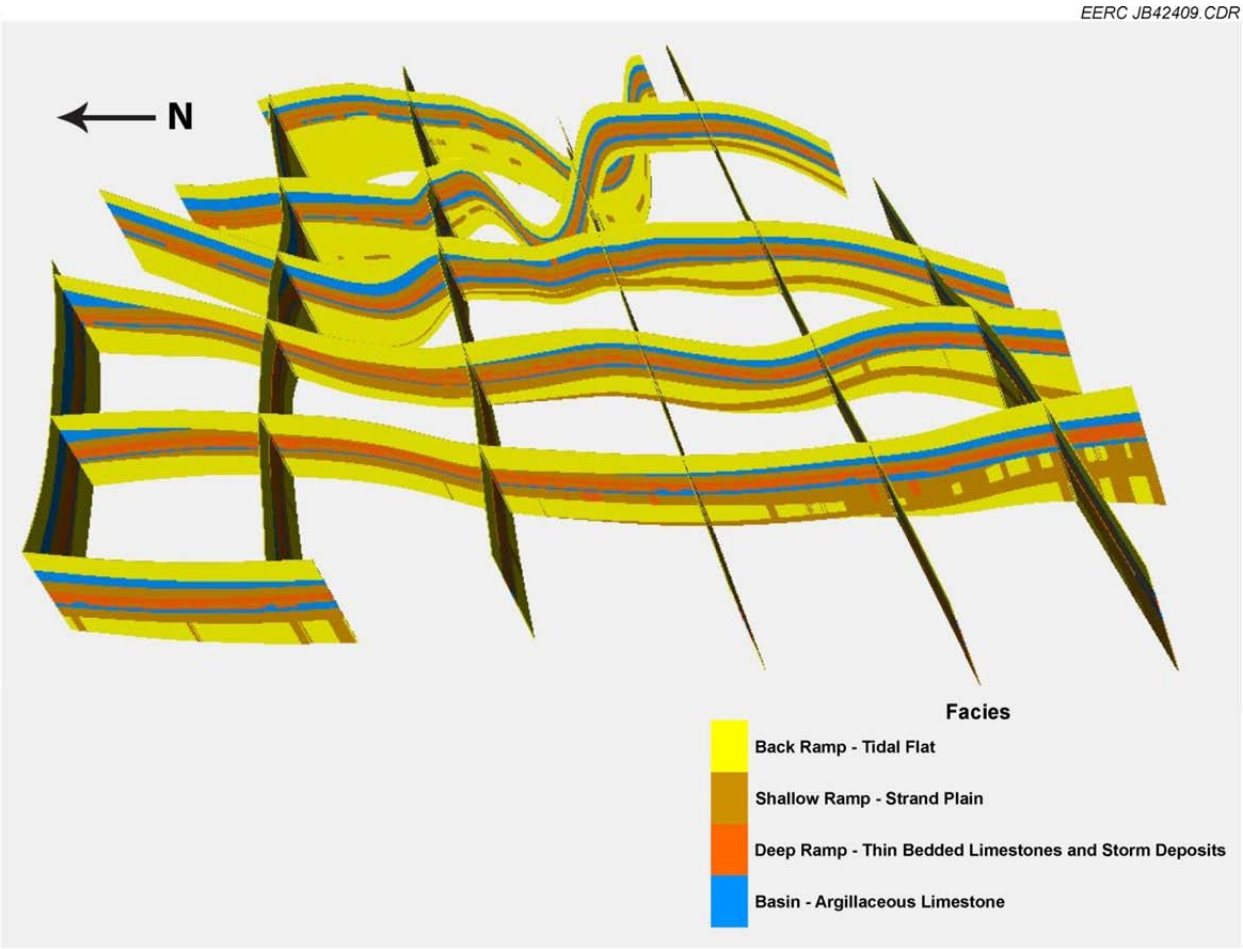

Figure B-8. Fence diagram of the depositional facies model clipped to the study area boundary. Data were imported from AGL petrophysical analysis and extrapolated across the entire field. Facies were populated with TGS with trends (see Figure B-6 for a map view layout).

EFFECTIVE POROSITY

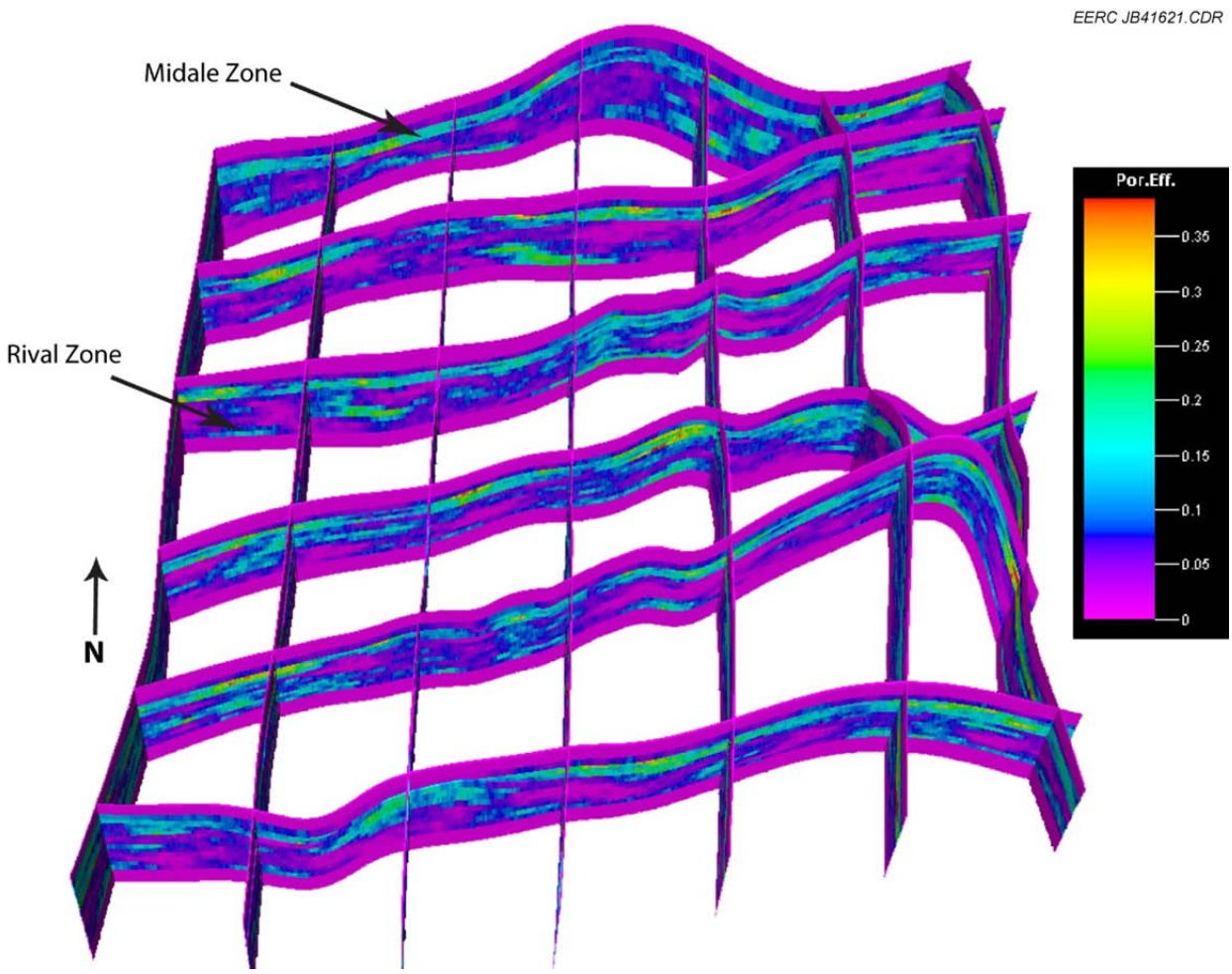

Figure B-9. Fence diagram showing the effective porosity property. Of note are the high porosities in the Midale Zone, separated by a consistent low-porosity zone (shaley marl), before seeing higher porosities again in the Rival Zone (see Figure B-6 for a map view layout).

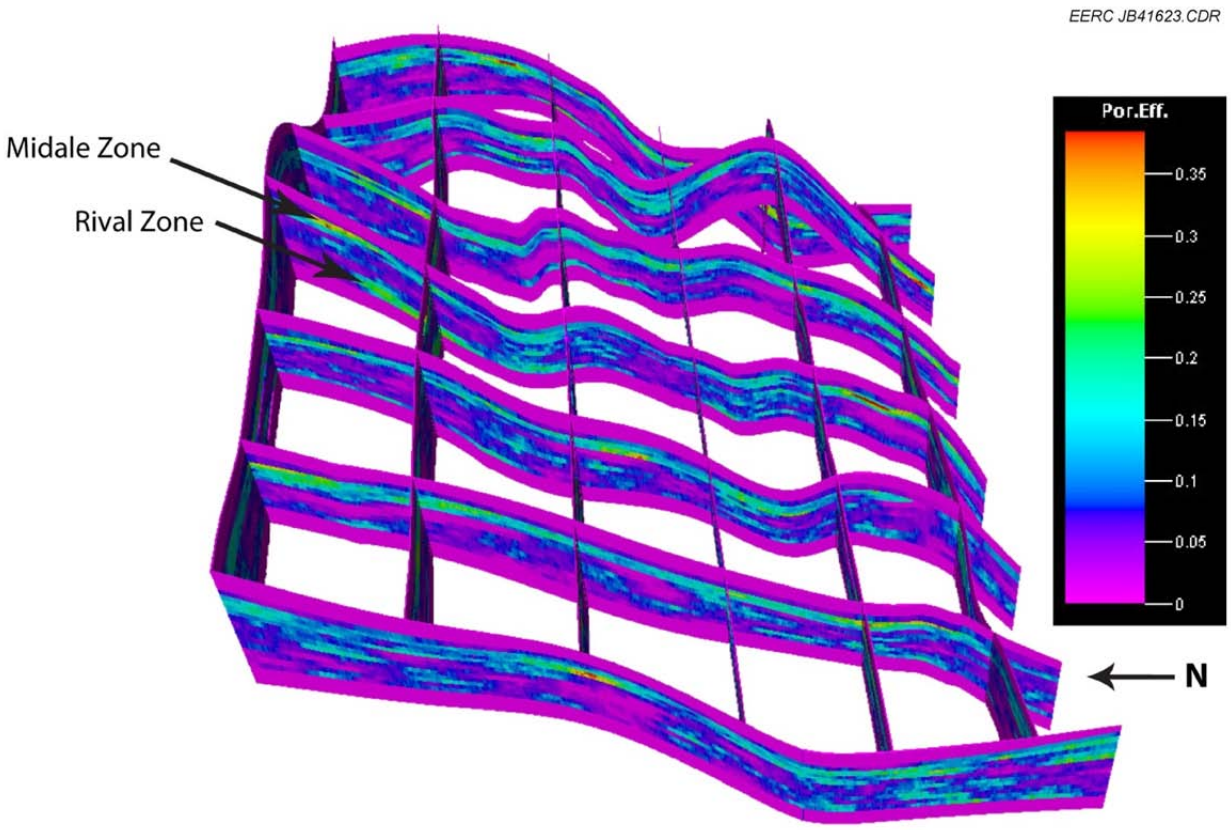

Figure B-10. Fence diagram showing the effective porosity property. Of note are the high porosities in the Midale Zone, separated by a consistent low-porosity zone (shaley marl), before seeing higher porosities again in the Rival Zone (see Figure B-6 for a map view layout).

PERMEABILITY

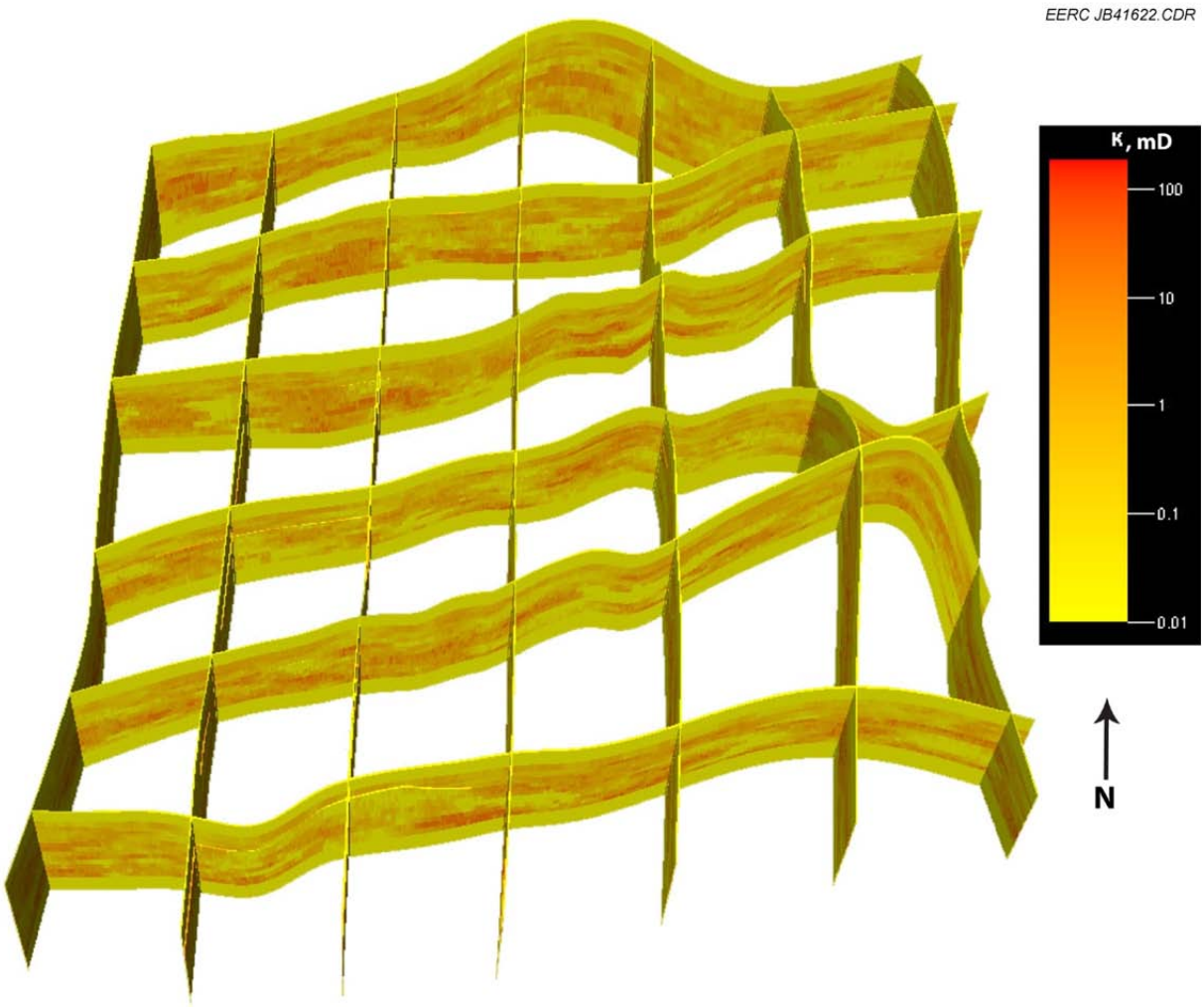

Figure B-11. Fence diagram of the permeability property (Figure B-6 shows a map view layout).

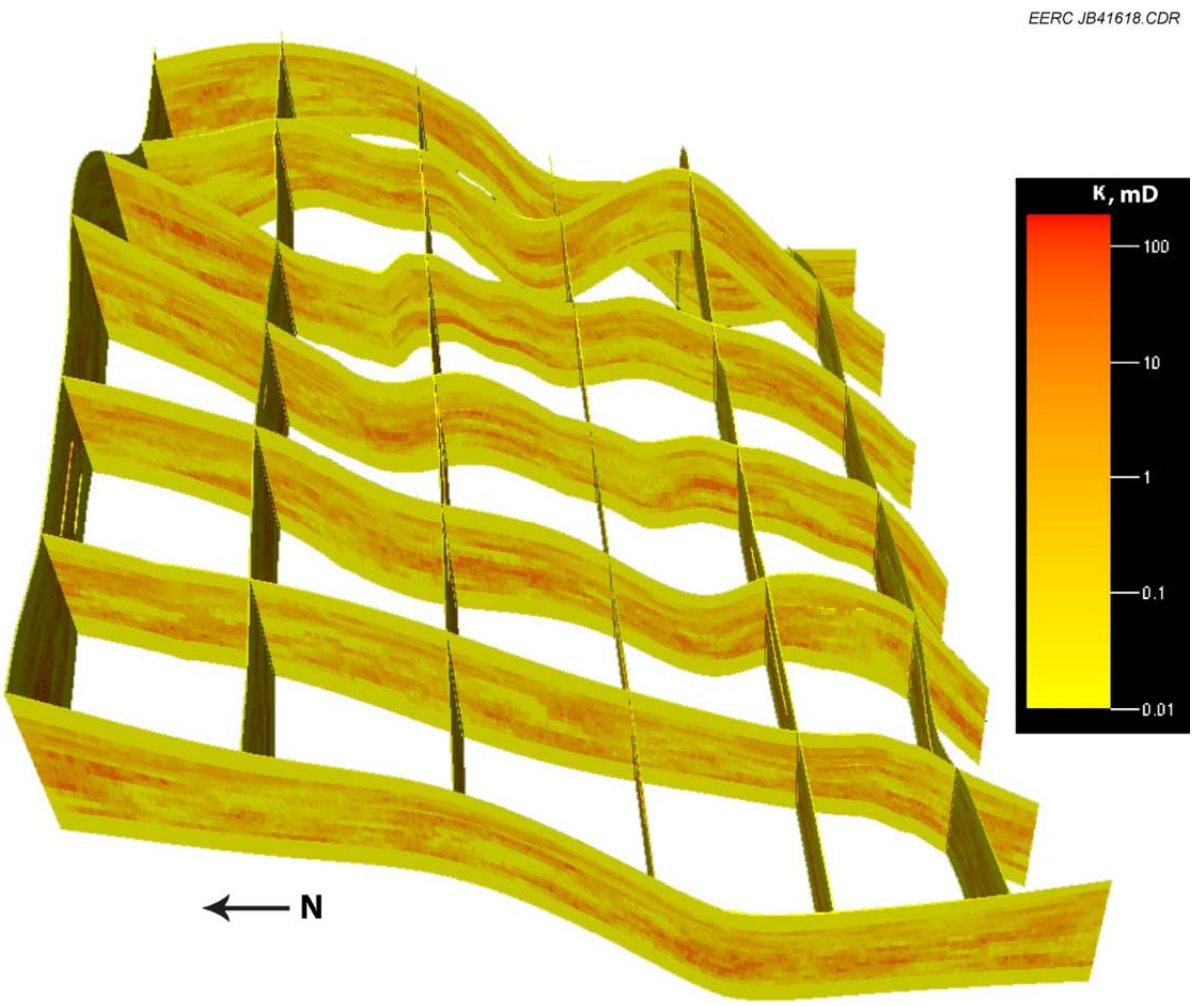

Figure B-12. Fence diagram of the permeability property (Figure B-6 shows a map view layout).

WATER SATURATION (ARCHIE)

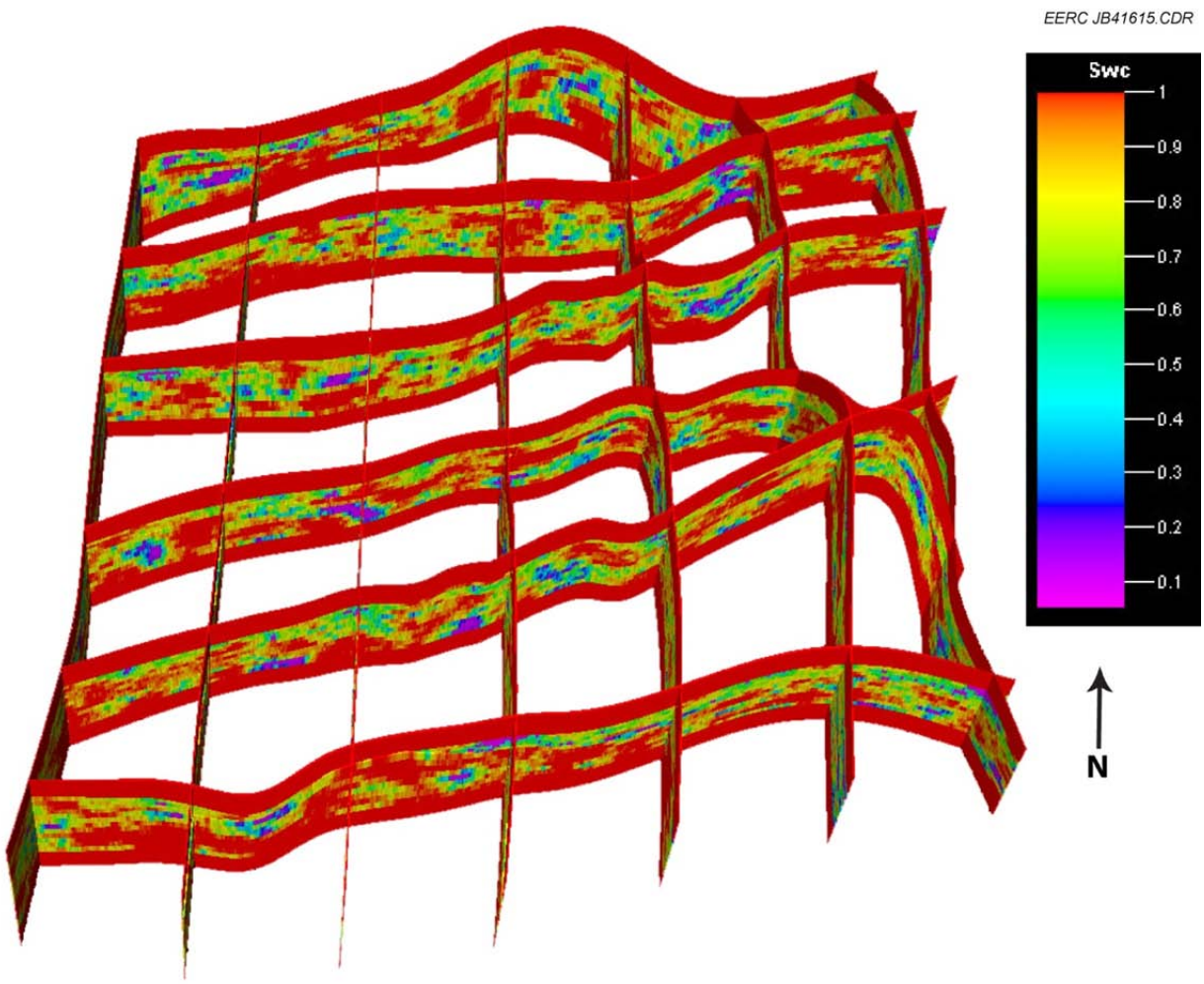

Figure B-13. Fence diagram of the Archie water saturation property. Most values were considered to be high compared to the literature (Laird, 1960) and thus were cokriged with core water saturation data for more certainty (Figure B-6 shows a map view layout).

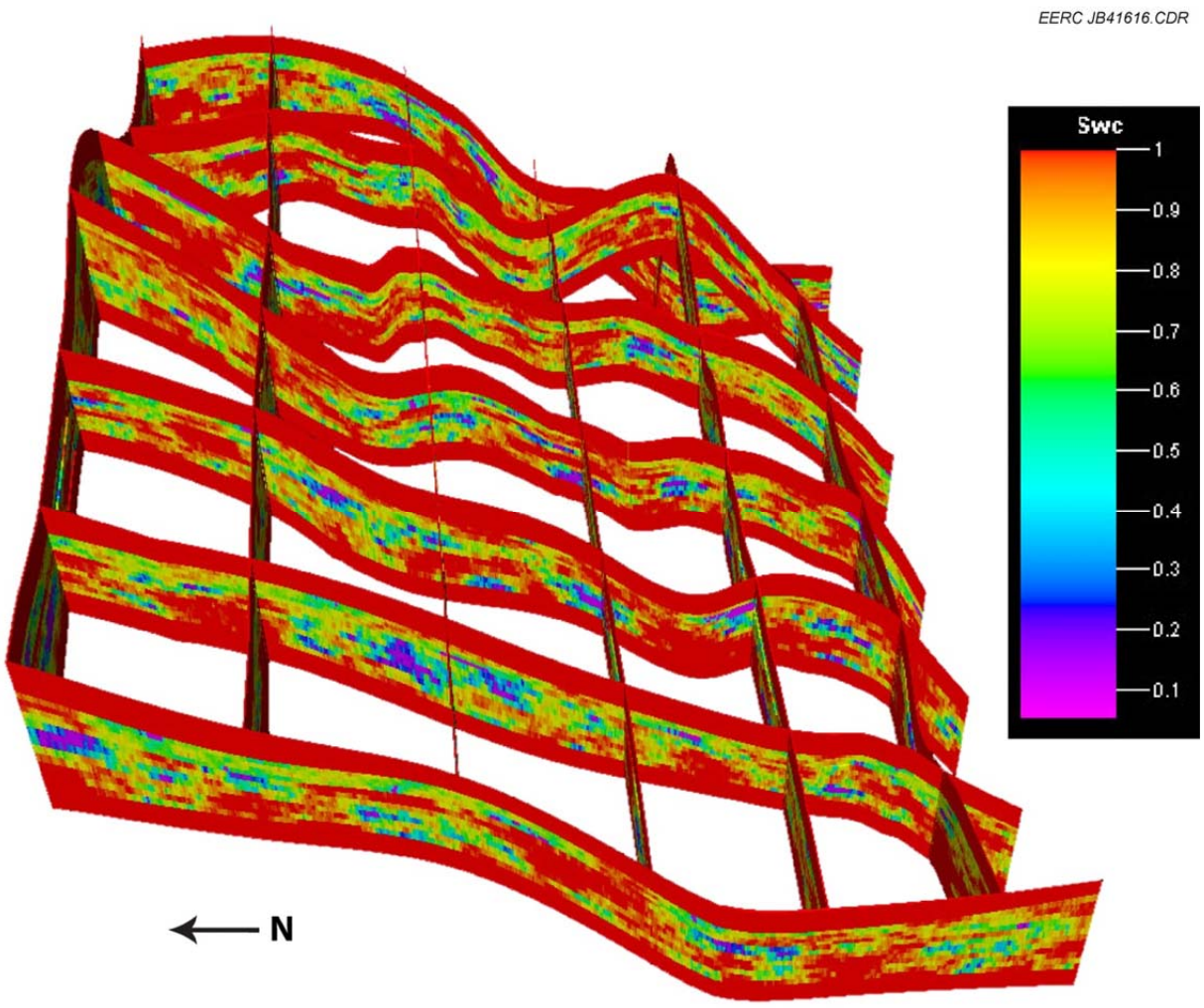

Figure B-14. Fence diagram of the Archie water saturation property. Most values were considered to be high compared to the literature (Laird, 1960) and thus were cokriged with core water saturation data for more certainty (Figure B-6 shows a map view layout).

WATER SATURATION (CORE ANALYSIS COKRIGED WITH ARCHIE)

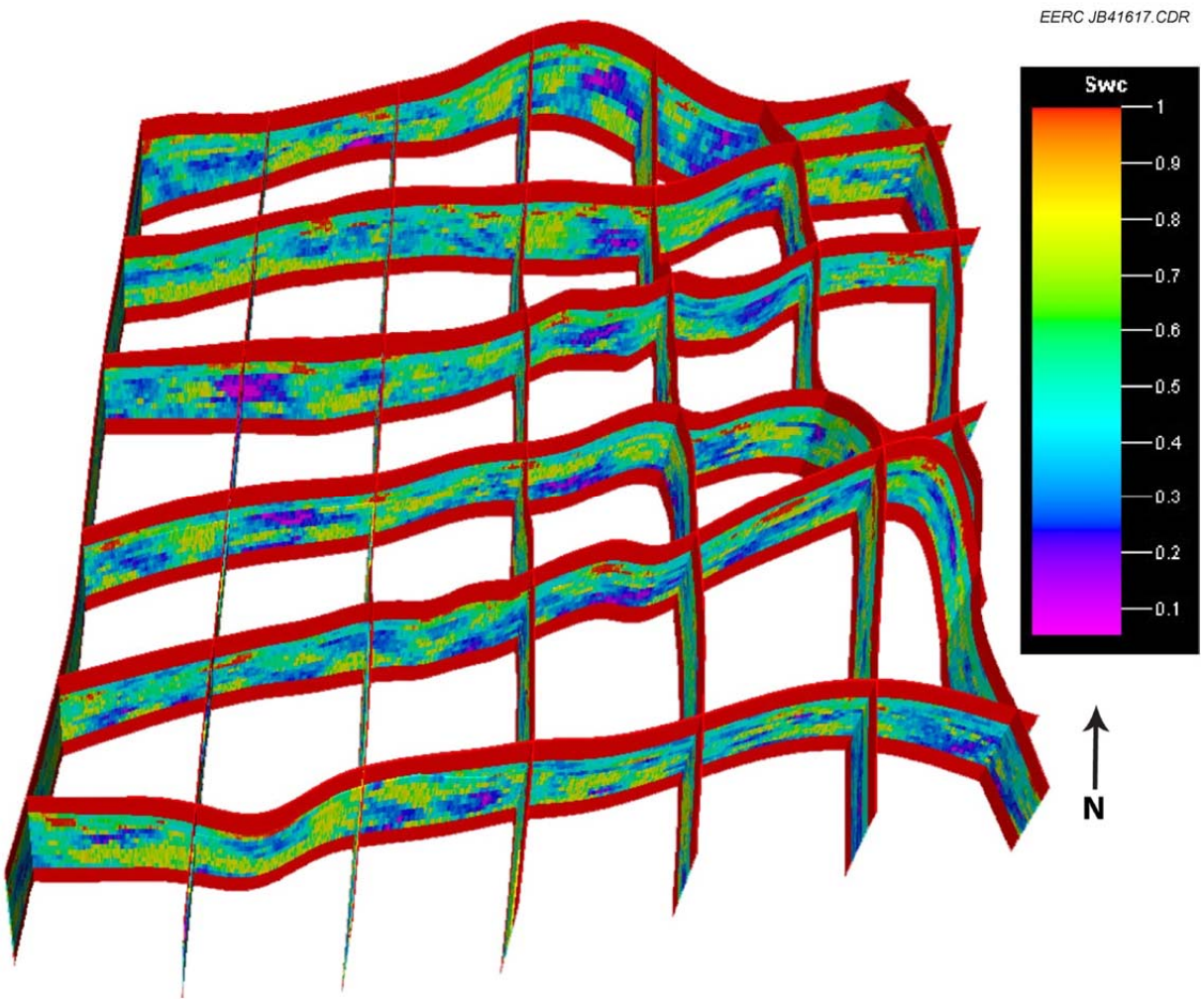

Figure B-15. Fence diagram of the cokriged water saturation property (Figure B-6 shows a map view layout).

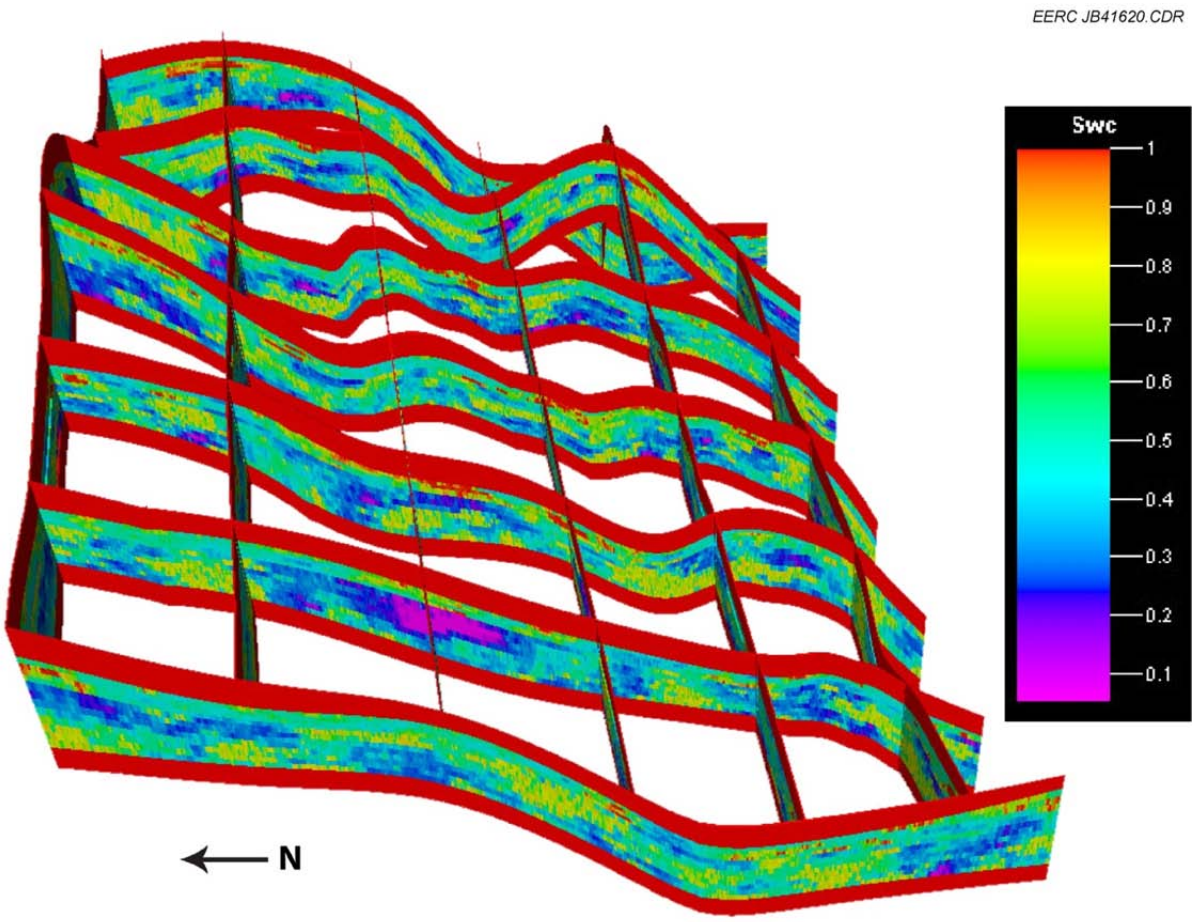

Figure B-16. Fence diagram of the cokriged water saturation property (Figure B-6 shows a map view layout).

NET-TO-GROSS

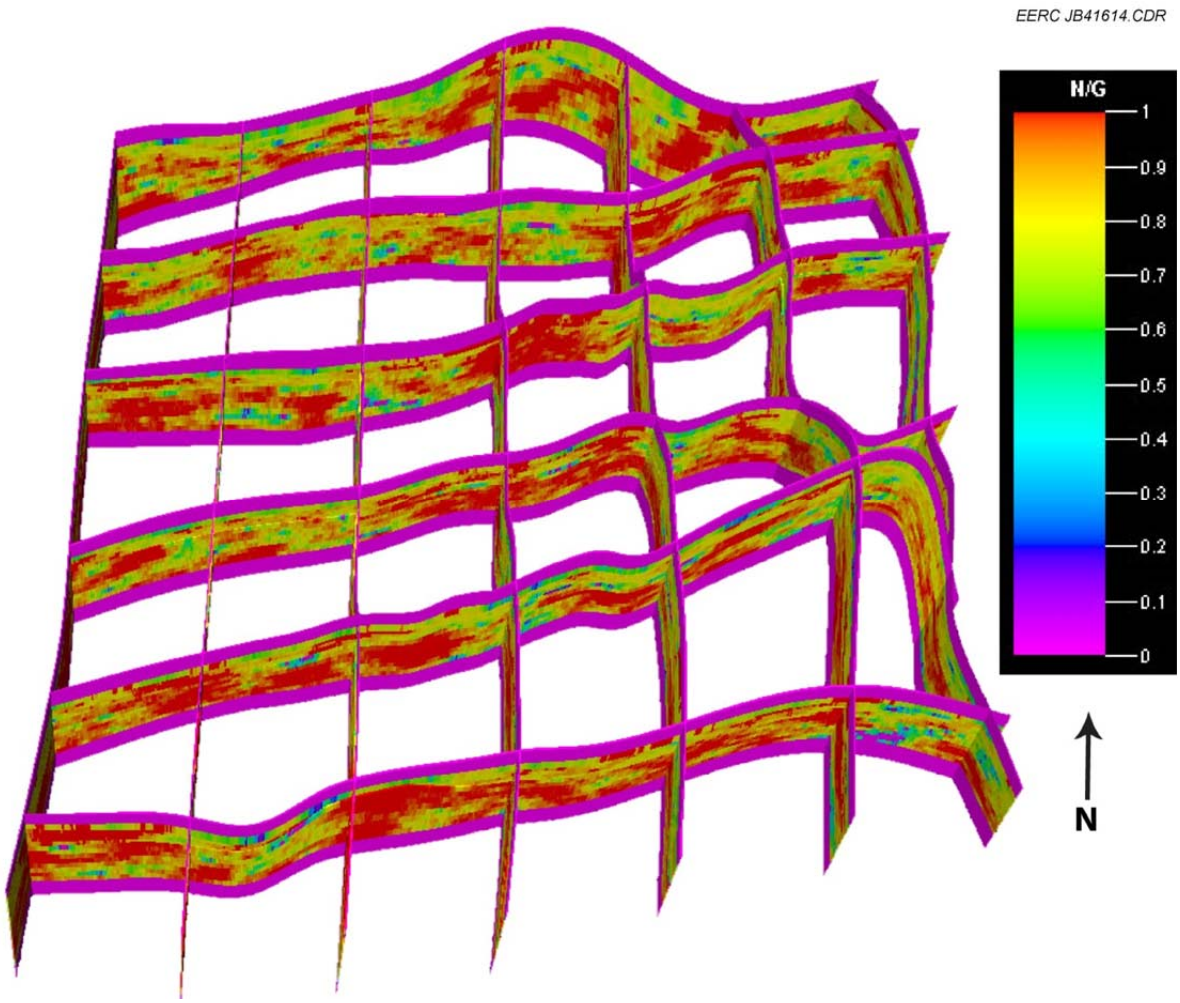

Figure B-17. Fence diagram of the net-to-gross property. Essentially, this property shows the distribution of shale (red color) within the reservoir (Figure B-6 shows a map view layout).

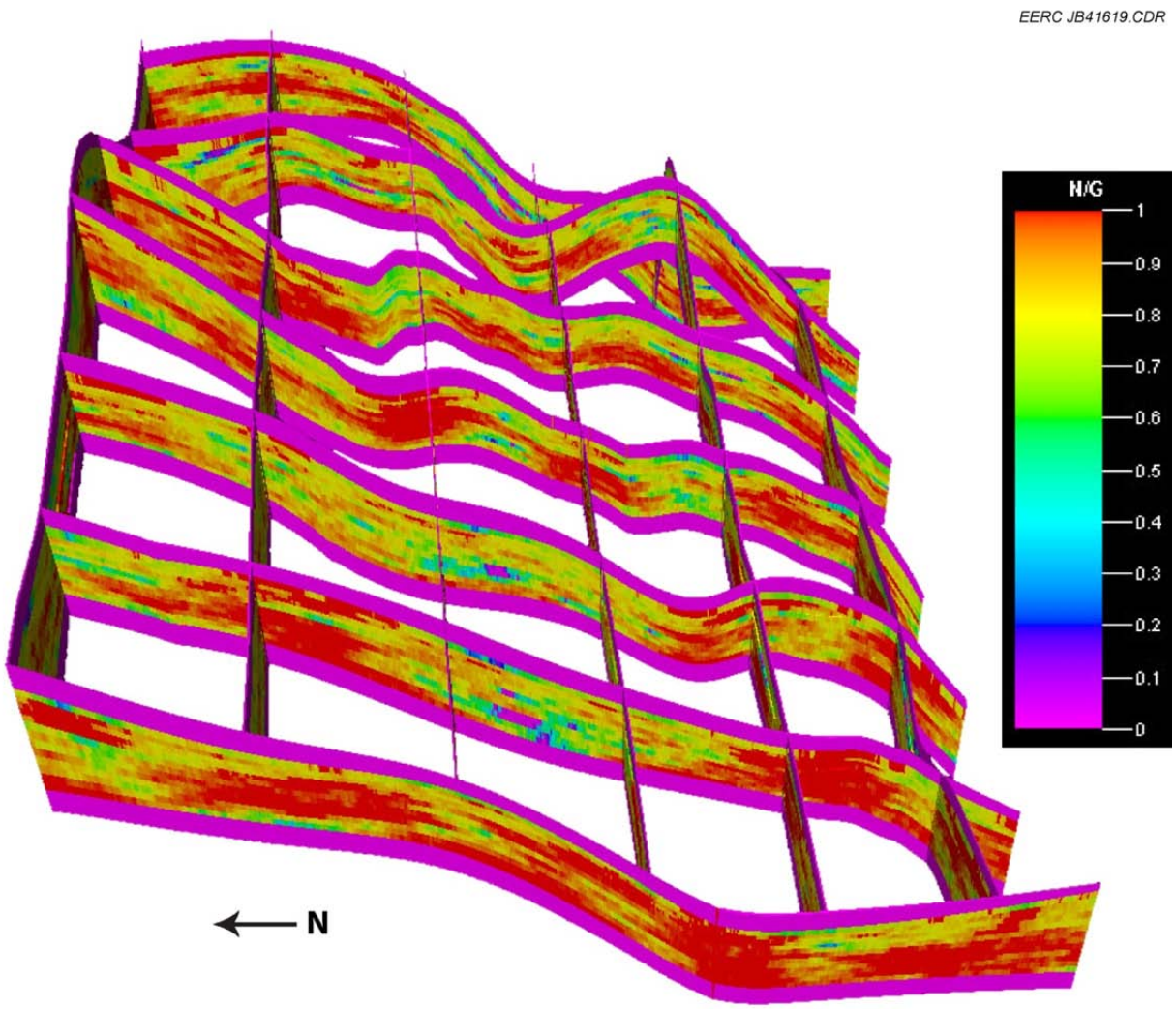

Figure B-18. Fence diagram of the net-to-gross property. Essentially, this property shows the distribution of shale (red color) within the reservoir (Figure B-6 shows a map view layout).

APPENDIX C

CO_2 PROPHET SIMULATION AND HISTORY MATCH GRAPHS

CO_2 PROPHET SIMULATION AND HISTORY MATCH GRAPHS

CO_2 Prophet was used to simulate the miscible CO_2 injection. First, field-scale simulation was performed to adjust the available data for the Rival Field such as cumulative water injection, cumulative water production, and cumulative oil production for the water injection period, spanning about 52 years. The adjusted model was then used to conduct the prediction runs for the subsequent CO_2 enhanced oil recovery (EOR) period. The results of both the history match and prediction runs for two patterns (seven-spot and line drive) are depicted in the following.

Seven-Spot Pattern

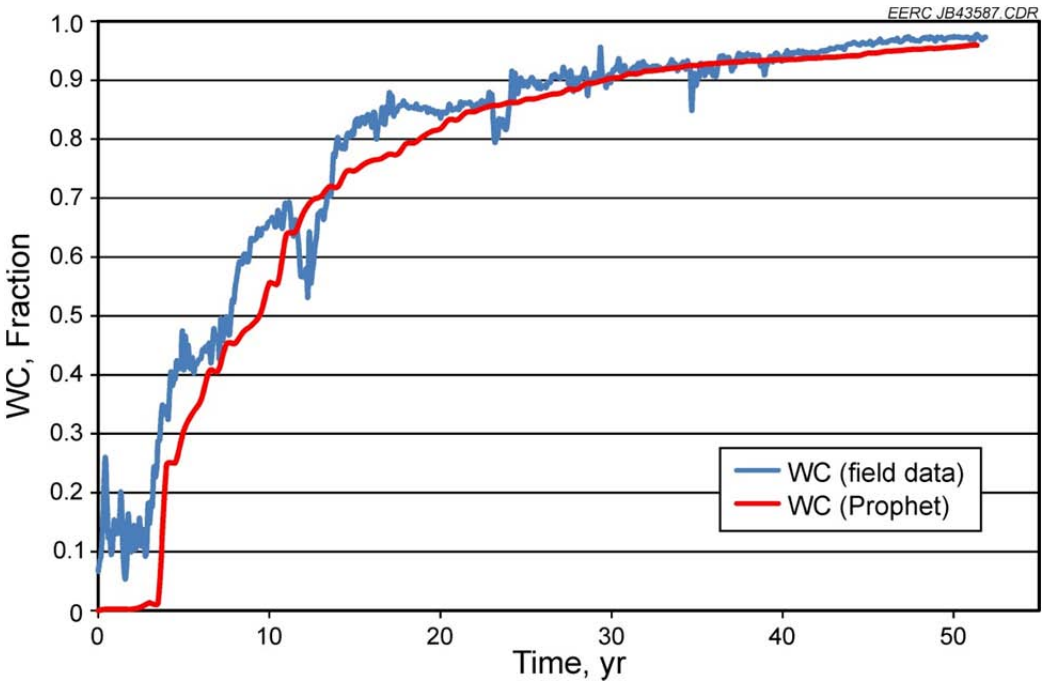

Figure C-1. History match of water cut (WC) vs. time for the seven-spot pattern.

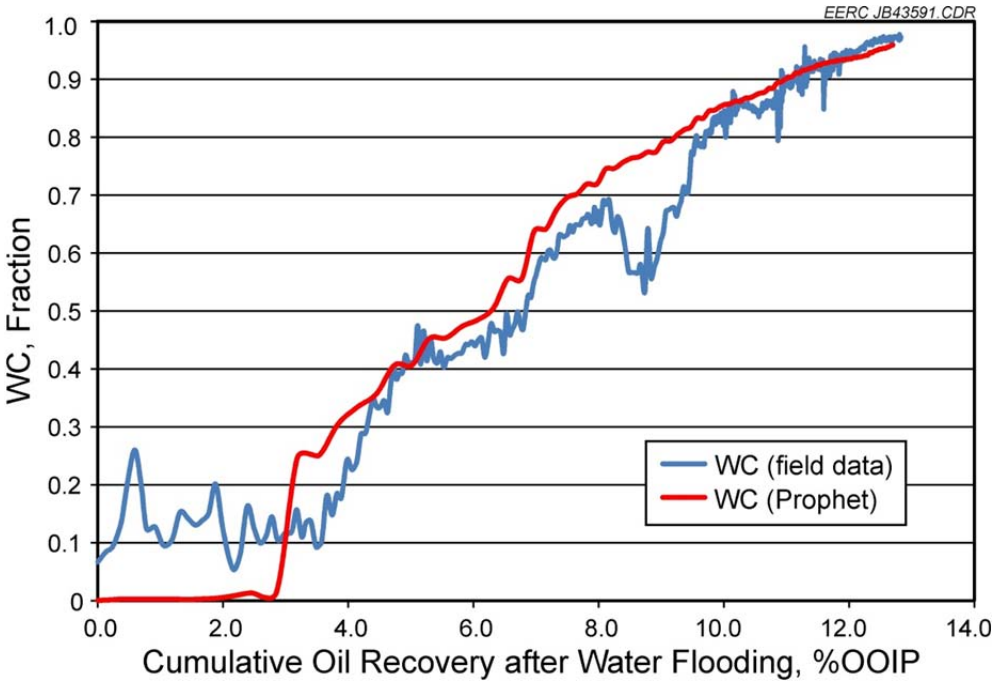

Figure C-2. History match of water cut vs. cumulative oil produced since the beginning of waterflood for the seven-spot pattern.

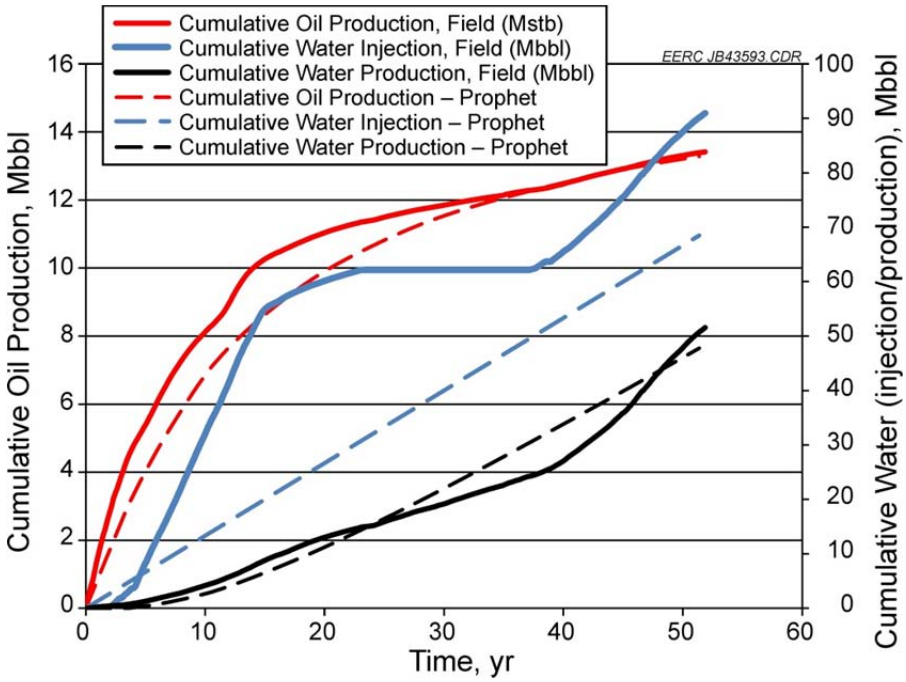

Figure C-3. History-matched historic oil production, water production, and water injection data for seven-spot pattern.

Line Drive Pattern

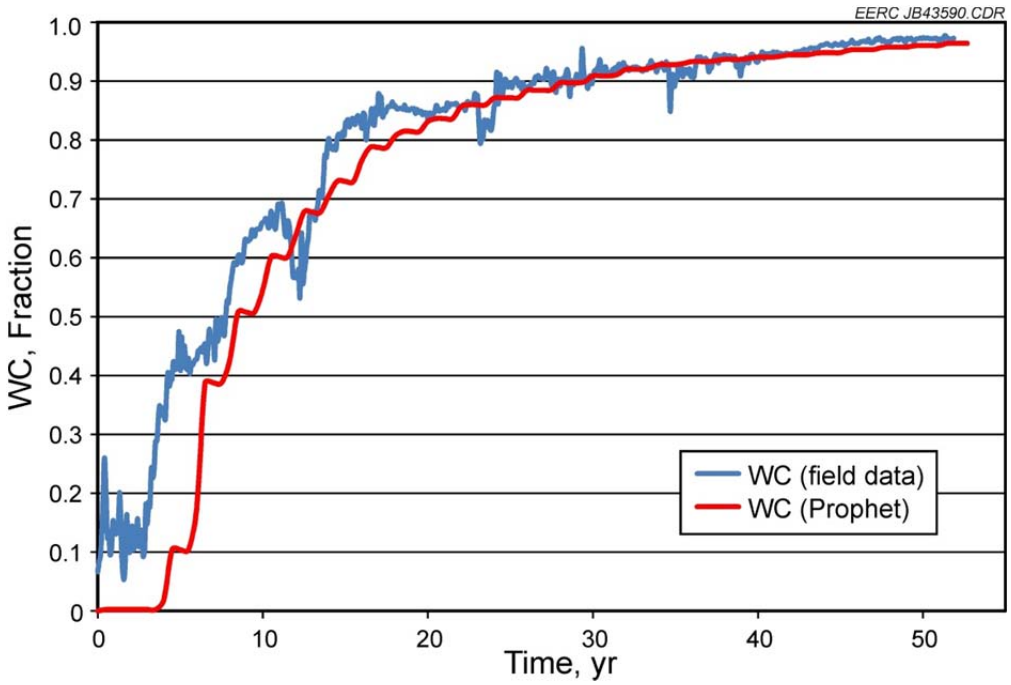

Figure C-4. History match of water cut vs. time for the line drive pattern.

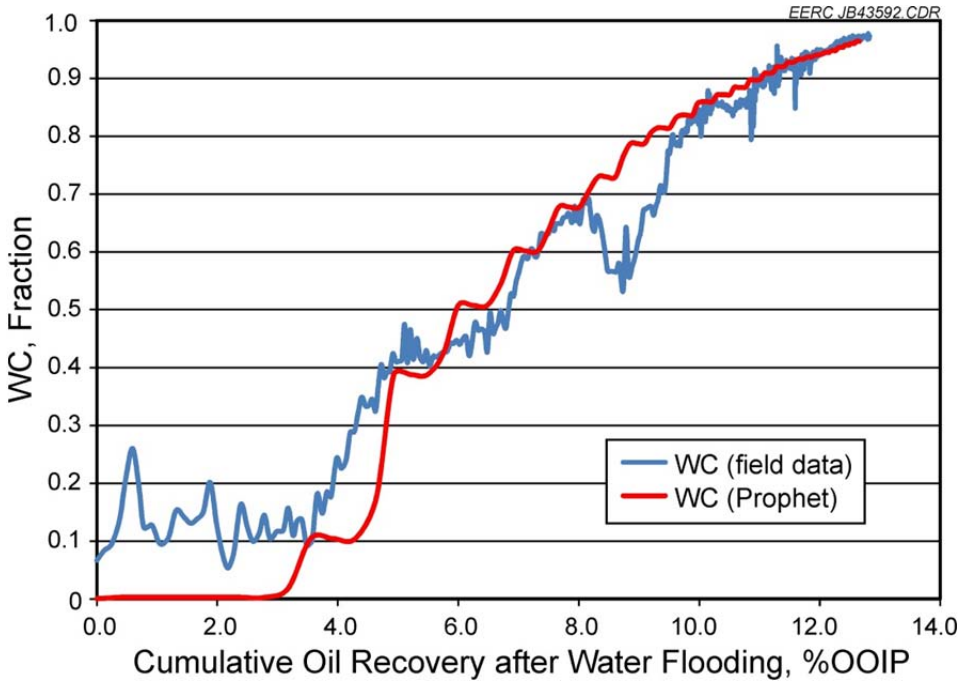

Figure C-5. History match of water cut vs. cumulative oil produced since the beginning of waterflood for the line drive pattern.

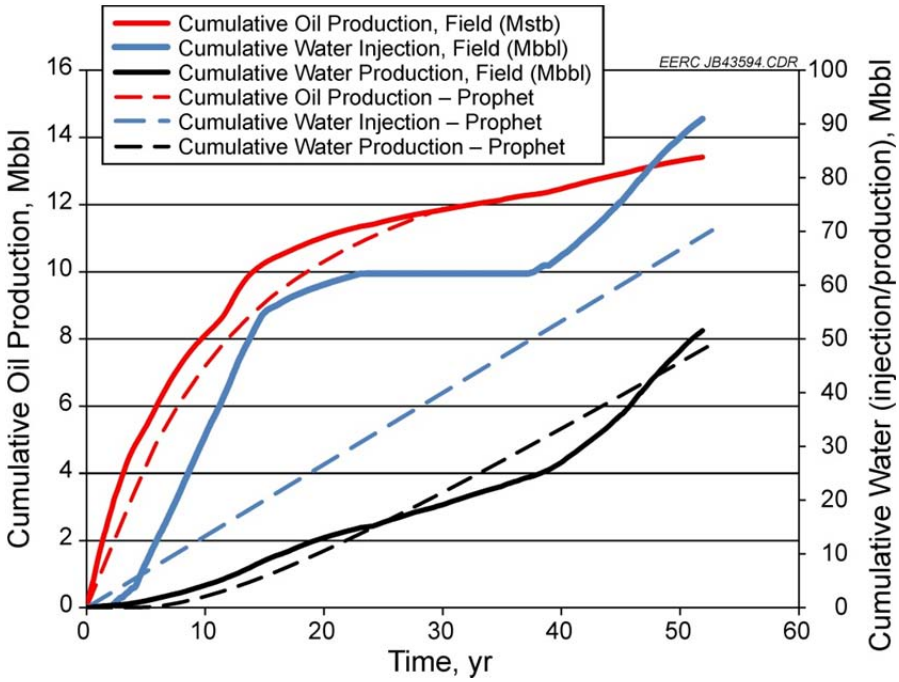

Figure C-6. History-matched historic oil production, water production, and water injection data for line drive pattern.

Table C-1. Results from CO_2 Simulation of 23 Cases Successfully Attempted

Spacing = 60 Acres

Pattern	Case	Cum. CO_2 Injection, HCPV	CO_2 Injection, Mscf/Day/Pattern	CO_2 Injection/ Year, Mt	Water Injection Time, Year	CO_2 Injection Time, Year	CO_2 Capt. Vol, Mscf	CO_2 Capt. Mass, Mt	CO_2 EOR Oil, Mstb	CO_2 Incremental EOR, % OOIP	CO_2 UT Factor, mscf/mstb	CO_2 Prod/Injection Ratio, scf/scf
Line	1	1	0.275	1	52.00	9.12	43,878	2.558	15.787	18.5	2780	0.73
Drive	2	1	0.551	2	52.00	4.54	43,844	2.556	15.650	18.5	2800	0.73
	3	2	0.275	1	52.00	18.75	61,662	3.595	24.422	28.6	2520	0.81
	4	2	0.551	2	52.00	9.29	61,611	3.592	24.235	28.5	2540	0.81
Seven-	1	1	0.275	1	52.00	9.28	38,298	2.233	13.193	15.5	2900	0.76
Spot	2	1	0.410	1.49	52.00	6.17	38,315	2.234	13.039	15.5	2940	0.76
	3	2	0.275	1	52.00	18.75	58,453	3.408	22.972	26.9	2540	0.82

Spacing = 80 Acres

Pattern	Case	Cum. CO_2 Injection, HCPV	CO_2 Injection, Mscf/Day/Pattern	CO_2 Injection/ Year, Mt	Water Injection Time, Year	CO_2 Injection Time, Year	CO_2 Capt. Vol, Mscf	CO_2 Capt. Mass, Mt	CO_2 EOR Oil, Mstb	CO_2 Incremental EOR, % OOIP	CO_2 UT Factor, mscf/mstb	CO_2 Prod/Injection Ratio, scf/scf
Line	1	1	0.367	1	52.50	9.23	43,853	2.557	15.757	18.5	2780	0.73
Drive	2	1	0.734	2	52.50	4.49	43,840	2.556	15.181	18.5	2890	0.73
	3	1	0.900	2.45	52.50	3.62	43,878	2.558	14.618	18.5	3000	0.73
	4	2	0.367	1	52.50	18.56	61,658	3.595	24.384	28.5	2530	0.81
	5	2	0.734	2	52.50	9.23	61,632	3.593	23.795	28.5	2590	0.81
	6	2	0.850	2.32	52.50	7.94	61,658	3.595	23.424	28.6	2630	0.81
Seven-	1	1	0.367	1	52.50	9.23	38,310	2.233	13.146	15.5	2910	0.76
Spot	2	1	0.550	1.50	52.50	6.08	38,310	2.233	12.749	15.5	3010	0.76
	3	2	0.367	1	52.50	18.71	58,470	3.409	22.925	26.9	2550	0.82
	4	2	0.450	1.23	52.50	15.22	58,445	3.407	22.797	26.9	2560	0.82

Spacing = 100 Acres

Pattern	Case	Cum. CO_2 Injection, HCPV	CO_2 Injection, Mscf/Day/Pattern	CO_2 Injection/ Year, Mt	Water Injection Time, Year	CO_2 Injection Time, Year	CO_2 Capt. Vol, Mscf	CO_2 Capt. Mass, Mt	CO_2 EOR Oil, Mstb	CO_2 Incremental EOR, % OOIP	CO_2 UT Factor, mscf/mstb	CO_2 Prod/Injection Ratio, scf/scf
Line	1	1	0.367	1	52.00	9.28	43,868	2.558	15.770	18.5	2780	0.73
Drive	2	1	0.734	2	52.00	4.54	43,878	2.558	15.657	18.5	2800	0.73
	3	2	0.367	1	52.00	18.76	61,655	3.594	24.402	28.6	2530	0.81
	4	2	0.734	2	52.00	9.28	61,645	3.594	24.279	28.6	2540	0.81
Seven-	1	1	0.367	1	52.00	9.28	38,308	2.233	13.210	15.5	2900	0.76
Spot	2	2	0.367	1	52.00	18.76	58,470	3.409	22.989	27.0	2540	0.82

REFERENCES

Laird, W.M., 1960, Oil fields in the Burke County area, North Dakota—geological, magnetic, and engineering studies: North Dakota Geologic Survey, Report of Investigation No. 36.

Schlumberger, 1991, Log Interpretation Charts: Houston, Schlumberger, 172 p.